CRYSTALLIZATION AND SOLID-STATE TRANSFORMATION OF PSEUDOPOLYMORPHIC FORMS OF SODIUM NAPROXEN

A Thesis
Presented to
The Academic Faculty

By

Young-soo Kim

In Partial Fulfillment
of the Requirements for the Degree
Doctor of Philosophy in
Chemical & Biomolecular Engineering

Georgia Institute of Technology

August, 2005

CRYSTALLIZATION AND SOLID-STATE TRANSFORMATION OF PSEUDOPOLYMORPHIC FORMS OF SODIUM NAPROXEN

Approved by:

Dr. Ronald W. Rousseau, Chairman
School of Chemical & Biomolecular Engineering
Georgia Institute of Technology

Dr. Amyn S. Teja, Associate Chair
School of Chemical & Biomolecular Engineering
Georgia Institute of Technology

Dr. Yulin Deng
School of Chemical & Biomolecular Engineering
Georgia Institute of Technology

Dr. Pete J. Ludovice
School of Chemical & Biomolecular Engineering
Georgia Institute of Technolog

Dr. Angus P. Wilkinson
School of Chemistry & Biochemistry
Georgia Institute of Technology

Dr. Ronald C. Zumstein, Vice President
Albemarle Corp.

Date Approved: July 2005

To my wife

ACKNOWLEDGEMENT

I would like to express my sincere gratitude to my thesis advisor, Dr. Ronald W. Rousseau for his tags on my research during meetings, and continual support throughout this study. I could not have even imagined this much achievement without his encouragement. Sincere appreciation is extended to my thesis committee, Dr. Amyn Teja, Dr. Pete Ludovice, Dr. Yulin Deng, Dr. Angus P. Wilkinson, and Dr. Ronald C. Zumstein for their helpful discussions. And, I would like to thank Albemarle Corporation for supplying sodium naproxen for the research.

I also thank the current and previous group members, Dr. Hatem Alsyouri, Karsten Bartling, Stephanie Barthe, Cosmas Bayuadri, George Dumont, Laurent Nassif, José R. Méndez del Río, Jennifer Luk, Jennifer Sherard, Izumi Kurosawa and Daniel Euhus. Everyone helped me with their enthusiastic discussion and advice.

I wish to acknowledge my wife and my family, including my parents, my brother, my sister, and my sister-in-law. My wife has encouraged me to take a step forward every time as my beloved and as my partner in my life. And, my family has helped me so much more than words can express.

TABLE OF CONTENTS

ACKNOWLEDGEMENT iv

LIST OF TABLES ix

LIST OF FIGURES xi

NOMENCLATURE xvi

ABBREVIATIONS xviii

SUMMARY xix

CHAPTER 1
INTRODUCTION 1

CHAPTER 2
BACKGROUND 6
2.1 CRYSTALLOGRAPHY 6
2.1.1 Lattice, unit cell, and crystal systems 6
2.1.2 Space groups 8
2.1.3 Plane spacings 11
2.2 POLYMORPHISM AND PSEUDOPOLYMORPHISM 12
2.2.1 Types of polymorphism 13
2.2.2 Classification of hydrates 18
2.2.3 Behavior of solubilities 19
2.3 STRUCTURAL THEORY OF POLYMORPHISM 23
2.4 MOLECULAR MODELING SOFTWARE 24
2.4.1 Crystal builder 24
2.4.2 Open force field 25
2.4.3 Charges 29
2.4.4 Energy minimizer 31
2.5 NAPROXEN/SODIUM NAPROXEN 33

CHAPTER 3
CHARACTERIZATION AND SOLID-STATE TRANSFORMATIONS OF THE PSEUDOPOLYMORPHIC FORMS OF SODIUM NAPROXEN 36
3.1 EXPERIMENTAL SECTION 37

3.1.1 Materials 37
3.1.2 Thermogravimetric analysis (TGA) 37
3.1.3 Differential scanning calorimetry (DSC) 38
3.1.4 Powder X-ray diffraction (PXRD) 38
3.1.5 High-Performance liquid chromatography (HPLC) 38
3.1.6 Microscopy 39
3.2 RESULTS AND DISCUSSION 39
3.2.1 Crystallization and hydrate transformation 39
3.2.2 Thermal analysis of the samples 43
3.2.3 Dehydration kinetics 49
3.3 CONCLUSIONS 58

CHAPTER 4
SOLUBILITY OF PSEUDOPOLYMORPHS OF SODIUM NAPROXEN 59
4.1 EXPERIMENTAL APPARATUS AND PROCEDURES 60
4.1.1 Apparatus 60
4.1.2 Experimental procedures 62
4.1.3 Sampling protocol 63
4.2 HIGH PERFORMANCE LIQUID CHROMATOGRAPHY 64
4.2.1 Equipment 64
4.2.2 Calibration 66
4.2.3 Sample dilution 69
4.3 ANALYSIS OF CRYSTALS 71
4.3.1 Optical microscopy 71
4.3.2 Powder X-Ray diffraction (PXRD) 71
4.4 RESULTS AND DISCUSSION 72
4.4.1 Solubility 72
4.4.2 Transition between pseudopolymorphs 76
4.4.3 Solubility data correlations 78
4.4.4 Relationships among heats of solution and heat of dehydration 81
4.4.5 Crystal habit of pseudopolymorphs of sodium naproxen 87
4.5 CONCLUSIONS 90

CHAPTER 5
CRYSTAL STRUCTURE OF ANHYDROUS SODIUM NAPROXEN, $C_{14}H_{13}O_3Na$ 92
5.1 CRYSTALLIZATION OF SINGLE CRYSTALS 93
5.2 RESULTS AND DISCUSSION 94

CHAPTER 6
PROPAGATION OF SOLID-STATE TRANSFORMATIONS BY DEHYDRATION AND STABILIZATION OF PSEUDOPOLYMORPHIC FORMS OF SODIUM NAPROXEN 99
6.1 EXPERIMENTAL SECTION 101
6.1.1 Materials 101
6.1.2 Powder X-ray Diffraction (PXRD) 101

6.1.3 Thermogravimetric Analysis (TGA) 102
6.1.4 Scanning Electron Microscopy (SEM) 102
6.1.5 Microscopy 102
6.1.6 Visualization 102
6.1.7 Dehydration of Crystalline Powders of Sodium Naproxen 103
6.1.8 Dehydration of Single Crystals of Sodium Naproxen 103
6.2 RESULTS AND DISCUSSION 104
6.2.1 Dehydration of Dihydrated Sodium Naproxen 104
6.2.2 Dehydration of Single Crystals of the Monohydrated Sodium Naproxen 109
6.2.3 Comparison of Structures and Stabilization Forces for Anhydrous and Monohydrated Sodium Naproxen 116
6.3 CONCLUSIONS 124

CHAPTER 7
STRUCTURE PREDICTION OF ANHYDROUS SODIUM NAPROXEN VIA MOLECULAR MODELING 126
7.1 SOFTWARE TO ASSIST IN SOLVING STRUCTURES FROM POWDER X-RAY DIFFRACTION PATTERN 129
7.1.1 PowderX 129
7.1.2 Autoindexing programs 131
7.1.3 GSAS - Rietveld refinement 132
7.2 RESULTS AND DISCUSSIONS 134
7.2.1 Determination of cell parameters from powder pattern 134
7.2.2 Determination of force fields for energy minimization 139
7.2.3 Generation of initial structures for structure solution 145
7.2.4 Energy minimization to obtain trial structures for refinement 148
7.2.5 Structure refinement 155
7.3 CONCLUSIONS 158

CHAPTER 8
CONCLUSIONS AND RECOMMENDATIONS 159
8.1 CONCLUSIONS 159
8.2 RECOMMENDATIONS 162

APPENDIX A
FITTING OF KINETIC MODELS TO ISOTHERMAL TGA DATA OF SODIUM NAPROXEN 164
A.1 1^{ST} WATER REMOVAL FROM THE DIHYDRATED SODIUM NAPROXEN 164
A.1.1 T = 24.0˚C 164
A.1.2 T = 26.4˚C 166
A.1.3 T = 29.5˚C 168
A.2 2^{ND} WATER REMOVAL FROM THE DIHYDRATED SODIUM NAPROXEN 170
A.2.1 T = 24.0˚C 170

A.2.2 T = 26.4˚C 172
A.3 1ST WATER REMOVAL FROM THE MONOHYDRATED SODIUM NAPROXEN 174
A.3.1 T = 24.1˚C 174
A.3.2 T = 26.9˚C 176
A.3.3 T = 29.8˚C 178

APPENDIX B
CALIBRATION CURVES 180
B.1 CALIBRATION CURVE TO MEASURE CONCENTRATIONS OF SODIUM NAPROXEN IN PURE WATER SOLUTIONS 180
B.2 CALIBRATION CURVE TO MEASURE CONCENTRATIONS OF SODIUM NAPROXEN IN 64 MOL% METHANOL IN AQUEOUS SOLUTIONS 181

APPENDIX C
DETERMINATION OF DENSITY OF ANHYDROUS SODIUM NAPROXEN BY THE METHOD OF FLOTATION 182

APPENDIX D
CRYSTALOGRAPHY INFORMATION OF THE ANHYDROUS SODIUM NAPROXEN 184

REFERENCES 187

LIST OF TABLES

Table 2-1. Seven crystal systems 8

Table 2-2. Thermodynamic rules for polymorphic transitions, where Form I is the higher-melting form..... 21

Table 3-1. The temperatures and the endotherms for peaks in DSC 47

Table 3-2. Converted heats of fusion of the sodium naproxen species 49

Table 3-3. Algebraic expressions for $g(\alpha)$ corresponding to suggested mechanisms of solid-state processes..... 51

Table 3-4. Activation energy for the released water..... 53

Table 3-5. Activation energies for different dehydration reactions..... 54

Table 4-1. Acquisition parameters..... 65

Table 4-2. Solubility of sodium naproxen in pure water 74

Table 4-3. Solubility of sodium naproxen in aqueous solutions containing 64 mol% methanol..... 74

Table 4-4. Solubility of sodium naproxen in pure water by Mendéz del Río (2004)..... 74

Table 5-1. Selected geometric parameters (Å, °) for sodium naproxen..... 97

Table 5-2. Crystallographic Data and Refinement Details 98

Table 6-1. Shrinkage and expansion of cell constants by dehydration of the monohydrated sodium naproxen to the anhydrous species..... 115

Table 6-2. Distances between Na and O by the Na–O type interactions..... 121

Table 6-3. Comparison of bond lengths and angles by hydrogen bonds..... 122

Table 7-1. Values for parameters in each task..... 134

Table 7-2. Peaks searched by 2nd Derivative method in PowderX 136

Table 7-3. Cell parameters searched by DICVOL in CRYSFIRE..... 137

Table 7-4. Forcefield available in Cerius2 and comparison 140

Table 7-5. RMS by energy minimization with PCFF force field 141

Table 7-6. RMS by energy minimization with CVFF force field..... 141

Table 7-7. VdW parameters for sodium ion (Na^+) 144

Table 7-8. RMS by energy minimization with vdW parameters for sodium from literatures..... 144

Table 7-9. Comparison of cell constants for the anhydrate to the monohydrate 146

Table 7-10. Results from energy minimization of the minimized structures of Model 1 and Model 2 154

Table 7-11. Parameter values for the final structure of anhydrous sodium naproxen 157

Table C-1. Prepared solutions and densities 183

Table D-1. Fractional hydrogen atomic coordinates and equivalent isotropic thermal parameters for anhydrous sodium naproxen 184

Table D-2. Fractional non-hydrogen atomic coordinates and equivalent isotropic thermal parameters for anhydrous sodium naproxen 185

Table D-3. Anisotropic thermal parameter with their e.s.d.'s in parentheses for anhydrous sodium naproxen 186

LIST OF FIGURES

Figure 2-1. (a) Three-dimensional lattice with lattice points represented by the solid circles and (b) a unit cell with cell dimensions 7

Figure 2-2. The fourteen Bravais lattices: BCC and FCC stand for Body-Centered Cubic and Face-Centered Cubic, respectively 9

Figure 2-3. Schematic diagram of the relationship between the 7 crystal systems, 14 Bravais lattices, 32 point groups, and 230 space groups 10

Figure 2-4. Bragg's equation representing the relationship between the interplanar spacing of hkl planes and the angle of incidence with Miller index 11

Figure 2-5. Molecular packing diagrams of the (a) α polymorph and (b) β polymorph of *p*-nitrophenol. 14

Figure 2-6. Unit cells of (a) Form I, (b) Form II, (c) Form III, (d) Form IV of sulfathiazole showing hydrogen bonds with dimer structure highlighted in green 15

Figure 2-7. Molecular conformation in (a) polymorph 1 and (b) polymorph 2 of piroxicam pivalate 17

Figure 2-8. Solubility curves exhibiting (a) monotropy, (b) enantiotropy, and (c) enantiotropy with metastable phases [19] 20

Figure 2-9. Dihedral angle 27

Figure 2-10. Improper torsion angle 27

Figure 2-11. Van der Waals interation 29

Figure 2-12. Schematic diagram of (S)-(+)-sodium naproxen 34

Figure 3-1. The path for the change between pseudopolymorphic forms of sodium naproxen 41

Figure 3-2. Powder X-ray diffraction patterns of three different pseudopolymorphic forms of sodium naproxen; (a) the anhydrate, (b) the monohydrate and (c) the dihydrate 42

Figure 3-3. TGA curves with nitrogen purge of (a) monohydrated and (b) dihydrated forms of sodium naproxen 44

Figure 3-4. Differential scanning calorimetry curves of three different pseudopolymorphic forms of sodium naproxen; (a) the anhydrate, (b) the monohydrate and (c) the dihydrate 46

Figure 3-5. (a) sodium naproxen molecule with the sodium and hydrogen atoms omitted and (b) a projection along the [100] plane of the monohydrate. In (a), two oxygen atoms and four covalent bonds are exaggerated. For clarity, only this portion of the molecule is depicted in (b). Additionally, in (b), the smaller circles represent oxygen atoms, the larger circles represent sodium atoms, and the shaded waves show water channels in the monohydrate. 56

Figure 4-1. Schematic diagram of a 3-port, 400-mL jacketed crystallization vessel and a water circulator system with a programmable temperature controller. 61

Figure 4-2. Schematic diagram of a 80-mL bottle with a cap and a water circulator system with a programmable temperature controller..... 61

Figure 4-3. A 5-mL plastic syringe, 0.2 μm syringe filter and a spinal needle. 61

Figure 4-4. HPLC separation of sodium naproxen and butyrophenone 65

Figure 4-5. Scheme of dilution for the calibration curve..... 68

Figure 4-6. Scheme of dilution for a sample..... 69

Figure 4-7. Solubility of sodium naproxen in pure water and in solution containing 64 mol% methanol. W in the legend means that the data were the solubility of sodium naproxen in pure water and W+M represents the data in the mixture of water and methanol. 75

Figure 4-8. Empirical fits to the solubility data in pure water and mixtures of water and methanol..... 77

Figure 4-9. Van't Hoff plot of the solubility of sodium naproxen in pure water 80

Figure 4-10. Van't Hoff plot of the solubility of sodium naproxen in the mixture of water and methanol..... 80

Figure 4-11. Alternative paths in which dihydrated sodium naproxen is dissolved in water 82

Figure 4-11. Photomicrographs of dihydrated sodium naproxen in pure water at 23°C .. 88

Figure 4-12. Photomicrographs of dihydrated sodium naproxen in aqueous solution containing 64 mol% methanol at 10°C 89

Figure 4-13. Photomicrographs of monohydrated sodium naproxen in aqueous solution containing 64 mol% methanol at 25°C 89

Figure 5-1. Schematic diagram of slow evaporation 93

Figure 5-2. A perspective drawing of two independent molecule A and B of anhydrate. 94

Figure 5-3. Newman projections of anhydrous sodium naproxen along the bonds of (a) C12a–C11a, (b) C12b–C11b, (c) C11a–C5a, (d) C11b–C5b, (e) C10a–O3a, and (f) C10b–O3b 95

Figure 6-1. PXRD patterns of sodium naproxen samples containing varying amounts of water. The weight % water is shown to the right of the diagram. Samples were obtained by dehydration of dihydrated sodium naproxen in a desiccator 105

Figure 6-2. Thermal analyses curves of (1) TGA and (2) dTG of samples with water content of (a) 7.39 wt% and (b) 9.01 wt% 107

Figure 6-3. Photomicrographs of a single crystal that initially was monohydrated sodium naproxen before being rapidly dehydrated in an oven. The progress of the experiment is shown at (a) t = 0 minute, (b) t = 10 minutes, (c) t = 20 minutes, (d) t = 30 minutes, (e) t = 40 minutes and (f) t = 50 minutes. The scale mark in every graph is 100 micro meters long. 110

Figure 6-4. (a) Miller indices of crystal faces and (b) a projection perpendicular to the $(0\bar{1}0)$ plane of the monohydrate of sodium naproxen showing water channels. In (b), sodium atoms and oxygen atoms in water are exaggerated for clarity and the larger circles represent sodium atoms and the smaller circles represent oxygen atoms in water. 111

Figure 6-5. Photomicrographs of single crystals on monohydrated sodium naproxen slowly dehydrated in a desiccator. Progress of the experiment is shown at (a) t = 0 hour, (b) t = 24 hours, (c) t = 33 hours and (d) t = 42 hours. 113

Figure 6-6. SEM analysis of a sample from rapid dehydration of the monohydrated sodium naproxen 115

Figure 6-7. (a) Sodium naproxen with the sodium and hydrogen atoms omitted, (b) and (c) projections perpendicular to the $(0\,\bar{1}\,0)$ plane and the $(\bar{1}\,00)$ plane of the monohydrate, respectively, (d) and (e) projections perpendicular to the $(0\,\bar{1}\,0)$ plane and the $(00\,\bar{1})$ plane of the anhydrate, respectively. In (a), two oxygen atoms and four covalent bonds are exaggerated for emphasis. For clarity, only this portion of the molecule is depicted in (c) and (e). In (b) and (d), only sodium atoms and oxygen atoms in water are exaggerated. In (b), (c), (d) and (e), the larger circles represent sodium atoms and the smaller circles represent oxygen atoms. 118

Figure 6-8. Planar projections of the unit cell of the monohydrate of sodium naproxen: perpendicular to (a) the (100) plane, (b) the (001) plane, and (c) the $(00\,\bar{1})$ plane. Only a small portion of sodium naproxen was depicted using the definition in Figure 6-7a. The larger circles represent sodium atoms and the smaller circles represent oxygen atoms; solid red lines and dotted blue lines between atoms represent the Na–O type interactions and hydrogen bonds, respectively. 120

Figure 6-9. (a) Geometry of free water, (b) placement of hydrogen atoms in water, (c) the definition of hydrogen bond angle and (d) bond length and angle by hydrogen bonds 122

Figure 7-1. Powder X-ray diffraction pattern for anhydrous sodium naproxen from Philips® PW1800 135

Figure 7-2. Powder pattern after smoothing peaks 135

Figure 7-3. Dimension of a unit cell for monohydrated sodium naproxen..... 139

Figure 7-4. Model 1 which uses the same coordinate system as the monohydrated sodium naproxen..... 147

Figure 7-5. Model 2 which has different coordinate system from the monohydrate..... 147

Figure 7-6. Powder X-ray diffraction patterns of (a) the anhydrous sodium naproxen, (b) Model 1 and (c) Model 2 149

Figure 7-7. Definition of torsion angles in sodium naproxen..... 150

Figure 7-8. Minimized structures and definitions of A and B molecules in (a) Model 1 and (b) Model 2..... 152

Figure 7-9. Simulated powder X-ray diffraction pattern of the structure in the lowest energy state in Table 7-10..... 154

Figure 7-10. Output from the Rietveld refinement and the difference between the observed experimental pattern and simulated pattern..... 156

NOMENCLATURE

A	peak area
C	concentration, g solute/kg solution
ΔE_a	activation energy for dehydration, kJ/mol
$F(calc)$	calculated structure factors
$F(obs)$	observed structure factors
H	enthalpy, J (Chapter 3)
$\hat{H}$	enthalpy per unit mass, J/g (Chapter 3)
$\Delta\hat{H}_{fus}$	specific enthalpy of fusion, kJ/mol
$\Delta\hat{H}_d$	heat of dehydration, kJ/mol
$\Delta\hat{H}_H$	heat of hydration, kJ/mol
$\Delta\hat{H}_{sol}$	heat of solution, kJ/mol
M	mass of water in the sample at time t, g (Chapter 3)
M	mass, g (Chapter 4)
M_T	initial mass of water in a sample for isothermal TGA experiments, g
R	gas constant
R^2	correlation coefficient
R_p	R factor
T	temperature, °C or K
T_d	dehydration temperature, °C
T_m	melting temperature
T_s	dissolution temperature, °C
T_t	triple point temperature

c_P	heat capacity
γ	liquid-phase activity coefficient
b	constant for a calibration curve
$\Delta_{\text{fus}}h$	enthalpy of fusion
k	constant for a calibration curve (Chapter 4)
k	rate constant, min^{-1} (Chapter 3)
m	mass, g (Chapter 3)
m	the number of water molecules per mother molecule, $m < n$ (Chapter 4)
n	the number of water molecules per mother molecule
t	time, min
w	mass of a sample, g
x	mass fraction (Chapter 3)
x	mole fraction of a solute (Chapter 4)
α	fraction of water removed from the hydrated crystal at time t
ε	separation distance at which the van der Waals potential is zero, kJ/ mol
σ	depth of the van der Waals potential well, nm

Subscripts

A	acetonitrile
I	internal standard
S	Sample or solution
W	water
0	the anhydrate (Chapter 4)
fus	fusion
(l)	liquid phase
(s)	solid phase
(v)	vapor phase

ABBREVIATIONS

CVFF	Consistent Valence Forcefield
DSC	Differential Scanning Calorimetry
HPLC	High-Performance Liquid Chromatography
PCFF	Polymer Consistent Forcefield
PXRD	Powder X-ray Diffraction
RMS	Root Mean Square
SEM	Scanning Electron Microscopy
SPC	Single Point Charge model for water
SPC/E	Extended SPC
TGA	Thermal Gravimetric Analysis

SUMMARY

Incorporation of water molecules in the crystal structure of an organic compound has strong effects on its physical and chemical properties. Therefore, the study on stability of water-incorporated pharmaceutical compounds and mechanisms of hydration and dehydration is very important for the pharmaceutical industries.

The main goals of the present research project were quantitative description of the crystallization and solid-state transformations of pseudopolymorphs of sodium naproxen in order to provide fundamental information concerning stability of the pseudopolymorphic forms. Furthermore, macroscopic phenomena of size reduction and anisotropic water-removal by dehydration were rationalized by microscopic aspects of crystal lattice structures.

Several pseudopolymorphic forms of sodium naproxen can crystallize from 0 mol% and 64 mol% methanol in aqueous solutions. The transition temperature between the dihydrate and the anhydrate was observed to be 29.8°C for 0 mol% methanol solutions, while interconversion between the dihydrate and the monohydrate occurred at 19.6°C for 64 mol% methanol solutions. The results showed the effects of temperature and solvent composition on the stability of pseudopolymorphs of organic compounds.

The heats of solution for each pseudopolymorph were estimated by fitting the solubility data with the van't Hoff equation, and their use was extended by the thermodynamic cycle developed in the present study. According to the thermodynamic

cycle, for an enantiotropic system, a form with a lower degree of hydration always has the lower heat of solution than a form with a higher degree of hydration, implying that a form with a lower degree of hydration is more stable.

The relative stabilities of the dihydrated, the monohydrated, and the anhydrous sodium naproxen at 0% relative humidity were investigated by dehydration of the dihydrated form and powder X-ray diffraction. The monohydrate is more stable than the dihydrate and the result was supported by isothermal TGA experiments.

This research explained why powder-like crystals of the anhydrous sodium naproxen were produced by dehydration of hydrated forms. The surfaces of the dehydrated crystals displayed cracks aligned along the *b*-axis of the monohydrate. These cracks made the anhydrous crystals, which were produced from the monohydrated species, very brittle and, eventually, such crystals were disrupted into much smaller entities. In addition, the existence of water channels in the unit cells of the monohydrate facilitates the dehydration in a direction more rapidly, especially, along the *b*-axis of the monohydrate. Rapid removal of water in a specific direction caused anisotropic dehydration.

CHAPTER 1

INTRODUCTION

Incorporation of solvent into the lattice of crystalline solids results in the formation of molecular adducts known as solvates. When the incorporated solvent is water, the solvates are called hydrates. A new and different unit cell, often leading to different physical properties, results with solvate formation; i.e., properties of solvates, such as density, solubility, dissolution rate and bioavailability, are different from those of non-solvated species. These physical property changes are analogous to those associated with polymorphism, and therefore solvates are often referred to as pseudopolymorphs to distinguish them from polymorphs.[1] Note that each pseudopolymorph may also have polymorphs. In the present study, since anhydrous and hydrated crystalline compounds of sodium naproxen were used, pseudopolymorphs of sodium naproxen mean anhydrous and hydrated forms of sodium naproxen.

The pharmaceutical importance of crystalline hydrates is summarized by Morris.[2] The physicochemical stability and/or bioavailability of pseudopolymorphs may raise issues during new drug development. Some hydrated compounds may convert to an amorphous form upon dehydration and some may become chemically labile. For example, cephradine dihydrate dehydrates to become amorphous and undergoes subsequent oxidation.[3] Dihydrophenylalanine[4, 5] anhydrate crystallizes as prism-shaped

crystals from ether and it is stable to oxidation; however, the dihydrated form grows as needle-like crystals and these crystals oxidize in air producing 70% phenylalanine in 10 minutes. Study of the bioavailability of ampicillin has shown that blood serum concentrations of ampicillin by the anhydrous form were higher and reached earlier than those by the trihydrated form.[6] It was deduced from the results of experiments that the differences of blood serum concentrations of ampicillin between the anhydrate and the trihydrate result from the differences in the aqueous solubility of those two forms.

Bulk drug substances are produced by several consecutive processes and unintentional interconversion among pseudopolymorphs may happen very frequently during the processes. For example, crystallization for the purpose of separation, purification, or simply solidification can lead to the production of hydrated forms. Since the formation of pseudopolymorphs is affected by variables such as temperature, pressure, and polarity of solvents, changing operating variables during crystallization may result in transformation between pseudopolymorphs.

Removal of solvent from the crystals by drying may have an effect on the interconversion. Drying is usually employed to remove solvent-residues from crystals after crystallization. If hydrated forms are wet and they are introduced into the drying process, not only solvents on the surface of the forms but also solvents incorporated in the lattice structures may be evaporated. Therefore, drying may result in the transformation of a hydrated form into a new form with a lower degree of hydration.

More unexpected interconversion may happen in a size reduction step such as milling. According to the study on transitions of carbamazepine[7], it was found that the dihydrated crystalline form was not phase-stable with respect to compression.

Sometimes, mechanical grinding of organometallic pseudopolymorphs using a mortar and pestle to prepare samples for powder X-ray diffraction experiments help water molecules become inserted into crystal lattice structures.[8]

The present study was motivated by the size reduction of crystals accompanying the drying process. Crystals of monohydrated sodium naproxen are formed with an average particle size of at least about 120 μm in the crystallization process developed by Phan et al.[9] The crystals then are dried to produce anhydrous sodium naproxen. During the drying process the dehydrated sodium naproxen becomes powder-like. This is not desired generally because larger crystals are easier to handle. Therefore, mechanisms of dehydration and macroscopic changes by dehydration are of great significance and they were examined in this research project. Additionally, because there has been little published work on pseudopolymorphism in sodium naproxen, this topic was also addressed in order to provide fundamental properties of pseudopolymorphism.

In this project, the following two areas were studied: (1) solvent-mediated transitions of pseudopolymorphic forms of sodium naproxen and (2) the solid-state transformations by dehydration. An outline of subsequent chapters is as follows:

- Chapter 2: background.
- Chapter 3: characterization of pseudopolymorphs of sodium naproxen and isothermal TGA (Thermal Gravimetric Analysis) experiments. The study on characterization of pseudopolymorphs of sodium naproxen was carried out by Di Martino et al.[10] However, they overlooked the existence of the monohydrate and their study was focused on the anhydrate and the dihydrate. Therefore, in Chapter 3, the monohydrated powder was

produced by dehydration of the dihydrate obtained using the method proposed by Di Martino et al.[10] and it was compared with the anhydrate and the dihydrate. In addition, the dihydrated sodium naproxen was dehydrated at constant temperatures in TGA to reveal mechanisms of dehydration.

- Chapter 4: crystallization and solubility of pseudopolymorphs with respect to the ratio of methanol and water. The solubility of pseudopolymorphs of sodium naproxen in solution was interpreted by thermodynamic model and the relationship between the heats of solution was explained by introducing the thermodynamic cycle.
- Chapter 5: structure determination of the anhydrate. The structure of only the monohydrate had been determined.[11] Single crystals of the anhydrate were obtained as described in Chapter 4. They then were used to determine the structure of the monohydrate.
- Chapter 6: solid-state transformation of monohydrated sodium naproxen. In this chapter, the size reduction by dehydration of the monohydrate was clearly explained using structural information of the monohydrate and the anhydrate.
- Chapter 7: structure determination of anhydrous sodium naproxen from the powder X-ray diffraction pattern. Since the anhydrous form is generated by dehydration of the monohydrated species, it was assumed that those two species have structural similarity. Therefore, when the trial model for the anhydrous species was generated, the structure for the

monohydrated sodium naproxen was used as an initial guess according to the assumption. The successful determination of the structure of the anhydrous form proved that the assumption was valid. Furthermore, study in this chapter was a good example of usage of known structure to determine the structures of other pseudopolymorphs.

CHAPTER 2

BACKGROUND

2.1 CRYSTALLOGRAPHY

2.1.1 Lattice, unit cell, and crystal systems

A crystalline species is defined as a solid that is composed of atoms, ions or molecules arranged in a periodic, 3-dimensional pattern.[12] A three-dimensional array is called a lattice as shown in Figure 2-1a. The requirement of a lattice is that each volume, which is called a unit cell, is surrounded by identical objects. The smallest periodic volume is taken from the lattice and depicted with vectors in Figure 2-1b. Three vectors, $\vec{a}$, $\vec{b}$, and $\vec{c}$, are defined in a right-handed sense for a unit cell. However, since three vectors are quite arbitrary a unit cell is described by six scalars, a, b, c, α, β, and γ without directions. By elementary vector analysis, the volume of a unit cell is defined by

$$V_c = |\vec{a} \times \vec{b} \cdot \vec{c}| \tag{2-1}$$

Several kinds of unit cells can be possible. For example, if a = b = c and α = β = γ = 90°, the unit cell is cubic and Fe, Cr, Mo have cubic unit cells. It turns out that only seven different kinds of unit cells are necessary to include all the possible lattices. These correspond to the seven crystal systems as shown in Table 2-1.

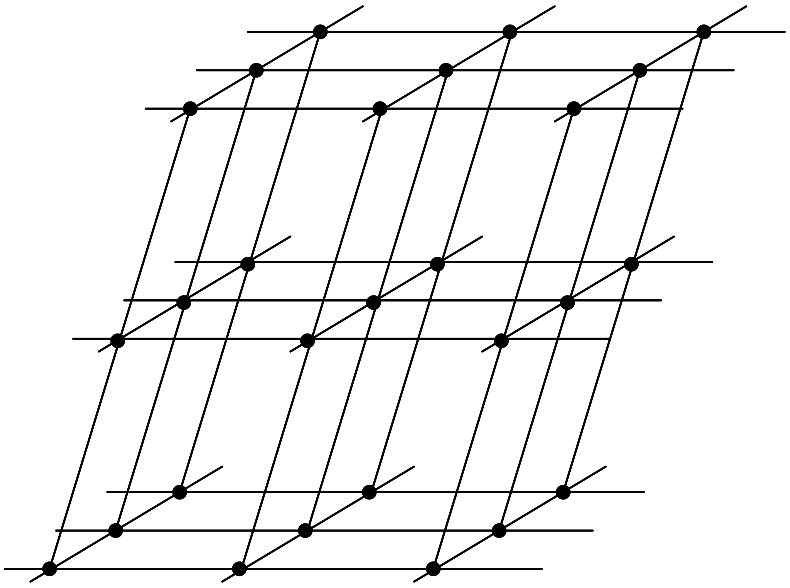

(a)

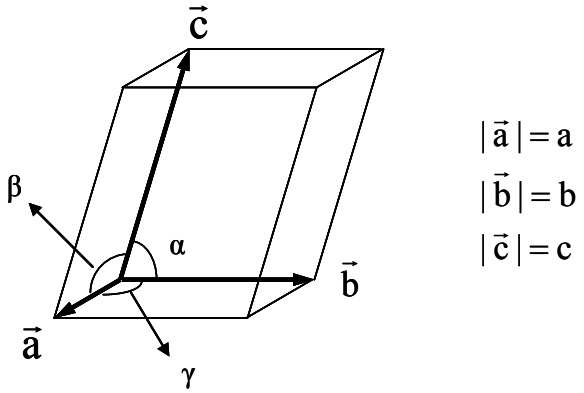

(b)

Figure 2-1. (a) Three-dimensional lattice with lattice points represented by the solid circles and (b) a unit cell with cell dimensions

Table 2-1. Seven crystal systems

Crystal System	Axial lengths and angles
Cubic	$a = b = c$
	$\alpha = \beta = \gamma = 90°$
Tetragonal	$a = b \neq c$
	$\alpha = \beta = \gamma = 90°$
Orthorhombic	$a \neq b \neq c$
	$\alpha = \beta = \gamma = 90°$
Rhombohedral (Trigonal)	$a = b = c$
	$\alpha = \beta = \gamma \neq 90°$
Hexagonal	$a = b \neq c$
	$\alpha = \beta = 90°, \gamma = 120°$
Monoclinic	$a \neq b \neq c$
	$\alpha = \gamma = 90° \neq \beta$
Triclinic	$a \neq b \neq c$
	$\alpha \neq \beta \neq \gamma \neq 90°$

2.1.2 Space groups

Seven different point lattices can be obtained simply by putting points at the corners of the unit cells of the seven crystal systems. However, there are more possible arrangements of points which do not violate the requirements of a lattice. The French crystallographer, Bravais, worked on this subject and in 1848 demonstrated that there are fourteen possible point lattices as shown in Figure 2-2. This result is commemorated by the use of the term Bravais lattice. The fourteen Bravais lattices are the result of combining the seven crystal systems and centered points.

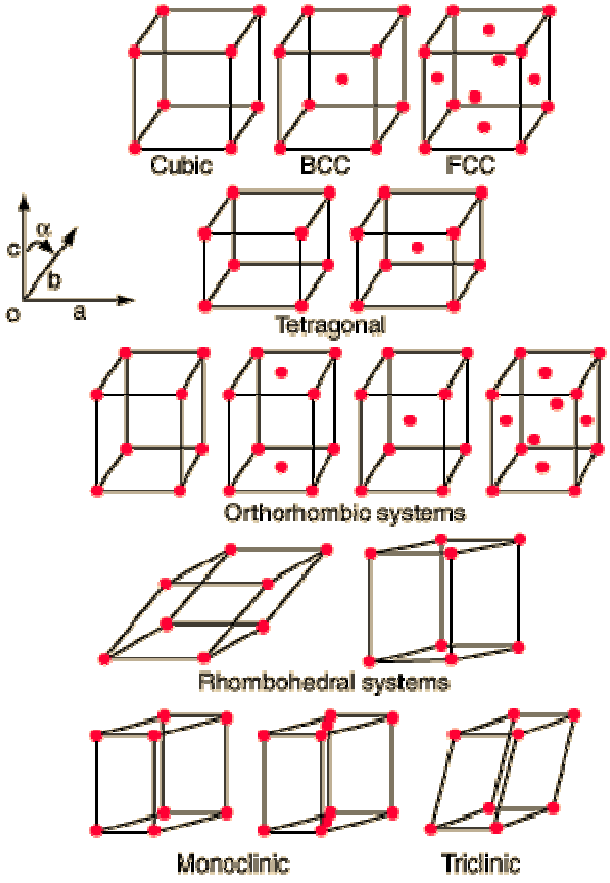

Figure 2-2. The fourteen Bravais lattices: BCC and FCC stand for Body-Centered Cubic and Face-Centered Cubic, respectively.

Symmetry operations are divided into two categories: *macroscopic* and *microscopic operations*. *Macroscopic operations* can be deduced from the arrangement of well-developed crystal faces without any knowledge of the atomic arrangement inside the crystals while *microscopic operations* depend on atomic arrangement. The atom's presence cannot be inferred from the external development of the crystal. Reflection, rotation, inversion and rotation-inversion are included in *macroscopic operations* and glide planes and screw axes belong to *microscopic operations*. The combination of macroscopic operations with the seven crystal systems leads to 32 possible groups and they are called 32 point groups. Finally, microscopic symmetry operations to describe how the atoms or molecules in crystals are combined to 32 point groups with 14 Bravis lattices, resulting in 230 combinations called 230 space groups. Figure 2-3 shows the relationship between the 7 crystal systems, 14 Bravais lattices, 32 point groups, and 230 space groups.

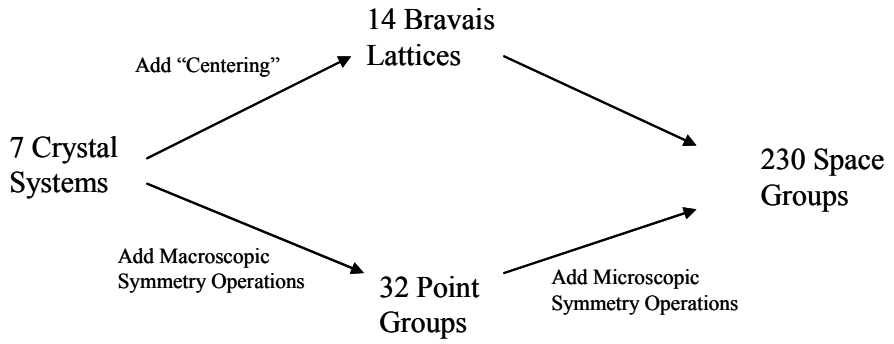

Figure 2-3. Schematic diagram of the relationship between the 7 crystal systems, 14 Bravais lattices, 32 point groups, and 230 space groups

2.1.3 Plane spacings

X-rays were discovered in 1895 by the German physicist Röntgen and under von Laue's direction, Friedrich and Knipping conducted experiments to record diffracted beams in 1912. W. L. Bragg analyzed the Laue experiment and was able to express the necessary conditions for diffraction in a considerably simpler mathematical form than that used by von Laue. In Figure 2-4, the relationship between the interplanar spacing and the angle of an incident beam is described by Bragg's equation.

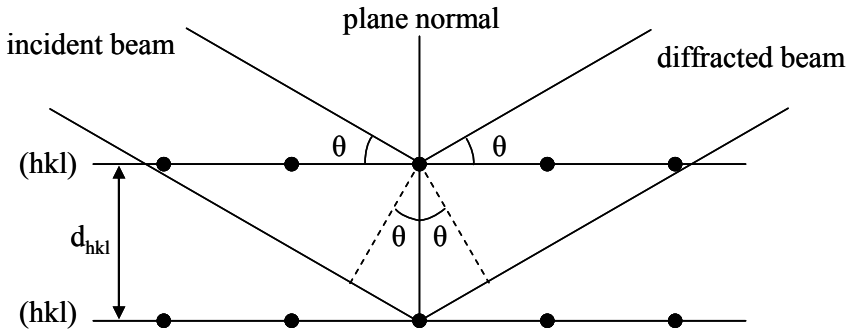

$\lambda = 2\, d_{hkl} \sin\theta$ (Bragg's equation)

Figure 2-4. Bragg's equation representing the relationship between the interplanar spacing of hkl planes and the angle of incidence with Miller index

Bragg's equation gives an easy way to understand powder X-ray diffraction pattern. Powder X-ray diffraction data collected on crystalline samples has information such as peak intensities and peak positions. Peak intensities are determined by the contents of unit cells and peak positions are closely related to the cell constants. Interplanar spacing is a function of Miller indices and cell constants. Therefore, if the cell constants are known for a crystalline compound, peak positions corresponding to Miller indices can be obtained from the Bragg's equation: the wavelength, λ, is machine-

specific. The determination of cell parameters in structure determination of powder X-ray diffraction pattern is a reverse process to find cell constants from peak positions. Here, note that cell constants for a unit cell are not affected by contents in the unit cell. Contents in the unit cell have effects on the peak intensities.

2.2 POLYMORPHISM AND PSEUDOPOLYMORPHISM

Many organic and inorganic pharmaceutical compounds can crystallize in two or more solid forms that have the same chemical composition. This phenomenon is termed polymorphism. Polymorphs have different relative intermolecular and/or interatomic distances as well as unit cells, resulting in different physical and chemical properties such as density, solubility, dissolution rate, bioavailability, etc. Solvates are crystalline solid adducts containing solvent molecules in the crystal lattice structure. When the incorporated solvent is water, the crystalline adducts are called hydrates. Incorporation of solvents in the lattice structure results in changes in physical and chemical properties of solvates. Since property changes by solvent-incorporation are analogous to polymorphism, the phenomenon of crystal solid adducts that possess solvents is called pseudopolymorphism. Note that each pseudopolymorph may have polymorphs also. In the present study, since anhydrous and hydrated forms of sodium naproxen are used, pseudopolymorphs of sodium naproxen mean hydrated forms of sodium naproxen, including the anhydrous species.

2.2.1 Types of polymorphism

The capability of forming different crystal lattices can be described through two mechanisms: *packing polymorphism* and *conformational polymorphism*.[13]

Packing polymorphism represents formation of different crystal lattices of conformationally relatively rigid molecules that can be rearranged stably into different three-dimensional structures through different intermolecular mechanisms. For example, *p*-nitrophenol has two polymorphs.[14] Different modes of intermolecular hydrogen bonding as shown in Figure 2-5 lead to the formation of the two structures. A detailed analysis of the charge density of the two forms indicates charge migration from the benzene ring region to the nitro and hydroxyl groups that accompanies the transformation of one form into the other. In addition, polarization of the oxygen lone-pair electrons was found to be substantially larger in the crystal forms than in the free molecule, resulting in considerably larger dipole moments in the solid state.

The four polymorphs of sulfathiazole in Figure 2-6 were analyzed to identify differences and similarities in molecular and structural features.[15] Graph set analysis was utilized to define the hydrogen bonding motif in the four crystal structures. Possible links between the observed patterns of hydrogen bonding, processes of nucleation, and the crystal growth observed from a number of solvent systems were deduced from their study.

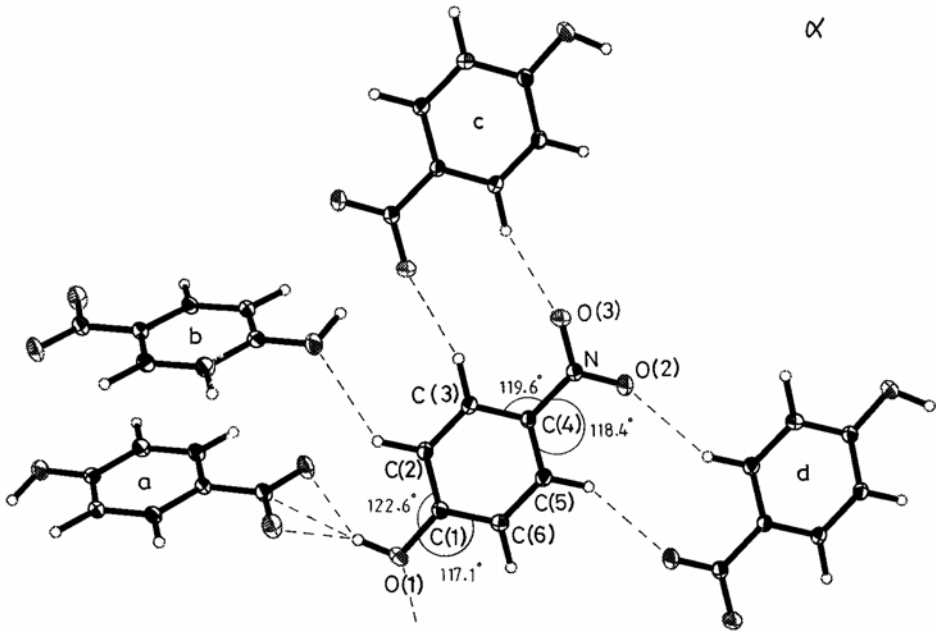

(a)

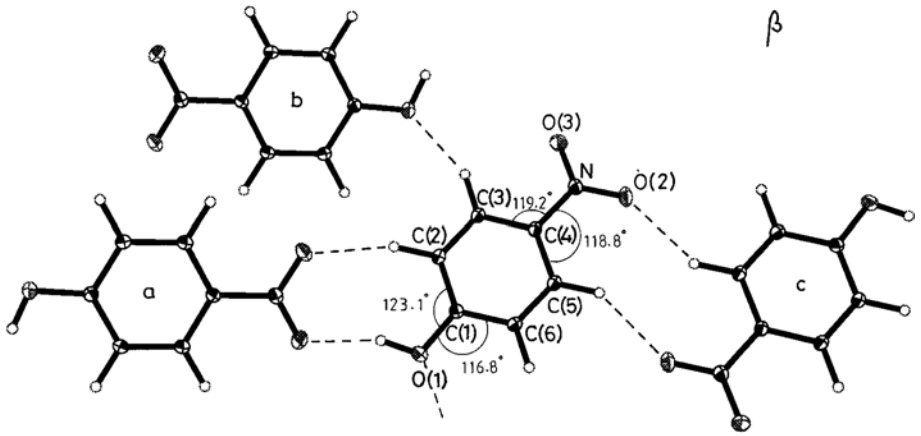

(b)

Figure 2-5. Molecular packing diagrams of the (a) α polymorph and (b) β polymorph of *p*-nitrophenol.

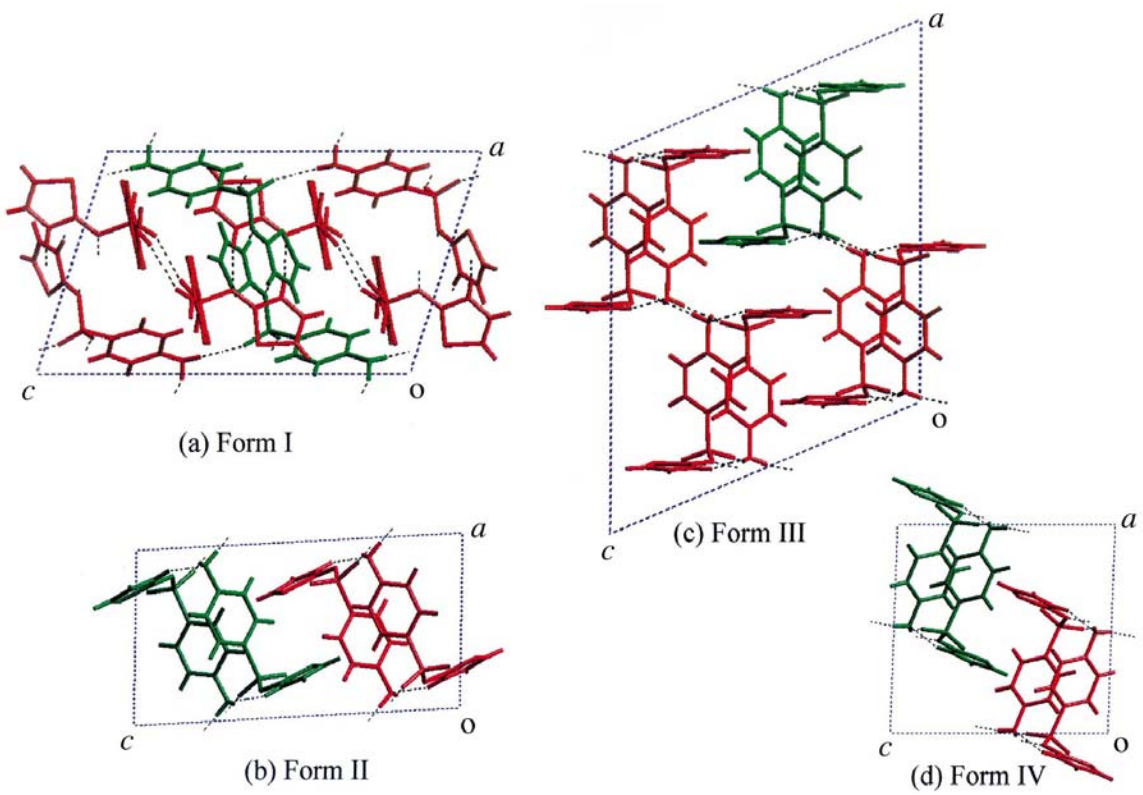

Figure 2-6. Unit cells of (a) Form I, (b) Form II, (c) Form III, (d) Form IV of sulfathiazole showing hydrogen bonds with dimer structure highlighted in green

When a nonconformationally rigid molecule can be folded into alternative crystal structures the polymorphism is categorized as conformational polymorphism. Studies of the conformational polymorphism of the two forms of piroxicam has shown that polymorph 1 has one molecule (Figure 2-7a) in the asymmetric unit and polymorph 2 has two independent molecules, A and B (Figure 2-7b).[16] The most significant difference in three molecules in Figure 2-7 is the torsion angles around the bonds C(4)–O(14) and C(3)–C(21): 100.6(7)° and –139.6(6)° for the molecule in polymorph 1, –88.0(1)° and 17.0(1)° for the molecule A, 96(1)° and -103.0(1)° for the molecule B. The intermolecular hydrogen bond in polymorph 1 involves the amido nitrogen atom as donor and the pyridine nitrogen atom as acceptor. Two centrosymmetrically related $N(23)-H\cdots N(29)$ hydrogen bonds maintain the dimer structure. Independent A and B molecules in polymorph 2 are located in distinct areas where different hydrogen bonding arrangements occur within the areas.

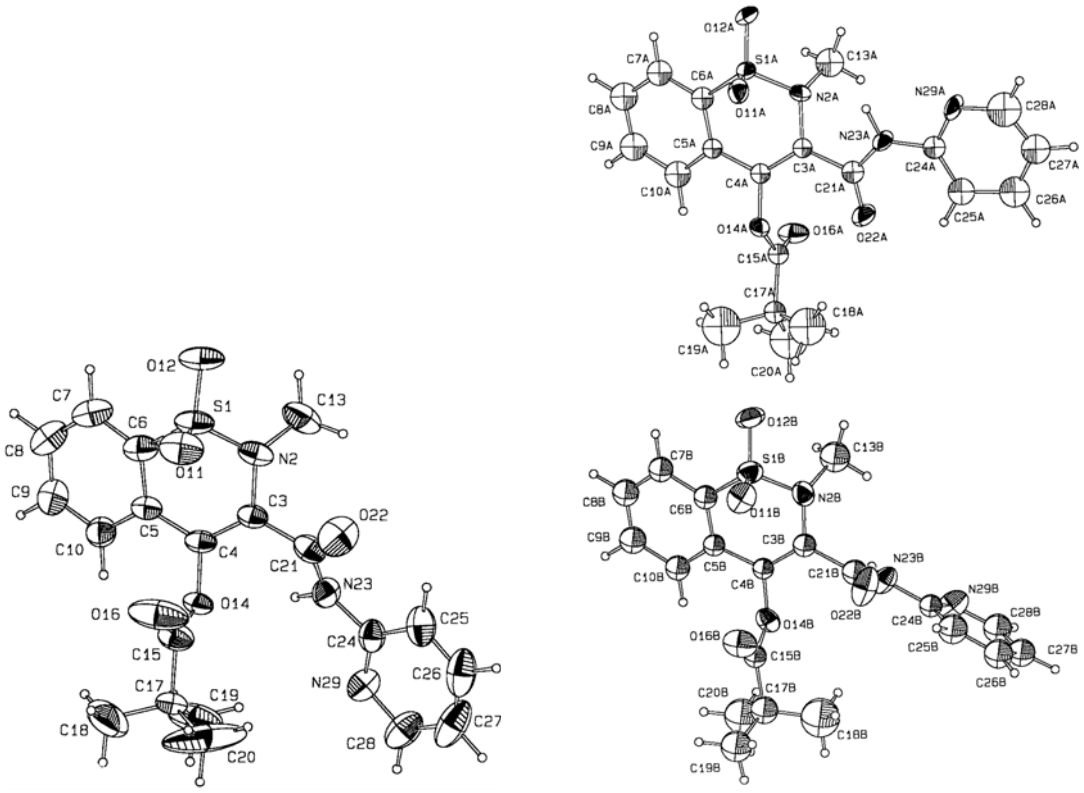

(a) (b)

Figure 2-7. Molecular conformation in (a) polymorph 1 and (b) polymorph 2 of piroxicam pivalate

2.2.2 Classification of hydrates

Crystalline hydrates have been classified by structural aspects into three classes: *isolated lattice sites*, *lattice channels* and *metal-ion coordinated water*.[2] These three classes are discernible by the commonly available analytical techniques.

Hydrates, which belong to the first class, *isolated lattice sites*, represent the structures with water molecules that are isolated and kept from contacting other water molecules directly in the lattice structure. Therefore, water molecules exposed to the surface of crystals may be easily lost. However, the creation of holes that were occupied by the water molecules on the surface of crystals does not provide access for water molecules inside the crystal lattice. The analyses by TGA and DSC for the hydrates in this class show sharp endotherms. Cephradine dihydrate[3] is an example of this class of hydrates.

The second class includes hydrates that have water molecules in channels. The water molecules in this class lie continuously next to the other water molecules, forming channels through the crystal. The TGA and DSC data show interesting characteristics of channel hydrate dehydration. Early onset temperature of dehydration is expected and broad dehydration is also characteristic for the channel hydrates. This is because the dehydration begins from the ends of channels that are open to the surface of crystals. Then, dehydration keeps on happening until all water molecules are removed through the channels. Ampicillin trihydrate[17] belongs to this class. Some hydrates have water molecules in two-dimensional space and they are called planar hydrates.

The third class is a category to which ion-associated hydrates belong. Hydrates contain metal-ion coordinated water and the interaction between the metal ions and water

molecules is the major force in the structure of crystalline hydrates. The metal–water interactions may be quite strong relative to the other non-bonded interactions and, therefore, dehydration occurs at very high temperatures.[18] In TGA and DSC thermograms, very sharp peaks corresponding to dehydration of water bonded with metal ions are expected at high temperatures.

2.2.3 Behavior of solubilities

Polymorphs and pseudopolymorphs can be also classified as either monotropes or enantiotropes, depending upon whether or not one form can transform reversibly to another.[19] In a monotropic system, as shown in Figure 2-8a, Form I can not transform to Form II because the transition temperature cannot appear before the melting temperature. For indomethacin, such a relationship exists between Forms I and II, and Form II and Form III. In Figure 2-8b, Form II is stable over a temperature range below the transition temperature at which two solubility curves meet and Form I is stable above the transition temperature. At the transition temperature, reversible transformation between two forms happens. Figure 2-8c shows the kinetic effects on thermodynamic property of solubility. If initial concentration is represented by X in Figure 2-8c and crystallization is carried out it would not be unusual that Form I, which is metastable, crystallizes out first from the solution. This is due to Oswald's law of stages.[a]

[a] "As unstable system does not necessarily transform directly into the most stable state, but into one which most closely resembles its own, i.e. into another transient state whose formation from the original is accompanies by the smallest loss of free energy."20. Ostwald, W., Studdien über die Bildung und Umwandlung fester Körper. *Zeitschrift für Physikalische Chemie* **1897,** 22, 289-330.

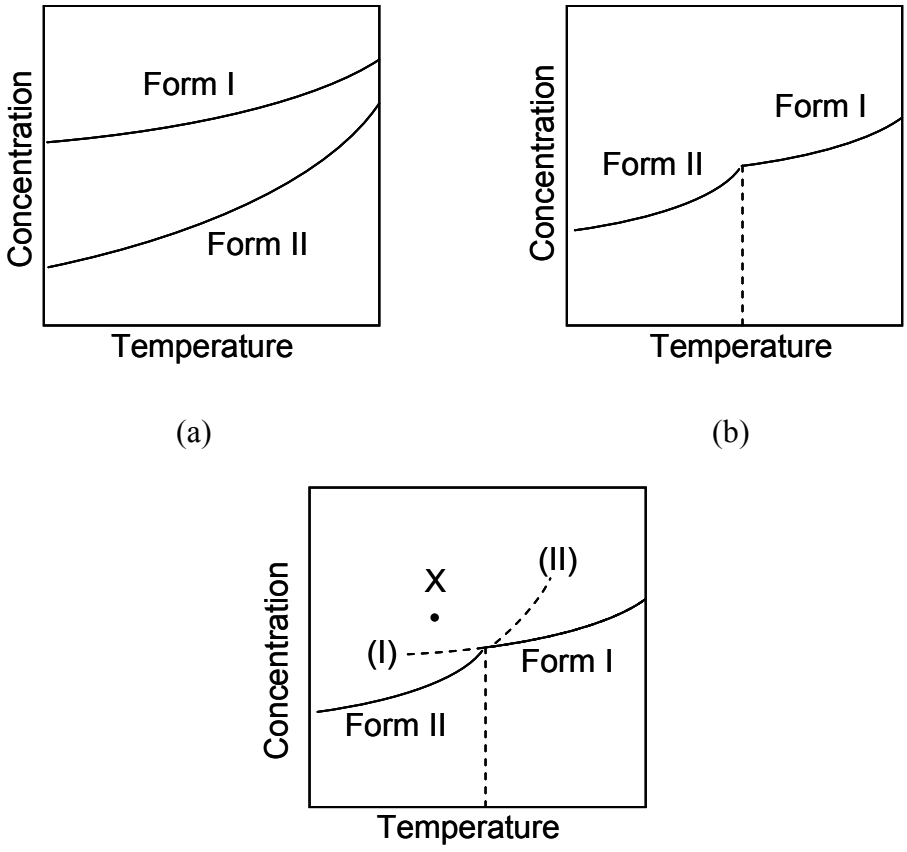

Figure 2-8. Solubility curves exhibiting (a) monotropy, (b) enantiotropy, and (c) enantiotropy with metastable phases [19]

When the decision on whether two polymorphs are enantiotropes or monotropes need to be made it is very useful to use the thermodynamic rules developed by Burger and Ramberger and tabulated in Table 2-2: the heat of transition rule, the heat of fusion rule, the infrared rule, and the density rule. Note that last two rules are significantly less reliable than the others.[21]

Table 2-2. Thermodynamic rules for polymorphic transitions, where Form I is the higher-melting form

Enantiotropy	Monotropy
Transition < melting I	Transition > melting I
I Stable > transition II Stable < transition	I always stable
Transition reversible	Transition irreversible
Solubility I higher < transition Solubility II higher > transition	Solubility I always lower than II
Transition II → I is endothermic	Transition II → I is exothermic
The heat of fusion of I < the heat of fusion of II	The heat of fusion of I > the heat of fusion of II

The stability of polymorphs is thermodynamically related to their free energy.[22] The more stable polymorph has the lower free energy at a given temperature. For the more stable form I,

$$G_I = H_I - TS_I \tag{2-2}$$

where G is the free energy, H is enthalpy, T is temperature and S is entropy. For the less stable form II,

$$G_{II} = H_{II} - TS_{II} \tag{2-3}$$

A fluid phase, which may be either the pure hypothetical supercooled liquid or even the gas or vapor phase, is taken as the standard state of a solid.[23] Since each of these standard states represents complete breakdown of the various crystalline forms, it will be independent of crystalline form and the free energy for the standard state is:

$$G^\circ = H^\circ - TS^\circ \tag{2-4}$$

Subtracting Equation 2-4 from Equation 2-2 for constant temperature T yields the following equations:

$$G_I - G^\circ = H_I - H^\circ - T(S_I - S^\circ) \tag{2-5}$$

$$\Delta G_I^\circ = \Delta H_I^\circ - T\Delta S_I^\circ \tag{2-6}$$

$$\Delta G_I^\circ = RT \ln(a_I / 1) \tag{2-7}$$

where a is activity. Similar equations are derived by using Equations 2-3 and 2-4:

$$G_{II} - G^\circ = H_{II} - H^\circ - T(S_{II} - S^\circ) \tag{2-8}$$

$$\Delta G_{II}^\circ = \Delta H_{II}^\circ - T\Delta S_{II}^\circ \tag{2-9}$$

$$= RT \ln(a_{II} / 1) \tag{2-10}$$

Subtracting Equation 2-7 from Equation 2-10 gives:

$$G_{II} - G_I = RT \ln(a_{II} / a_I) \tag{2-11}$$

Since polymorph II is less stable than polymorph I and, consequently, G_{II} is greater than G_I

$$a_{II} > a_I \tag{2-12}$$

and since activity and concentration are related by assumption that activity coefficients of two polymorphs are approximately identical,

$$x_{II} > x_I \tag{2-13}$$

where x is concentration. From Equation 2-13, the less stable polymorph II above the transition temperature in Figure 2-8c has higher solubility at constant temperature.

2.3 STRUCTURAL THEORY OF POLYMORPHISM

The classification of polymorphic substances into monotropic and enantiotropic classes from the view of the lattice theory is not appropriate. A more basic question to researchers in the lattice theory is whether or not the crystal lattice structures of polymorphs are related. At a transition point with the temperature and the pressure fixed, it is possible for interconversion to happen between two polymorphs only in the case that the structures of the polymorphs are related. If complete rearrangement is required by atoms or molecules during transformation, no point of contact for reversible interconversion exists. Therefore, the existence of enantiotropes or monotropes in thermodynamics and phase theory is corresponding to related or unrelated lattice structures in structural theory.[24]

Transformation between polymorphs that have completely different lattice structures exhibits the dramatic changes in properties. The difference in energy between polymorphs is not always considerable as shown with diamond/graphite. In most cases, polymorphs in this category are required to break bonds and rearrange atoms or molecules and, consequently, the polymorphs have a monotropic relation.

For the study of polymorphs that are structurally related, three issues should be dealt with. First, structural relationships between the polymorphs should be established. Second, it should be explained why a particular substance is able to arrange its structural units in two closely related lattices. Third is a description of the manner and conditions under which rearrangement of the units from one lattice type to another can happen.

2.4 MOLECULAR MODELING SOFTWARE

Cerius^2 is a computational modeling software package made by Accelrys Software Incorporated. It is based on UNIX workstations, providing powder tools for application in life and materials science modeling and simulation. The software has several modules to define the system, calculate energy components, determine thermodynamic properties, and minimize the potential energy of the system. The software uses graphic user interface and displays the system graphically in the model window.

The modules of interest in Cerius^2 software for the present study were *Crystal Builder*, *Open Force Field*, *Charges* and *Energy Minimizer*.

2.4.1 Crystal builder

The first step in molecular modeling is to define the model to be studied. If the model is available in CIF or PDB formats, it can be directly loaded into the software. However, information available is fractional atomic coordinates and cell constants including space group in many cases. The main function of the *Crystal Builder* is to input those data and display the model in the model window. Another important function of the *Crystal Builder* is to generate crystalline superlattice structure. Equivalent molecules by symmetry in the unit cell become independent molecules, leading to the space group of P1.

2.4.2 Open force field

Energy calculations require force fields including bonded and non-bonded interactions between atoms of the present model. The force fields is a parameter file specifying which particular equations and parameter settings are to be used for every valence and non-bonded interactions. The energy of the model structure can be expressed as a superposition of the two-body, three-body, and four-body interaction expressions defined by the force field. The superposition of N-body system in terms of such a superposition is called the energy expression.

The potential energy of the model is expressed by summation of valence terms and non-bonded interactions.

$$E_{total} = E_{valence} + E_{non-bonded} \tag{2-14}$$

where valence terms describe the interactions between bonded atoms of the molecules and non-bonded terms describe interactions between atoms which are not necessarily bonded to one another.

The valence terms are also superposition of bond stretching (E_{bond}), angle bending (E_{angle}), molecular torsions ($E_{torsion}$) and molecular inversions ($E_{inversion}$) as follows:

$$E_{valence} = E_{bond} + E_{angle} + E_{torsion} + E_{inversion} \tag{2-15}$$

Bond stretching is expressed either as a simple harmonic oscillator

$$E_{bond} = \frac{1}{2} k_b (R - R_e)^2 \tag{2-16}$$

or as the Morse function

$$E_{bond} = D_b [e^{-\alpha(R-R_e)} - 1]^2 \tag{2-17}$$

where R and R_e are a distance between atoms and an equilibrium bond distance between two atoms involved with the bond, respectively, k_b is a force constant, D_b represents a finite energy for breaking the bond and α is Morse scale factor. The Morse function leads to nearly zero forces for very large R and the harmonic function results in increasingly large restoring forces as R is increased from R_e. k_b can be written from Equation 2-16 as

$$k_b = \left(\frac{\delta^2 E_{bond}}{\delta R^2} \right)_{R=R_e} \tag{2-18}$$

and combining Equations 2-17 and 2-18 leads to

$$\alpha = \left(\frac{k_b}{2D_b} \right)^{1/2} . \tag{2-19}$$

The angle bending has two simple expressions,

$$E_{angle} = \frac{1}{2} k_a (\cos\theta - \cos\theta_e)^2 \tag{2-20}$$

and

$$E_{angle} = \frac{1}{2} C_a (\theta - \theta_e)^2 \tag{2-21}$$

where θ and θ_e are an angle between two bonds and an equilibrium angle and k_a is a force constant for cosine θ expansions and C_a is a force constant for θ expansions. Two force constants are related by

$$C_a = \frac{k_a}{(\sin\theta_e)^2} . \tag{2-22}$$

The torsion interaction for two bonds IJ and KL connected via a common bond JK is taken of the form

$$E_{torsion} = \frac{1}{2} k_t [1 - n_t \cos(\varphi - \varphi_e)]^2 \tag{2-23}$$

where φ and φ_e are a dihedral angle and an equilibrium dihedral angle, respectively, k_t is a force constant for torsion interaction and n_t is the phase factor which can be +1 or -1. Dihedral angle is defined in Figure 2-9.

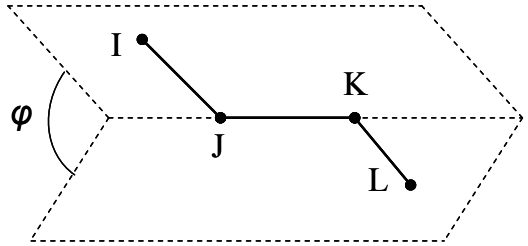

Figure 2-9. Dihedral angle

The last term of valence terms is planar inversion for an atom I bonded to exactly three other atoms, J, K and L. It describes how difficult it is to force all three bonds into the same plane (inversion) or how favorable it is to keep the bonds in the same plane. Inversion term is expressed by the form

$$E_{inversion} = \frac{1}{2} k_i \chi^2 \tag{2-24}$$

where k_i is the force constant and χ is the improper torsion which is depicted in Figure 2-10.

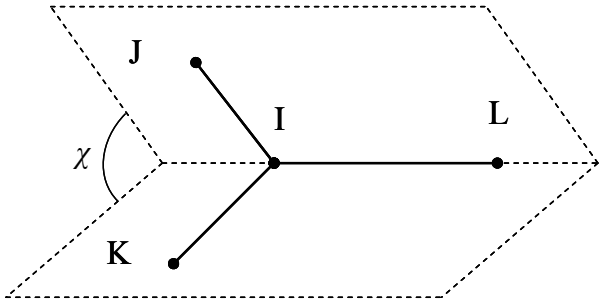

Figure 2-10. Improper torsion angle

The non-bonded interaction term in Equation 2-14 is summation of electrostatic force (E_{elec}) and van der Waals force (E_{vdW}).

$$E_{non-bonded} = E_{elec} + E_{vdW} \tag{2-25}$$

Electrostatic force accounts for the atomic interactions due to charge differences between atoms. Attractive or repulsive forces may be exerted on the atoms depending on the partial charges of each atom. Generally, electrostatic force is considered stronger than van der Waals force. Electrostatic force is calculated using

$$E_{elec} = C_0 \frac{q_1 q_2}{\varepsilon_{elec} R} \tag{2-26}$$

where C_0 is Coulomb force constant, ε_{elec} is dielectric constant and q_1 and q_2 are charges of atom 1 and 2.

Two atoms at a long distance exhibit attraction forces and, at close distances, repulsion forces are also exerted on the atoms. This continuous attraction-repulsion force is described accurately by the van der Waals force which is expressed by the Lennard-Jones 12-6 potential shown in Equation 2-27.

$$E_{vdW} = 4\,\varepsilon_{vdW}\left[\left(\frac{\sigma}{R}\right)^{12} - \left(\frac{\sigma}{R}\right)^{6}\right] \tag{2-27}$$

where σ , which is called size parameter, is the depth of the van der Waals potential well and ε_{vdW} ,which is called energy parameter, is the separation distance at which the van der Waals potential is zero. Equation 2-27 can be rearranged with size parameter, R^*, which is the distance at which the van der Waals potential is the minimum.

$$E_{vdW} = \varepsilon_{vdW}\left[\left(\frac{R^*}{R}\right)^{12} - 2\left(\frac{R^*}{R}\right)^{6}\right] \tag{2-28}$$

Sometimes, most simple form of the Lennard-Jones potential can be used instead of Equations 2-27 and 28.

$$E_{vdW} = \frac{A}{R^{12}} - \frac{B}{R^6} \tag{2-29}$$

with definition of A and B as follows

$$A = 4\varepsilon_{vdW}\sigma^{12} = \varepsilon_{vdW}\left(R^*\right)^{12} \tag{2-30}$$

and

$$B = 4\varepsilon_{vdW}\sigma^{6} = 2\varepsilon_{vdW}\left(R^*\right)^{6}. \tag{2-31}$$

Van der Waals interaction and variables in Equations 2-27 and 28 are depicted in Figure 2-11.

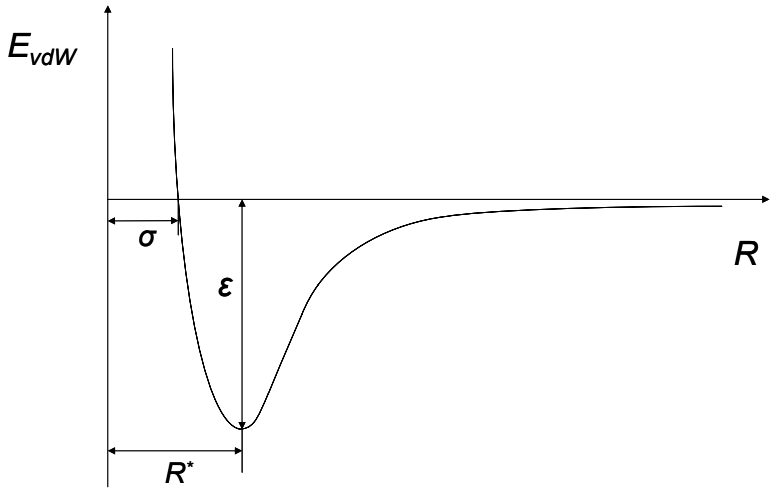

Figure 2-11. Van der Waals interation

2.4.3 Charges

The difficulty in using Equation 2-26 is how to determine partial charges of each atom. Charges for small molecules have been possibly fit to the electrostatic potentials calculated from high-quality Hartree-Fock wave functions.[25] For large molecules, a

method for predicting accurate charges is desperately needed. In the present study, Gasteiger method[26] was used for charge-assignment.

Gasteiger partial charges are assigned by two stages. In the first stage, seed charges are assigned to each atom in the molecule. For example, carboxylate oxygen atoms are each assigned the value of -0.5. In the second stage, these initial charges are shared across bonds, moving a certain amount of charge from one atom to another. The partial charge moved and its direction are determined by difference in electronegativities of the atoms on each end of the bond. The relaxation algorithm is then iterated several times, attenuating the charge moved with each iteration.

Electronegativity of an atom was defined by Mulliken.[27]

$$\chi_{iv} = \frac{1}{2}\left(I_{iv} + E_{iv}\right) \tag{2-32}$$

where I_{iv} and E_{iv} are the ionization potential and the electron affinity of atom i, respectively. The orbital electronegativity of the molecular depends on the hybrid state and partial charge, Q, of i.

$$\chi_{iv} = a_{iv} + b_{iv}Q_i + c_{iv}Q_i^2 \tag{2-33}$$

and

$$a_{iv} = \frac{I_{iv}^0 + E_{iv}^0}{2} \tag{2-34}$$

$$b_{iv} = \frac{I_{iv}^+ + E_{iv}^+ - E_{iv}^0}{4} \tag{2-35}$$

$$c_{iv} = \frac{I_{iv}^+ - 2I_{iv}^0 + E_{iv}^+ - E_{iv}^0}{4} \tag{2-36}$$

where superscripts 0 and + represent the neutral atom and the positive ion, respectively. Total partial charge for *i* is the summation of the contribution, $q_i^{<\alpha>}$ of the atomic charge on α-th iteration.

$$Q_i = \sum_{\alpha} q_i^{<\alpha>} \tag{2-37}$$

$$q_i^{<\alpha>} = \left(\frac{1}{2}\right)^{\alpha} \left[\sum_j \frac{\chi_{j\mu}^{<\alpha>} - \chi_{i\nu}^{<\alpha>}}{\chi_{i\nu}^{+}} + \sum_k \frac{\chi_{k\lambda}^{<\alpha>} - \chi_{i\nu}^{<\alpha>}}{\chi_{i\nu}^{+}} \right] \tag{2-38}$$

where *j* and *k* are dummy variables for the summation.

2.4.4 Energy minimizer

Energy expression is a mathematical equation which has physical meanings based on force fields. Minimum energy state of a model is determined by the condition which can be obtained from the minimum of the mathematical equation. That is, minimum energy state is determined by minimizing the energy expression.

Energy Minimizer module has several minimization algorithms such as steepest descent method, quasi-Newton method, truncated Newton method and conjugate gradient method. In a steepest descent method, the "best direction" and the "best value" along the search direction should be determined from an initial value. The best direction is determined by the gradient direction expressed as

$$x_{\alpha+1} = x_\alpha + h \nabla f(x_\alpha) \tag{2-39}$$

where x_α is a vector of variables on α-th iteration, *f* is a function and *h* is the best value along the search direction.[28] When an arbitrary step size *h* is used this method is called steepest descent method. If a maximum value to reach the minimum position along the search direction is used the method is called the optimal steepest ascent.

In a Newton method, Hessian matrix is employed to determine the distance along the search direction.

$$x_{\alpha+1} = x_\alpha - H_\alpha^{-1} \nabla f(x_\alpha) \tag{2-40}$$

and Hessian matrix, H, is defined for a function, f, of two variables, x and y, as follows.

$$H = \begin{bmatrix} \dfrac{\partial^2 f}{\partial x^2} & \dfrac{\partial^2 f}{\partial x \partial y} \\ \dfrac{\partial^2 f}{\partial x \partial y} & \dfrac{\partial^2 f}{\partial y^2} \end{bmatrix} \tag{2-41}$$

However, Hessian matrix is composed of the second derivatives of f that vary from step to step.[28] Quasi-Newton method attempts to avoid these difficulties by approximating H with another matrix using only first partial derivatives of f.

Searching direction on α-th iteration, s_α, in conjugate gradient method, is calculated by the equation:

$$s_\alpha = -\nabla f(x_\alpha) + \left[\frac{\nabla f(x_\alpha)^T \nabla f(x_\alpha)}{\nabla f(x_{\alpha-1})^T \nabla f(x_{\alpha-1})} \right] s_{\alpha-1} \tag{2-42}$$

and

$$s_0 = -\nabla f(x_0)\,. \tag{2-43}$$

Unlike a Newton method which requires the second derivatives of f in Hessian matrix, a conjugate gradient method uses only the first derivative and improves the searching direction by storing information from the previous iteration.[29]

Default setting in *Energy Minimizer* is "Smart Minimizer". The minimizer begins with a steepest descent method, followed by a quasi-Newton method, and finishes with a truncated Newton method which is a variation of the Newton method.

2.5 NAPROXEN/SODIUM NAPROXEN

Naproxen[a] is a member of the non-steroidal anti-inflammatory drug (NSAIDs) family. NSAIDs reduce inflammation (swelling), pain, and temperature. Naproxen is used to treat mild to moderate pain, osteoarthritis, rheumatoid arthritis, ankylosing spondylitis, primary dysmenorrheal, tendonitis, bursitis, and other conditions. Naproxen and sodium naproxen are available in prescription strength; naproxen sodium is also available in nonprescription strength.

The first large-scale synthesis of naproxen produced 500 kg of material in 1970.[30] Friedel-Crafts acylation of 2-methoxynaphthalene (nerolin) produced 2-acetyl-6-methoxynaphthalene, which was converted to a naphthylacetic acid by the Willgerodt reaction. α-Methylation yields the d,l-acid, which can be efficiently resolved using cinchonidine. Naproxen was introduced to the market by Syntex in 1976.[31]

There are three general approaches to producing an optically active compound: (1) use of the chiral pool, (2) separation of racemates (classical resolution, direct crystallization, kinetic resolution using an enzyme), and (3) asymmetric synthesis. One of the examples of manufacturing using chiral pool is the process to produce the top-selling ACE inhibitors, enalapril, captopril, and lisinopril, which are all derived from L-proline.[32] Technology which is employing separation of racemates was applied to optically pure (S)-ibuprofen.[32] The several asymmetric technologies were designed for naproxen manufacture such as Zambon process.[33]

[a] (S)-(+)-6-Methoxy-α-methyl-2-naphthaleneacetic acid

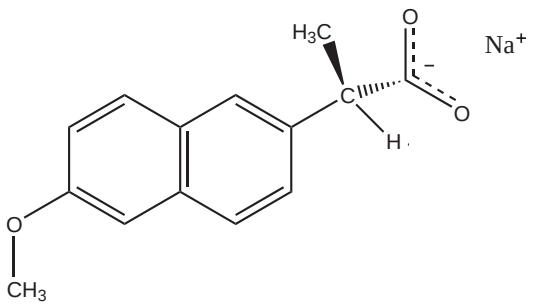

Figure 2-12. Schematic diagram of (S)-(+)-sodium naproxen

The sodium salt of naproxen shown in Figure 2-12 has much higher solubility in water than its acid free form. This property has given rise to its production by many pharmaceutical markets. A conventional process used for the production of sodium naproxen involves reacting naproxen dissolved in toluene with an aqueous sodium hydroxide solution, with subsequent removal of water. The resulting compound is anhydrous sodium naproxen with an average particle size in the range of about 30 to 70μm. The form of crystals of the compound is small needle-like particles having an aspect ratio of about 10.

Development of a process to produce crystals significantly larger than about 70 μm was a major improvement to the product.[9] The improved process forms concurrently or in any sequence a solids-free liquid mixture from (i) naproxen having a chiral purity of at least about 82 %, but below 98 %, (ii) water, (iii) at least one water-soluble inorganic basic sodium compound in an amount proportioned to neutralize from about 50 to 97 % of acid, and (iv) an organic solvent. Removing water from the mixture leaves the monohydrate of naproxen sodium with an average particle size of at least about 120 μm, and a chiral purity of at least 98 % (S)-enantiomer (Phan, H. V. et al., 1999). Note that the average particle size becomes larger and crystals from the process are monohydrated.

The process of producing larger crystals has the advantage of reducing centrifugation cycle time. Also, product handling is simplified in various operations such as drying, flowing, screening or tableting. The monohydrated compound, however, requires a dehydration process to produce commercially available anhydrous sodium naproxen.

Crystal structures have been determined for naproxen[34] and for monohydrate[11] of sodium naproxen. Study of the conformation of naproxen and the importance of intramolecular hydrogen-bond-like (HBL), e.g. C–H···O–C, interactions identified the four stable conformers for which HBL interactions play an important role.[35] Bansal et al.[36] observed differences in dissolution rates of hydrated tablets obtained by wet granulation from the anhydrous form, and the anhydrate and dihydrate of sodium naproxen have been characterized.[10] The optically pure (S)-(+)-sodium naproxen was used in the present study.

CHAPTER 3

CHARACTERIZATION AND SOLID-STATE TRANSFORMATIONS OF THE PSEUDOPOLYMORPHIC FORMS OF SODIUM NAPROXEN

Pharmaceutical solids may come in contact with water during processing steps, such as crystallization, lyophilization, wet granulation, aqueous film-coating, or spray-drying, and they may be exposed to humid air during storage. Absorbed water molecules may reside on crystal surfaces or in crystal lattice structures, but when the absorbed water enters the lattice structure it can change the packing in the unit cell, resulting in the formation of hydrates.

The anhydrate and dihydrate of sodium naproxen have been characterized.[10] Relatively little work had been done on sodium naproxen monohydrate prior to the current research. Our purpose here is twofold: (1) to characterize the monohydrated form, especially by comparing it to both the anhydrate and the dihydrate, and (2) to determine the energetics associated with dissolution of the anhydrate and transformation of the hydrated sodium naproxen to species of lower degrees of hydration.

3.1 EXPERIMENTAL SECTION

3.1.1 Materials

Naproxen sodium, supplied by Albemarle Corp., was used in experiments without further purification or processing. Cooling recrystallization was used to produce the dihydrated crystalline form of sodium naproxen; 35 g of anhydrous sodium naproxen was dissolved in 100 mL of pure water (HPLC-grade purchased from Fisher Scientific) at 35 ºC. The solution was cooled until recrystallization occurred. The slurry then was heated to 25 ºC and filtered under vacuum, and the resulting filter cake was dried under ambient conditions. The monohydrated form of sodium naproxen was prepared by drying the dihydrate in a desiccator for 2 days. Every sample was analyzed with X-ray powder diffraction to ensure that either the anhydrate or the desired hydrate had been formed.

3.1.2 Thermogravimetric analysis (TGA)

The loss of mass from sodium naproxen samples was analyzed with a TG/DTA 320 instrument (Seiko Instruments Inc.). Samples of mass 10 to 15 mg were heated from 21 ºC to 150 ºC in aluminum pans that were 5 mm in diameter. An empty aluminum pan was used as the reference. A heating rate of 10 ºC/min was employed with a nitrogen purging rate of 90 mL/min. Open pans without lids were used and prominent peaks were observed. All TGA runs were carried out with open pans, as recommended by Di Martino et al.[10]

3.1.3 Differential scanning calorimetry (DSC)

Heat flow from the samples for the dehydration and melting endotherms was measured with a DSC 220C instrument (Seiko Instruments Inc.). The temperature axis and cell constant of the DSC were calibrated with indium. The temperature range of the experiments was from 23 ºC to 290 ºC in aluminum pans that were 7 mm in diameter. DSC runs were performed at a ramping rate of 10 ºC/min under nitrogen purge at a rate of 90 mL/min. Quantitative evaluation of energies associated with phase transformations required the use of open pans in the DSC experiments.[10]

3.1.4 Powder X-ray diffraction (PXRD)

Crystals were analyzed and identified by powder x-ray diffraction (PXRD) analysis using Philips® PW1800 automatic powder diffractometer with APD 3720 analysis software. About 1 to 2 g of crystals was required. Each crystal sample was ground to a fine powder with a mortar and pestle before being pressed into the sample holder. Copper Kα radiation was used. The radiation for Copper Kα1 is 1.54056Å. The PXRD patterns were made over a diffraction-angle (2θ) range of 1.02 to 80˚, with a step size of 0.02 º and a counting time of 1 second per step.

3.1.5 High-Performance liquid chromatography (HPLC)

HPLC (Shimadzu®) was used for the measurement of solution concentration, hence solubility. The chromatographic separation was performed on a reverse-phase column Varian Microsorb-MV 100-3 C18 column. A wavelength of 254 nm was used in the SPD-10AV detector. The voltage signal from the detector was interpreted by the

Shimadzu CLASS-VP Chromatography Data System version 4.2 software program running on a personal computer. Two mobile phases were prepared. One was pure acetonitrile (Acros Organics) and the other was a mixture of 2% acetic acid (Sigma–Aldrich) and 98% water (volume ratio). Each mobile phase was connected to the delivery module of the HPLC. The flow rates from each reservoir were 0.5 mL/min and, totally, 1.0 mL/min. Butyrophenone (Sigma–Aldrich) was dissolved into acetonitrile and used as the internal standard.

3.1.6 Microscopy

Crystal samples were analyzed under the Leica DM LM microscope with the objective lens of 20X. The microscope was equipped with Sony DKC-5000 digital camera that converted the focused light into a digital signal. This signal was visualized by Image-Pro Plus version 4.5.

3.2 RESULTS AND DISCUSSION

3.2.1 Crystallization and hydrate transformation

Crystallization of sodium naproxen from water at the conditions described above produced a dense network of needle-like crystals. Although the mass of crystals prevented subsequent rotation of a magnetic stirrer, the residual mother liquor was easily expressed from the crystal mass during filtration. The crystals were less than 25 μm in thickness and as long as several millimeters. Unfortunately, crystals of this size were unacceptable for single-crystal x-ray diffraction analysis.

Over the range of temperatures examined in the present research, only the dihydrate of sodium naproxen was formed on crystallization from water, which is consistent with earlier work by Di Martino et al.[10] Other known pseudopolymorphs of sodium naproxen can be produced using different protocols. For example, Kim et al.[11] reported that recrystallization from a solvent comprised of pure methanol and the water absorbed from the atmosphere during the evaporation resulted in formation of monohydrated crystals. We were able to obtain anhydrous crystals using the procedure of Kim et al., by immediately coating the recovered crystals with oil, thereby preventing absorption of water from the atmosphere. Phan et al.[9] also reported formation of the monohydrate from a mixture of water and organic solvents. We formed the monohydrated species of sodium naproxen in our experiments by recrystallization from sodium naproxen solutions in a mixture of methanol and water (80:20, volume ratio).

The experimental procedures shown schematically in Figure 3-1 were developed to provide samples of the various hydrated forms of sodium naproxen. As shown, the monohydrate was obtained by placing the dihydrate in a desiccator for about two days at room temperature. Prepared samples of the monohydrate were analyzed with PXRD and compared to the simulated PXRD pattern of the monohydrate. The two are identical, showing that the dried samples from the dihydrate are the same as the samples recrystallized from methanol by Kim et al.[11]

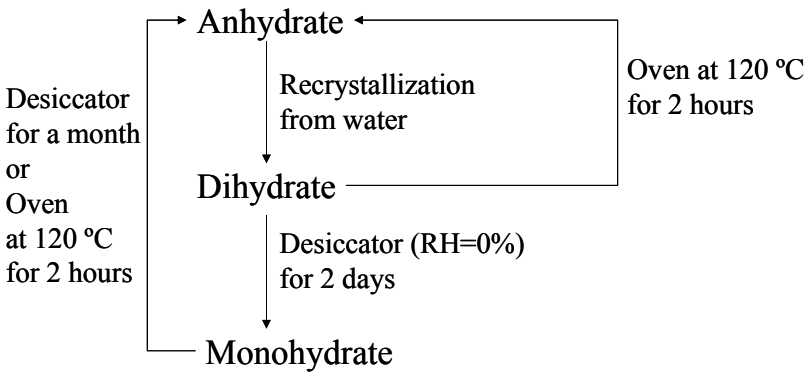

Figure 3-1. The path for the change between pseudopolymorphic forms of sodium naproxen

The anhydrate of sodium naproxen was obtained by heating the dihydrate in an oven at 120ºC for 2 hours or by leaving it in a desiccator for a month. Alternatively, the monohydrate prepared from the dihydrate could be dried in an oven or in a desiccator to produce the anhydrate. The PXRD pattern of the anhydrate obtained in any of these methods was the same as that of the original anhydrous compound obtained from Albemarle. It can be concluded, therefore, that crystallization and subsequent controlled dehydration of the dihydrate can be used to produce any of the three pseudopolymorphic forms.

The powder x-ray diffraction patterns shown in Figure 3-2 were generated for each of the sodium naproxen species under investigation. The peak positions and intensities show differences among the structures of the species, confirming that the three forms are distinct compounds. Obviously, the differences result from the variable water content in the crystal structures.

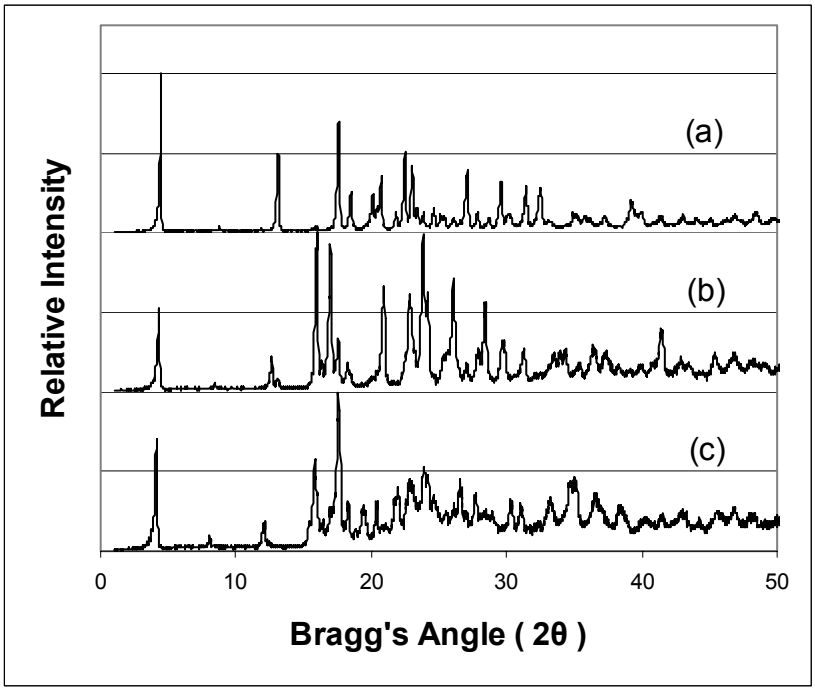

Figure 3-2. Powder X-ray diffraction patterns of three different pseudopolymorphic forms of sodium naproxen; (a) the anhydrate, (b) the monohydrate and (c) the dihydrate

3.2.2 Thermal analysis of the samples

The theoretical water contents of the monohydrate and dihydrate forms of naproxen sodium are 6.666 wt% and 12.499 wt%, respectively. Analysis of the TGA data in Figure 3-3 provided results quite close to the theoretical values: 0.048± 0.012 (mean ±S.D.) wt% for the anhydrate, 6.832 ± 0.286 wt% for the monohydrate, and 12.957 ± 0.655 wt% for the dihydrate.

More detailed analysis of the TGA thermograms in Figure 3-3 shows the existence of two separate dehydration steps for the dihydrate, whereas the monohydrate shows only one. Although the two dehydration steps for the dihydrate were not completely separated, the first corresponds to the removal of water that is not found in the monohydrate, while the second corresponds to that of water that is also found in the monohydrate. Because the nitrogen purge facilitates dehydration, the stabilization of the initial sample weights was carried out without nitrogen purge.

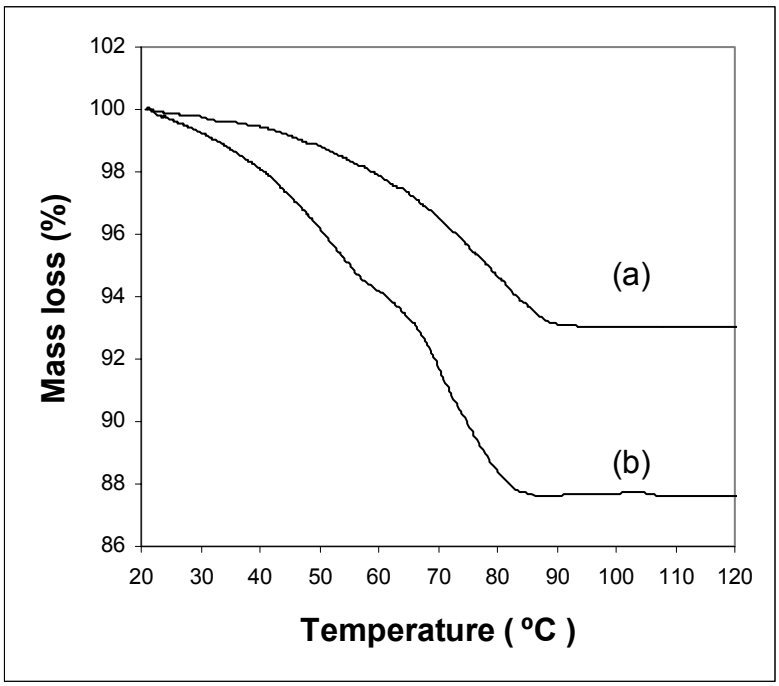

Figure 3-3. TGA curves with nitrogen purge of (a) monohydrated and (b) dihydrated forms of sodium naproxen

Figure 3-4 shows DSC thermograms for the three pseudopolymorphs of sodium naproxen. Table 3-1 gives the estimated energies of the transformations associated with the peaks in Figure 3-4. The anhydrate shows only one endothermic peak, which corresponds to melting. The dihydrate has one peak for melting and two peaks corresponding to removal of two different types of water from the unit cell. The first released water produces the first dehydration endotherm in the DSC thermogram for the dihydrate. This water is easily removed at ambient temperature, and will be discussed below. Because the peaks for the dehydration endotherms are not separated clearly, the endothermic energy for each water molecule removed from the dihydrate could not be determined directly. Therefore, the dehydration energy for the dihydrate in Table 3-1 is the sum of dehydration energies for the first and second released water.

The monohydrate of sodium naproxen exhibits two peaks, one for melting and the other associated with the endotherm for dehydration. The minute peak at about 60 ºC corresponds to an endotherm associated with a slight over-hydration of the monohydrate sample.

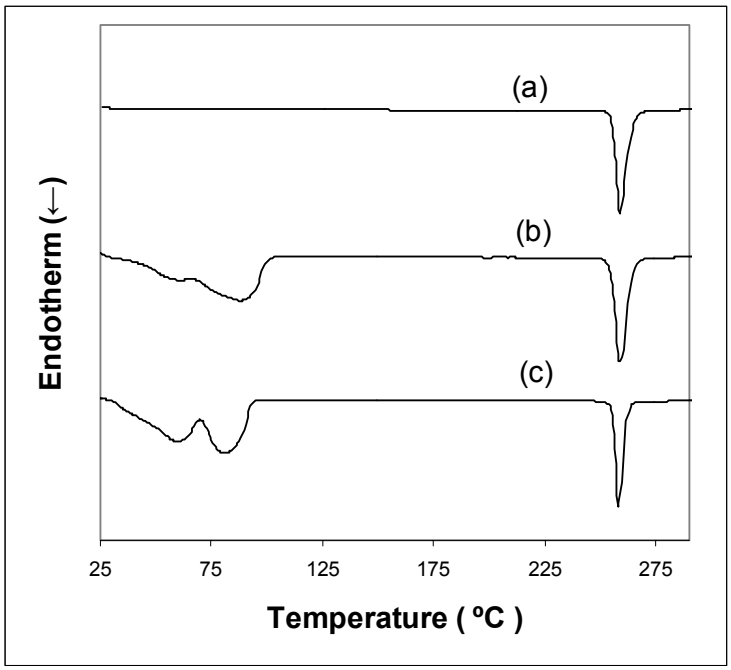

Figure 3-4. Differential scanning calorimetry curves of three different pseudopolymorphic forms of sodium naproxen; (a) the anhydrate, (b) the monohydrate and (c) the dihydrate

The heats of dehydration in Table 3-1 are based on the mass of sample; in other words, 207.3 J/g of the monohydrated species and 376.8 J/g of the dihydrated species. If the anhydrous species is used as the basis, these values become 220.5 and 427.6 J/g of anhydrate, respectively. If we assume that the heat of hydration for the monohydrate is equivalent to that for removal of the second water from the dihydrate, then the heat of dehydration for removal of the first water can be found by difference: 207.1 J/g of anhydrate. Because there is less than 10% difference between the two heats of dehydration, the interactions of the first released water with the atoms that surround it in the crystal structure are energetically similar to those between the second water and its surrounding atoms.

Table 3-1. The temperatures and the endotherms for peaks in DSC

Compound	1st peak Temperature (°C)	2nd peak Temperature (°C)	Heat of Dehydration (J/g sample)	Minimum Temperature (°C)	Melting (°C)	Heat of Fusion (J/g sample)
Anhydrate	–	–	–	258.3 ± 0.2	255.1 ± 0.1	110.7 ± 0.5
Mono-hydrate	86.0 ± 1.5	–	207.3 ± 0.5	258.5 ± 0.3	254.7 ± 0.4	102.8 ± 0.9
Dihydrate	60.7 ± 1.5	82.2 ± 1.3	376.8 ± 1.8	258.1 ± 0.3	255.3 ± 0.2	94.5 ± 1.3

Results are means with their standard deviations.

It is expected that the heats of fusion of the three sodium naproxen species should be the same since melting occurs after removal of water and the crystal structures of the dehydrated species have been shown identical. However, the heats of fusion estimated in Table 3-1 are based on the initial sample mass, which includes whatever water had been present. These values can be converted to energy per unit mass of the anhydrous species as follows:

$$\Delta H_{\text{fus},n} = m_n \Delta \hat{H}_{\text{fus},n} = m_0 \Delta \hat{H}_{\text{fus},0} \tag{3-1}$$

where $\Delta H_{\text{fus},n}$ (J) is the enthalpy change with fusion measured by the DSC, $\Delta \hat{H}_{\text{fus},n}$ is the heat of fusion per unit initial sample mass as estimated directly by the DSC, $\Delta \hat{H}_{\text{fus},0}$ is the heat of fusion per unit mass of dehydrated sample, *m* is the mass of the sample, and the subscripts *n* and 0 denote the species with *n* moles of water per mole of anhydrate and the anhydrous species, respectively. Rearranging Equation 3-1,

$$\Delta \hat{H}_{\text{fus},0} = \frac{m_n}{m_0} \Delta \hat{H}_{\text{fus},n} = \frac{1}{x_0} \Delta \hat{H}_{\text{fus},n} = \left(\frac{1}{1 - x_{\text{H}_2\text{O}}} \right) \Delta \hat{H}_{\text{fus},n} \tag{3-2}$$

where *x* is mass fraction of the indicated species. This equation and the values of x_{H_2O} determined from TGA analyses were used to obtain the estimates of heat of fusion given in Table 3-2. Clearly, the converted heats of fusion for the three species are quite similar to each other and provide additional evidence that the dehydrated species have the same structure as anhydrous sodium naproxen.

Table 3-2. Converted heats of fusion of the sodium naproxen species

Compound	x_{H_2O}	$\Delta\hat{H}_{fus,n}$ (J/g)	$\frac{1}{1-x_{H_2O}}$	$\Delta\hat{H}_{fus,0}$ (J/g)
Anhydrate	0.00048 ± 0.00012	110.7 ± 0.5	1.00048*	110.8*
Monohydrate	0.06832 ± 0.00286	102.8 ± 0.9	1.07333*	110.3*
Dihydrate	0.12957 ± 0.00655	94.5 ± 1.3	1.14886*	108.6*

* values are calculated with means.

3.2.3 Dehydration kinetics

The DSC and TGA data on the dihydrate of sodium naproxen show the removal of two different types of water molecules from the crystal structure; these are referred to as first and second waters. The first generates the initial DSC peak and the second leads to the subsequent peak. In the following analysis, we evaluate the DSC and isothermal TGA data on both the monohydrate and dihydrate of sodium naproxen so as to elucidate the role water plays in the structures of these two species and to determine why the two waters in the dihydrate behave differently.

The rate of removal of water from a hydrated crystal can be written as

$$\frac{d\alpha}{dt} = kf(\alpha) \tag{3-3}$$

where α is defined as the fraction of water removed from the hydrated crystal at time t; that is,

$$\alpha = \frac{M_T - M}{M_T} \tag{3-4}$$

where M_T is the initial mass of water in the sample and M is the mass of water in the sample at time t. The relationship between water content in a crystal sample and time is

embodied in the function $f(\alpha)$, which in turn depends on the mechanism of water removal. Integration of Equation 3-3 gives[37]

$$\int_0^1 \frac{d\alpha}{f(\alpha)} = g(\alpha) = \int_0^t k\,dt = kt \tag{3-5}$$

The rate constant k may be considered to follow an Arrhenius dependency on T:

$$k = k_0 \exp\left(-\frac{\Delta E_a}{RT}\right) \tag{3-6}$$

where ΔE_a is the activation energy for dehydration, R is the gas constant, and T is temperature. The activation energy can be estimated from the rate constants determined from measurements of isothermal dehydration kinetics at several temperatures, provided $g(\alpha)$ is known. Table 3-3 gives selected expressions from the Šesták[38] and Dong et al.[37] for $g(\alpha)$ corresponding to various solid-state processes.

Table 3-3. Algebraic expressions for $g(\alpha)$ corresponding to suggested mechanisms of solid-state processes

Model Identifier	g(α)	Mechanism (descriptor of equation)
A2	$\left(-\ln(1-\alpha)\right)^{\frac{1}{2}}$	One-dimensional growth of nuclei (Avrami-Erofeev equation, $n = 2$)
A3	$\left(-\ln(1-\alpha)\right)^{\frac{1}{3}}$	Two-dimensional growth of nuclei (Avrami-Erofeev equation, $n = 3$)
A4	$\left(-\ln(1-\alpha)\right)^{\frac{1}{4}}$	Three-dimensional growth of nuclei (Avrami-Erofeev equation, $n = 4$)
R1	α	One-dimensional phase boundary reaction (zero-order mechanism)
R2	$1-\left(1-\alpha\right)^{\frac{1}{2}}$	Two-dimensional phase boundary reaction (contracting cylinder)
R3	$1-\left(1-\alpha\right)^{\frac{1}{3}}$	Three-dimensional phase boundary reaction (contracting sphere)
D1	α^2	One-dimensional diffusion
D2	$\left(1-\alpha\right)\ln\left(1-\alpha\right)+\alpha$	Two-dimensional diffusion
D3	$\left(1-\left(1-\alpha\right)^{\frac{1}{3}}\right)^2$	Three-dimensional diffusion (Jander's equation)
D4	$\left(1-\frac{2}{3}\alpha\right)\left(1-\alpha\right)^{\frac{2}{3}}$	Three-dimensional diffusion (Ginstling-Brounshtein equation)

Several isothermal dehydrations were performed in the TGA apparatus, and the resulting relationships between α and t determined using the following procedure for each of the water molecules in the dihydrate and for the lone water in the monohydrate of sodium naproxen. The function in Table 3-3 that provided the best fit to the dehydration data was identified, and the corresponding values of k determined. By fitting the Arrhenius expression to these values, an estimate of the activation energy of the given process was obtained.

For the first water released from the dihydrate and the lone water from the monohydrate, TGA data were fit from α at t = 5.5 min to α = 0.9. (*Note*. α is determined for each of the water molecules, and M_T in each instance is the mass associated with that specific water.) For the second water molecule removed from the dihydrate, the data were fit from α = 0.3 to α = 0.9. The interpretation of data on the second water removed from the dihydrate was complicated by a long transient between removal of the first and the second water molecules from the dihydrate. That is why the range of α was taken to begin at 0.3, thereby removing the transient and obtaining higher correlation coefficient, R^2 for the resulting fits to the data. Table 3-4 gives the results of the analyses leading to the best fits of data for both water molecules in the dihydrate and for the water in the monohydrate.

As shown in Table 3-4, model R2 provided the best fit to the data involving removal of the first water from the dihydrate, but model D3 was best for the second water and for the lone water removed from the monohydrate. This implies that different resistances control the removal rate of water: a phase boundary reaction for the first water of the dihydrate and diffusion for both the second water of the dihydrate and the lone water of the monohydrate. The phase-boundary reaction is taken to be dissociation of water from the crystal lattice.

Table 3-4. Activation energy for the released water

Released Water	Model	T (ºC)	k (min^{-1})	R^2	Arrhenius Plot	
					ΔE_a(kJ/mole)	R^2
First water from the dihydrate	R2	24.0	0.02443	0.9987	67.2	0.9850
		26.4	0.03214	0.9980		
		29.5	0.04015	0.9990		
Second water from the dihydrate	D3	24.0	0.002277	0.9941	98.6	0.9383
		26.4	0.003712	0.9908		
		29.5	0.004747	0.9934		
Water from the monohydrate	D3	24.1	0.000896	0.9948	92.5	0.9997
		26.9	0.001266	0.9958		
		29.8	0.001804	0.9970		

The activation energy for removal of the first water from sodium naproxen dihydrate is close to the lowest value among activation energies given in Table 3-5 for removal of water from several different crystal species. This is why, as shown experimentally with DSC and TGA data of the current research, the first water is very easy to remove, and it is easier to remove than the second water in sodium naproxen dihydrate. The activation energy for removal of the second water from the dihydrate was very similar to that for removing the lone water from the sodium naproxen monohydrate, and both are larger than the activation energy for removal of the first water from the dihydrate.

Table 3-5. Activation energies for different dehydration reactions

Compound	Activation Energy (kJ/mole)	Reference
Cefamandole sodium monohydrate → anhydrate	71	39
Neotame monohydrate → anhydrate	75 ± 9	37
Theophylline monohydrate → anhydrate	140	40
Sulfaguanidine monohydrate → anhydrate	67 – 168*	41
Mercaptopurine monohydrate → anhydrate	191 – 264**	42

* These values vary depending on crystallinity of the samples as well as environmental factors

** These values vary depending on the method of determination

Dong et al.[37] postulated a dehydration mechanism for neotame monohydrate that consisted of two steps: (a) dissociation of water from the crystal lattice and then (b) diffusion of the water through channels in the crystal. Dissociation may involve breakage of hydrogen bonds or disruption of other attractive forces. It appears that a similar view is appropriate for the current system, but it is complicated by the existence of two different types of behavior for the two water molecules in the dihydrate.

A packing diagram of sodium naproxen monohydrate crystals was constructed based on x-ray diffraction data,[11] and is shown in Figure 3-5. The diagram reveals channels for water transport within the crystals. Figure 3-5a shows the sodium naproxen molecule with the sodium atom omitted; in the crystal structure of Figure 3-5b, only the two oxygen atoms in the carboxyl group, four covalent bonds from the two oxygen atoms to the naphthyl group, a sodium atom, and an oxygen atom in the water of hydration were drawn to make it clear where water channels are in the monohydrate.

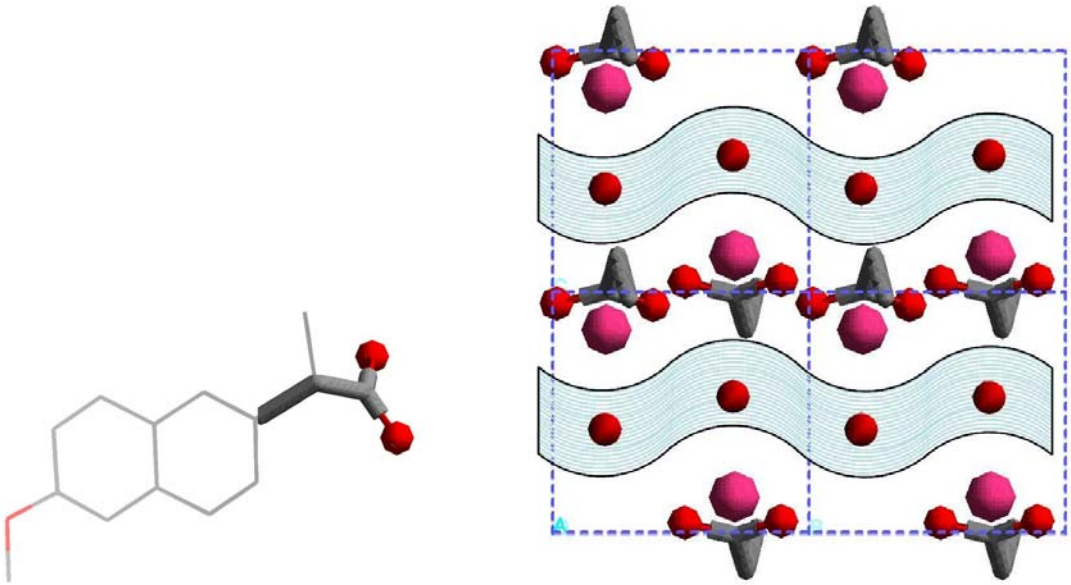

(a) (b)

Figure 3-5. (a) sodium naproxen molecule with the sodium and hydrogen atoms omitted and (b) a projection along the [100] plane of the monohydrate. In (a), two oxygen atoms and four covalent bonds are exaggerated. For clarity, only this portion of the molecule is depicted in (b). Additionally, in (b), the smaller circles represent oxygen atoms, the larger circles represent sodium atoms, and the shaded waves show water channels in the monohydrate.

Allen et al.[43] suggested that water released at low temperature has very weak interactions with nearby molecules in the crystal lattice. Morris[2] classified hydrates as follows: (1) isolated-site hydrates, which should yield sharp DSC endotherms and narrow TGA mass losses upon dehydration, (2) channel hydrates, which have early onset temperatures of dehydration and broader DSC and TGA traces than isolated-site hydrates, and (3) ion-associated hydrates, which have strong metal-water interactions and comparatively higher dehydration temperature and molar heat of dehydration than the other hydrates. He also suggested that dehydration is affected by diffusion of water molecules from the unit cells to the crystal surface; accordingly, if there is ready access of the leaving water to channels for diffusion, dehydration occurs easily and at low temperatures. The first water removed from sodium naproxen dihydrate has an earlier onset temperature than the second water, which we show in Figure 3-5 to be in channels. We infer, therefore, that since these channels exist in the monohydrate and facilitate dehydration, they must also exist in the dihydrate where removal of the first water is even easier.

3.3 CONCLUSIONS

Three different pseudopolymorphic forms of sodium naproxen were prepared by crystallization from aqueous solutions and by dehydration of higher hydrated crystalline samples. The changes in pseudopolymorphic form by dehydration in an oven and/or a desiccator imply that dehydration endotherms obtained by DSC were associated with the removal and evaporation of water incorporated in crystal structures and simultaneous transformation to lower degrees of hydration.

Analysis of TGA and DSC data demonstrated that there are two types of water molecules in the crystal structure of dihydrated sodium naproxen. Isothermal TGA data were employed to show the difference of activation energies associated with removal of these two different forms of water from the crystal structure. As expected, the first water removed from the dihydrate had a lower activation energy, explaining why it was easily removed at a low temperature. It was furthermore concluded that the relatively low activation energies and temperature ranges to remove those two different water molecules result from weak interactions with nearby molecules in the crystals lattice.

CHAPTER 4

SOLUBILITY OF PSEUDOPOLYMORPHS OF SODIUM NAPROXEN

Sodium naproxen has been produced since the 1970s and many modifications have been made to optimize the process to improve production rate with less cost. Although the physical and chemical properties of the pseudopolymorphs of sodium naproxen were studied by Di Martino et al. (2001),[10] little has been done on the solubility of sodium naproxen. In this chapter, solubilities of sodium naproxen in pure water and in aqueous solutions containing 64 mole% methanol were obtained by measuring the equilibrium concentrations over a range of temperature.

4.1 EXPERIMENTAL APPARATUS AND PROCEDURES

4.1.1 Apparatus

Two different equilibrium cells were prepared for solubility experiments of sodium naproxen in pure water system and a solvent containing 64 mol% methanol in water. One was a 3-port, 400-mL jacketed crystallization vessel shown in Figure 4-1 used as the equilibrium cell to measure solubility of sodium naproxen in pure water. The other cell was a bottle with a cap as in Figure 4-2 for solubility experiments of sodium naproxen in the methanol-water mixtures. The bottle was used to avoid evaporation of solvents and concomitant changes in the ratio of water and methanol during the experiments. The bottle was immersed in water at desired temperatures. Magnetic stirrers provided mixing. Each equilibrium cell was connected to a water circulator system with a programmable temperature controller when it was used. UV protector was prepared and equilibrium cells were maintained in the protector because Moore and Chappuis (1988)[44] reported that aqueous solutions containing the sodium salt of the naproxen underwent a quick and strong degradation fostered by light, especially, UV. Apparatus used for sampling is shown in Figure 4-3. Liquid samples were withdrawn from an equilibrium cell using a 5-mL plastic syringe and a stainless steel needle. A 0.2-μm syringe filter was used to prevent fine solid crystals from entering into the syringe.

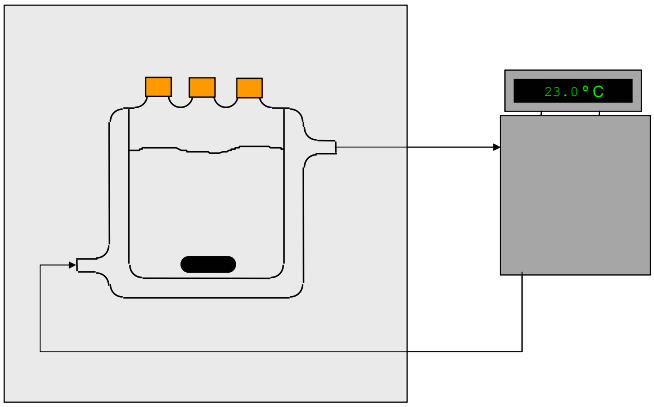

Figure 4-1. Schematic diagram of a 3-port, 400-mL jacketed crystallization vessel and a water circulator system with a programmable temperature controller.

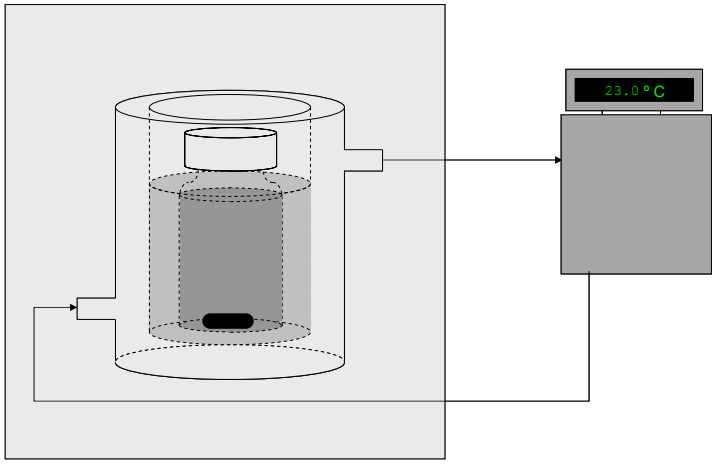

Figure 4-2. Schematic diagram of a 80-mL bottle with a cap and a water circulator system with a programmable temperature controller.

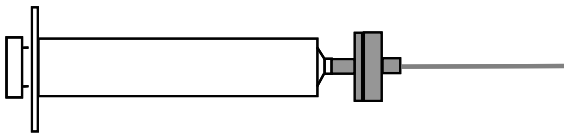

Figure 4-3. A 5-mL plastic syringe, 0.2 μm syringe filter and a spinal needle.

4.1.2 Experimental procedures

Anhydrous sodium naproxen, supplied by Albemarle Corp., was used in all experiments without further purification or processing and HPLC-grade water was used to dissolve sodium naproxen. A first rough measurement of solubility was performed at ambient temperature because solubility data were not available when the experiment started. One hundred milliliters of water and about 5 g of sodium naproxen were loaded in a vessel containing a magnetic stirrer which mixed the solution in the vessel. Since the concentration of 5 g in 100 mL water is much lower than the solubility at the ambient temperature, the initial amount of sodium naproxen dissolved very quickly. Two grams of sodium naproxen was added to the solution after the solution became clear. Once the dissolution rate slowed, 1g of sodium naproxen was added to the solution until it was not dissolved any more.

Accurate measurement of solubility of sodium naproxen in pure water was performed after the rough measurement. Predetermined amounts of water and sodium naproxen were loaded in a 3-port 300-mL jacketed vessel containing a magnetic stirring bar. Cooling crystallization was performed to form crystals at the desired temperature and sampling was carried out.

The procedures for determining the solubility of sodium naproxen in aqueous methanol solutions were the same as those for pure water. A lot of the mixture of water and methanol was prepared in advance for the experiments. This mixture solvent was used to dissolve sodium naproxen and dilute the solution in the equilibrium cell. A bottle with a cap was used as the equilibrium cell for the solubility in the mixture to avoid methanol from evaporating.

4.1.3 Sampling protocol

Sampling of the liquid was performed over a desired temperature range. Before recrystallization was performed the solution was heated to 50˚C and held for 2 hours to make sure that no crystals existed in the equilibrium cell. Then, the vessel was cooled until crystals formed. After recrystallization occurred the solution was heated to raise the temperature by 2˚C intervals to find an appropriate temperature for sampling. Because solutions in the cell became gel-like after nucleation and, consequently, it was impossible to take samples from the solution, as many crystals as possible should by dissolved by increasing the temperature of the solutions and the liquid portion could be taken from the cell. After the temperature to take samples was found the system conditions were held constant for about 12 hours.

When the system reached equilibrium, sampling the solution was sampled. A 0.2-μm sterile syringe filter was secured to a 5-mL plastic syringe and a spinal needle was attached to the filter. The needle had a fine inner diameter (~1.7 mm), which excluded crystals larger than the inner diameter. Furthermore, the 0.2- μm filter in the syringe removed any crystal which was withdrawn through the needle. After a sample was taken from the solution the filter was detached from the syringe and two or three drops of the solution in the syringe were injected into a 1.5-mL vial containing HPLC-grade water for immediate dilution. After the vial was weighed, the contents in the vial were mixed for several seconds by a vortexer. The temperature was measured using a Type-K thermocouple right after sampling.

4.2 HIGH PERFORMANCE LIQUID CHROMATOGRAPHY

4.2.1 Equipment

A high performance liquid chromatography (HPLC) made by Shimadzu Corp. was used to determine the concentration of sodium naproxen at equilibrium in aqueous solutions and in the mixture of water and methanol. The chromatographic separation was performed on a reverse-phase Varian Microsorb-MV 100-3 C18 column. A wavelength of 254 nm was used in the SPD-10AV detector. The voltage signal from the detector was interpreted by the Shimadzu CLASS-VP Chromatography Data System version 7.2.1 software program running on a personal computer. Two mobile phases were prepared. One was pure acetonitrile (Acros Organics) and the other was a mixture of 2 % acetic acid (Sigma–Aldrich) and 98% water (volume ratio). The mixture was prepared by mixing, for example, 2 mL of acetic acid and 98 mL of water. Each mobile phase was connected to the delivery module of the HPLC. The flow rates from each reservoir were 0.5 mL/min and, totally, 1.0 mL/min. The acquisition parameters are listed in Table 4-1 and the typical separation by HPLC is depicted in Figure 4-4.

Table 4-1. Acquisition parameters

Items	Parameters
Pumps Mode	Low Pressure Gradient Parameters
Total Flow Rate	1.0 mL/min
Pressure Limit	0.0 ~ 20.0 Mpa
Lamp for Detector	Deuterium (D2)
Wavelength for Acquisition	254 nm
Sampling Frequency	5 Hz
Acquisiton Time/Controller Stop Time	20 minutes
Injection Volume	10 μL
Sampling Speed	10 μL/sec

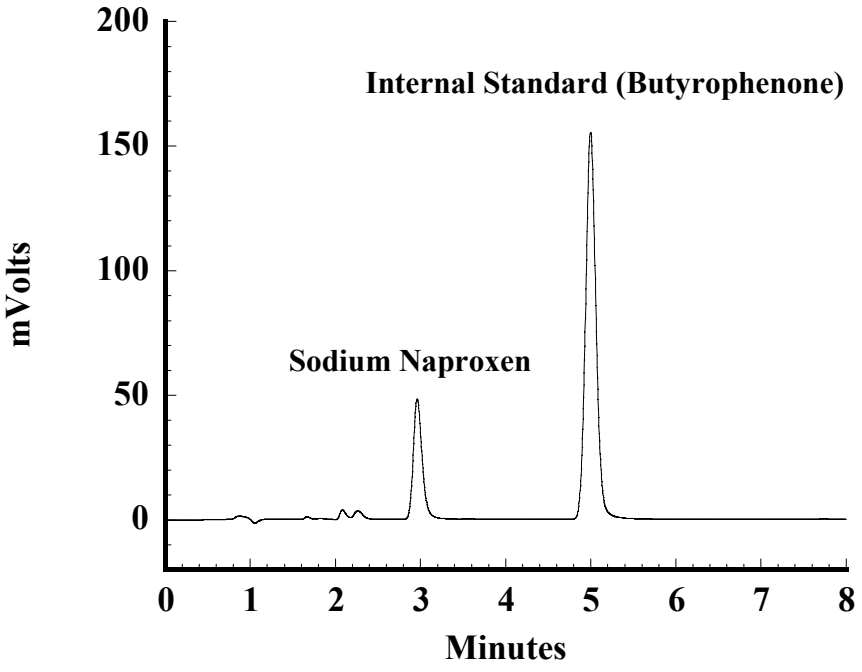

Figure 4-4. HPLC separation of sodium naproxen and butyrophenone

4.2.2 Calibration

Peak areas were calculated by integration of peak intensity of a sampl, and they are related to a concentration of the sample using a calibration curve. For this research, an internal standard was employed and the ratio of a sample area to an internal standard peak area was related to the ratio of a sample concentration to an internal standard concentration proportionally. The following equation represents the relationship:

$$\frac{A_S}{A_I} = k\frac{C_S}{C_I} + b \tag{4-1}$$

where A and C are peak area and concentration, respectively, subscript S and I represent sample and internal standard, respectively, and k and b are constants for the linear equation which is called a calibration curve. The linear curve is determined by preparing sample solution and internal solution with a known concentration, running HPLC and recording corresponding areas. Figure 4-5 shows a schematic diagram of dilution for the calibration curve.

After initial solutions with desired concentrations, C_{S0} and C_{I0} in Figure 4-5, are prepared concentrations after dilution are determined by following equations:

$$C_{S1} = \frac{C_{S0} \cdot M_{S0}}{(M_{S0} + M_{W0})} \times 1000 \tag{4-2}$$

$$C_{I1} = \frac{C_{I0} \cdot M_{I0}}{(M_{I0} + M_{W0})} \times 1000 \tag{4-3}$$

where M denotes mass and subscript W represents water. Units for concentration and mass are g solute/kg solution and g, respectively. Butyrophenone (Sigma–Aldrich) was dissolved into acetonitrile and used as the internal standard. Dilution of sample for calibration is very important because it can be expected only at low concentration that the

ratio of concentrations for sample and internal standard is proportional to that of corresponding areas. Final concentrations for the sample and the internal standard are calculated by equations:

$$C_{S2} = \frac{C_{S1} \cdot M_{S1}}{(M_{S1} + M_{I1} + M_{A1})} \times 1000 \quad (4\text{-}4)$$

$$C_{I2} = \frac{C_{I1} \cdot M_{I1}}{(M_{I1} + M_{S1} + M_{A1})} \times 1000 \quad (4\text{-}5)$$

where subscript A means acetonitrile. After final solution is injected into HPLC corresponding peak areas are obtained from the chromatogram. The ratios of $\frac{A_S}{A_I}$ versus $\frac{C_S}{C_I}$ are plotted and constants, *k* and *b*, for the linear equation are obtained by linear regression.

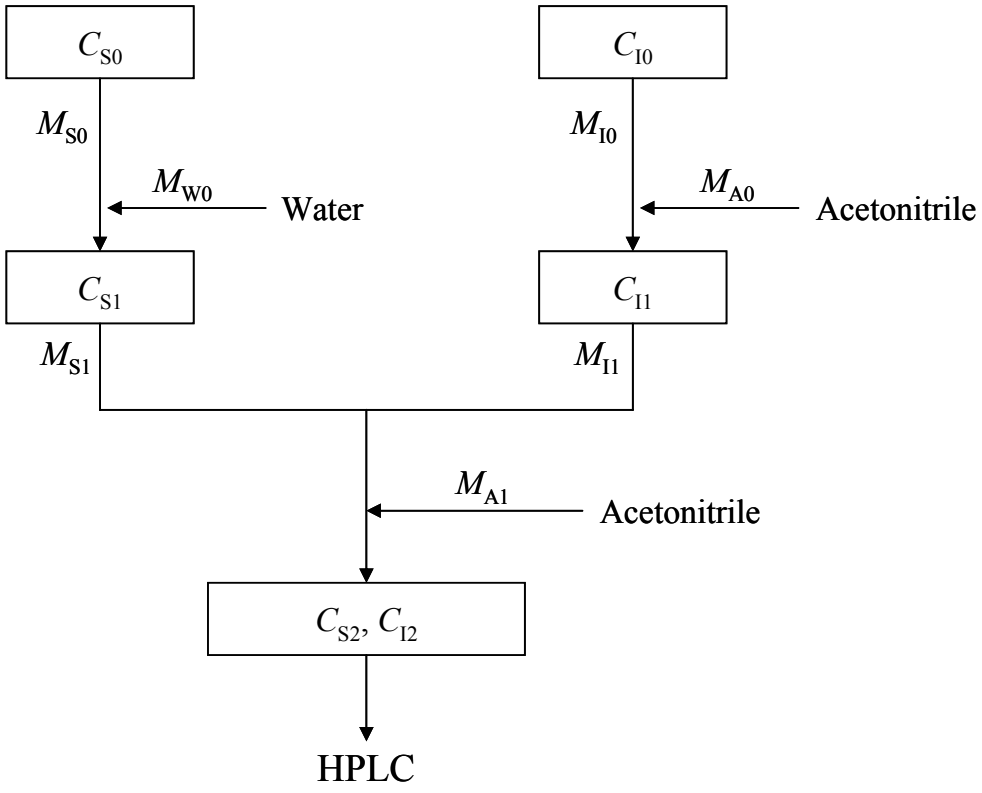

Figure 4-5. Scheme of dilution for the calibration curve

4.2.3 Sample dilution

Dilution was performed to prevent crystallization of sodium naproxen which reduces the accuracy of HPLC analysis and/or clogs tubing in HPLC. Furthermore, concentrations of samples and internal standards in diluted solution should fall into the range of concentrations for the calibration curve.

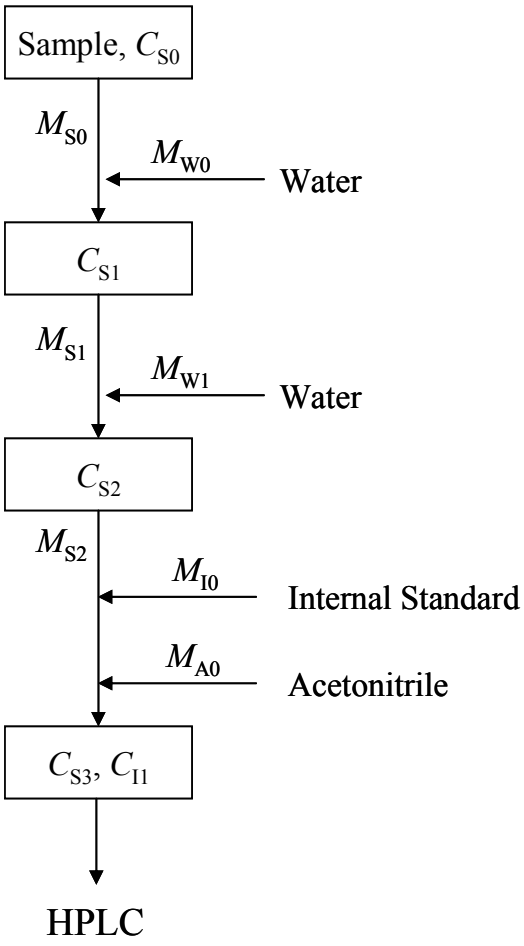

Figure 4-6. Scheme of dilution for a sample

The initial sample, C_{S0}, is unknown in the sample dilution steps while the initial sample to make a calibration curve is a predetermined concentration. At the third dilution step, an internal standard solution, whose concentration is already known, is also added. After the sample is diluted three times it is injected into the HPLC and peak areas corresponding to sodium naproxen and the internal standard are obtained. The injected concentration of sodium naproxen is determined by the rearranged equation:

$$C_{S3} = \frac{\left(\frac{A_{S3}}{A_{I1}} - b\right)}{k} \cdot C_{I1}. \tag{4-6}$$

Once the injected concentration of sodium naproxen is determined every concentration at each dilution step is obtained by equations:

$$C_{S2} = \frac{C_{S3} \cdot \left(M_{S2} + M_{I0} + M_{A0}\right)}{1000 \cdot M_{S2}} \tag{4-7}$$

$$C_{S1} = \frac{C_{S2} \cdot \left(M_{S1} + M_{W1}\right)}{1000 \cdot M_{S1}} \tag{4-8}$$

$$C_{S0} = \frac{C_{S1} \cdot \left(M_{S0} + M_{W0}\right)}{1000 \cdot M_{S0}}. \tag{4-9}$$

C_{S0} in Equation 4-9 is the initial concentration of liquid in the equilibrium cell.

4.3 ANALYSIS OF CRYSTALS

4.3.1 Optical microscopy

Crystals change in size and shape during recrystallization. This is caused by kinetic factors such as mixing intensity and ramping rate for temperature and by thermodynamic factors such as polymorphism and solvent compositions. In the present study, an optical microscope was used to observe how pseudopolymorphism and solvent composition affected the size and the shape of crystals.

A small amount of slurry from the equilibrium cell was taken and dropped on a slide glass which then was covered with a cover glass. The slide and cover glasses were stored in a refrigerator for samples at a low temperature before analyses because the crystal samples in solution were very sensitive to temperature and they tended to dissolve very rapidly on the slide glass, which is at a higher temperature than the crystals. Samples prepared were analyzed under a ML 9000 instrument made by MEIJI, Japan, with a 10X objective lens. The microscope was equipped with a Sony digital camera DKC-500 that converted the focused light into a digital signal. This signal was visualized by Image-Pro Plus version 4.5.

4.3.2 Powder X-Ray diffraction (PXRD)

An optical microscope gives information about the habit or shape of crystals. However, analysis with an optical microscope is not enough to distinguish a pseudopolymorphic form from the other forms because the habit of crystals may change

by kinetic factors. Therefore, the crystals were identified by powder x-ray diffraction (PXRD) analysis.

Slurry at a desired temperature was filtered by using a vacuum pump to draw solution through a filter and then the resulting filter cake was dried for 24 hours under ambient conditions. The dried sample was gently ground into powder with a mortar and pestle. Then, the powder samples were analyzed by using Philips® PW3040-PRO automatic powder diffractometer with X'Pert Data Collector 2.0d software. Square aluminum holders with recessed cavities that are 15 mm × 20 mm × 1.8 mm were used and about 1 to 2 g of crystals was required for an analysis. Copper Kα radiation was used. The radiation for Copper Kα1 is 1.541Å. A voltage and a current are 40 kV and 30mA, respectively. The PXRD patterns were made over a diffraction-angle (2θ) range of 3 to 40º, with a step size of 0.02º and a counting time of 1 second per step. X'Celerator was used and diffraction patterns were collected very quickly.

4.4 RESULTS AND DISCUSSION

4.4.1 Solubility

Di Martino et al. (2001) reported solubilities of the anhydrous and dihydrated species.[10] However, it was pointed out by Mendéz del Río (2004) that the data showed extremely low solubility values.[45] In this study, solubility data of pseudopolymorphs of sodium naproxen were obtained by the method mentioned above.

The solubility of sodium naproxen in pure water and in aqueous methanol solutions was determined. The results are listed in Tables 4-2 and 4-3. The solubility

data determined by Mendéz del Río (2004)[45] are also listed in Table 4-4 to compare the solubility data which were obtained by the focused-beam reflectance method (FBRM) while equilibrium cell and HPLC were used in this study as described above. All experimental data, including those obtained by using FBRM, are plotted in Figure 4-7.

The solubility over a temperature range from 9.1°C to 27.2°C was determined from pure water. Sodium naproxen grew as needle-like crystals which were thin and very long. The crystals filled up the equilibrium cell and the magnetic stirrer was even prevented from rotating. Furthermore, the liquid in the cell was captured in networks built by the thin and long needle-like crystals, which make it impossible to take a liquid sample.

Solubilities of sodium naproxen in pure water were determined by Mendéz del Río (2004) over a broader and higher temperature range from 15.2ºC to 39.7ºC.[45] The solubility by the equilibrium cell method was compared to that by FBRM. The difference between two data sets over an overlapped range was from 3.9% to 9.6%, showing a good consistency between two data sets.

Solubility data from aqueous solutions containing 64 mol% were determined over a temperature range from 10.2ºC to 34.5ºC. The temperature range is broader than that for solubility from pure water because there was no problem to take equilibrated solutions from the cell at higher temperatures, resulting from the crystal habit, which has a very small needle-like shape at lower temperature range and plate-like at higher temperature range.

Table 4-2. Solubility of sodium naproxen in pure water

Temperature (°C)	Solubility (g anhydrous sodium naproxen/kg solution)
9.1	78.9
16.9	128.6
23.1	186.5
27.2	240.2

Table 4-3. Solubility of sodium naproxen in aqueous solutions containing 64 mol% methanol

Temperature (°C)	Solubility (g anhydrous sodium naproxen/kg solution)
10.2	224.5
15.2	260.7
17.0	279.4
24.8	323.8
27.7	333.6
29.7	341.2
34.5	365.6

Table 4-4. Solubility of sodium naproxen in pure water by Mendéz del Río (2004)

Temperature (°C)	Solubility (g anhydrous sodium naproxen/kg solution)
15.2	104.3
17.3	121.5
20.0	145.5
22.9	181.2
26.6	223.7
27.9	240.2
28.3	246.1
30.3	273.7
34.1	308.1
36.9	333.7
39.7	364.1

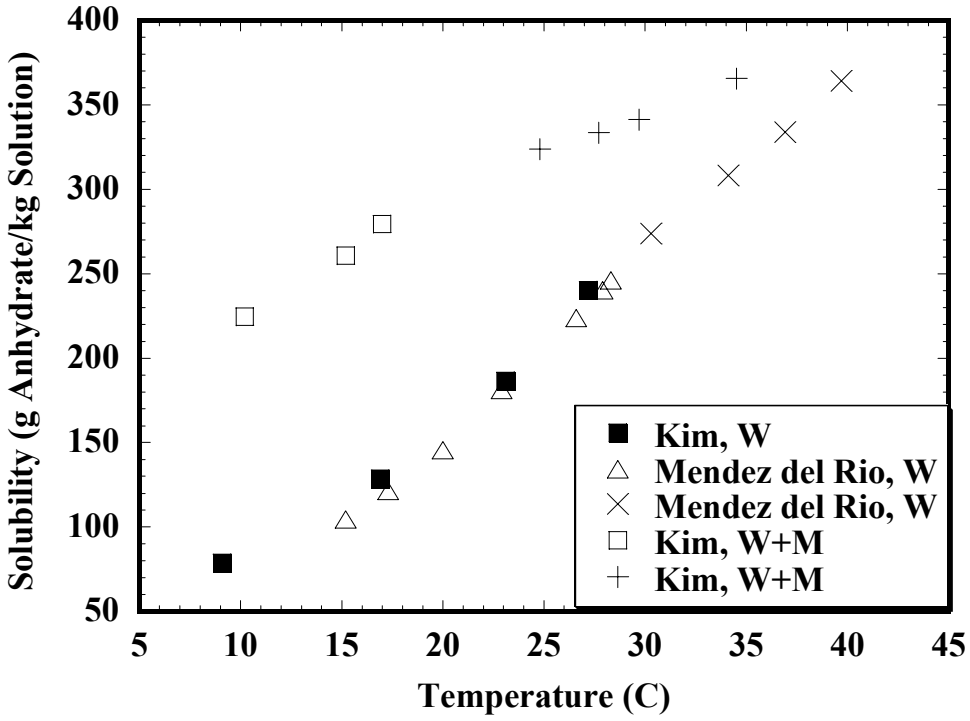

Figure 4-7. Solubility of sodium naproxen in pure water and in solution containing 64 mol% methanol. W in the legend means that the data were the solubility of sodium naproxen in pure water and W+M represents the data in the mixture of water and methanol.

4.4.2 Transition between pseudopolymorphs

Discontinuities in data are observed by taking a close look at Figure 4-7. They imply the transition between pseudopolymorphic forms and the transition was proved by analyzing crystal samples from each temperature range by PXRD. Sodium naproxen in pure water existed as dihydrated species at the low temperature range and it transformed to the anhydrous species at transition temperature. For sodium naproxen in solutions containing 64 mol% methanol, the dihydrated form of sodium naproxen is stable at the lower temperature range, while the monohydrated form is stable at higher temperature range.

Empirical fits were applied to all solubility curves to visualize the discontinuities. Exponential fits were used and the results are shown in Figure 4-8. The empirical functions were found to be good fits for all solubilities, giving coefficients of correlation (R^2) above 0.99.

It is noted that the monohydrated sodium naproxen does not exist in the solubility curve from pure water. Clearly, the monohydrated species in pure water is unstable thermodynamically or stable over a very small temperature range.

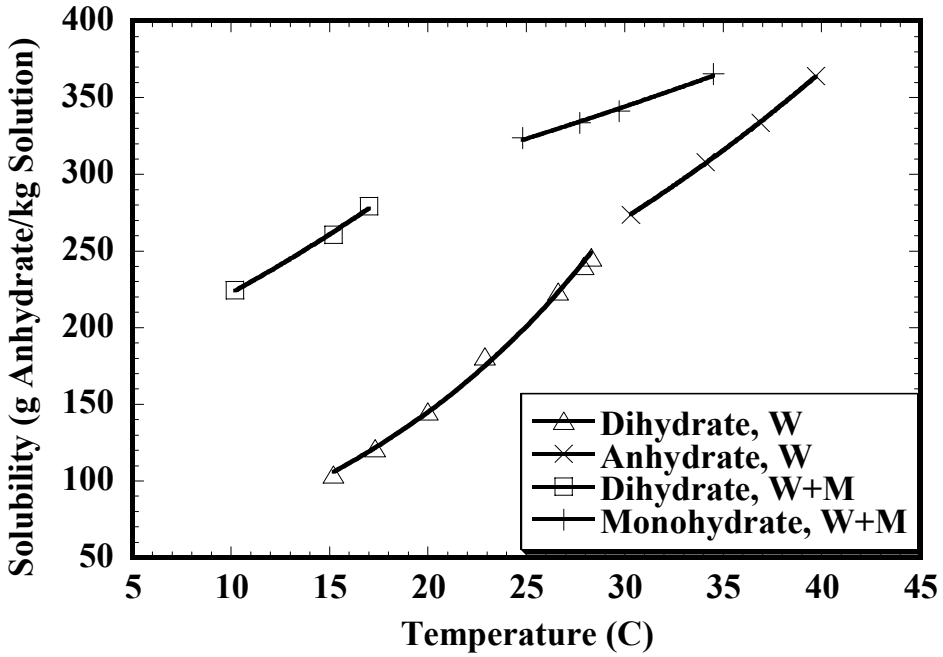

Figure 4-8. Empirical fits to the solubility data in pure water and mixtures of water and methanol.

4.4.3 Solubility data correlations

The thermodynamic framework for the solubility of solids in liquids has been outlined by Prausnitz et al. (1999).[46] The general expression that is used to relate solubility data to system temperature is as follows:

$$\ln\left(\frac{1}{x\gamma}\right) = \frac{\Delta_{\text{fus}}h}{RT_t}\left(\frac{T_t}{T}-1\right) - \frac{\Delta c_P}{R}\left(\frac{T_t}{T}-1\right) + \frac{\Delta c_P}{R}\ln\frac{T_t}{T} \qquad (4\text{-}10)$$

where x is the mole fraction, γ is the liquid-phase activity coefficient, $\Delta_{\text{fus}}h$ is the enthalpy of fusion, R is the gas constant, T_t is the triple point temperature, c_P is the heat capacity and $\Delta c_P = c_{P(liquid)} - c_{P(solid)}$.

The simplest correlation can be derived by three assumptions. First, the difference between the triple-point temperature and melting temperature is assumed to be small and consequently, the difference in the enthalpies of fusion at these two temperatures is taken to be negligible. Hence, the melting temperature, T_m, is substituted for T_t and the enthalpy of fustion at is T_m used. Second, the difference in the heat capacity of the solute in its solid-state and in its liquid-state, Δc_P, is relatively small. Therefore, the second and the third terms on the right-hand side of Equation 4-10 can be neglected. Also the difference between the second and the third terms are considered to be negligible because, as $\frac{T_t}{T}$ goes to unity, $\ln\frac{T_t}{T}$ goes to $\frac{T_t}{T}-1$. Third, if the solution behaves ideally, γ may be taken to be unity. With these assumptions, Equation 4-10 becomes as:

$$\ln x = -\frac{\Delta\hat{H}_{\text{fus}}}{RT} + \frac{\Delta\hat{S}_{\text{fus}}}{R} \qquad (4\text{-}11)$$

This is known as the van't Hoff equation.

Non-ideal behavior of the solution was reflected by replacing the enthalpy of fusion, $\Delta\hat{H}_{\text{fus}}$, with the heat of solution, $\Delta\hat{H}_{\text{sol}}$, and the entropy of fusion, $\Delta\hat{S}_{\text{fus}}$, with the entropy of dissolution, $\Delta\hat{S}_{\text{d}}$, suggested by Beiny and Mullin (1987)[47] and the van't Hoff equation is re-written:

$$\ln x = -\frac{\Delta\hat{H}_{\text{sol}}}{RT} + \frac{\Delta\hat{S}_{\text{d}}}{R}. \tag{4-12}$$

The solubilities were replotted on a van't Hoff plot (log x *vs.* $1/T$) as shown in Figures 4-9 and 4-10. Van't Hoff plots make more clear the discontinuity between data for dihydrated naproxen sodium and those for anhydrous sodium naproxen in Figure 4-9 and between the dihydrate and the monohydrate in Figure 4-10. Since fits shown are based on Equation 4-12 the slopes of the fits to each data set are $\Delta\hat{H}_{\text{sol}} / R$. The apparent heats of solution for both forms of sodium naproxen in water from Figure 4-9 are estimated to be 56.2 kJ/mol for the dihydrate and 33.8 kJ/mol for the anhydrate. The quality of the fit to each data set is given by correlation coefficients of 0.9993 and 0.9991 for the dihydrate and the anhydrate in Figure 4-9, respectively. The lines intersect at 29.8°C, which is called the transition temperature, indicating the temperature where two pseudopolymorphic forms have the same solubility.

For the solubility data of sodium naproxen in solutions containing 64 mol% methanol, the heats of solution are estimated to be 28.1 kJ/mol for the dihydrate and 14.1 kJ/mol for the monohydrate from Figure 4-10. The correlation coefficients are 0.9952 for the dihydrate and 0.9888 for the monohydrate. The transition temperature of sodium naproxen in the mixture is 19.6°C.

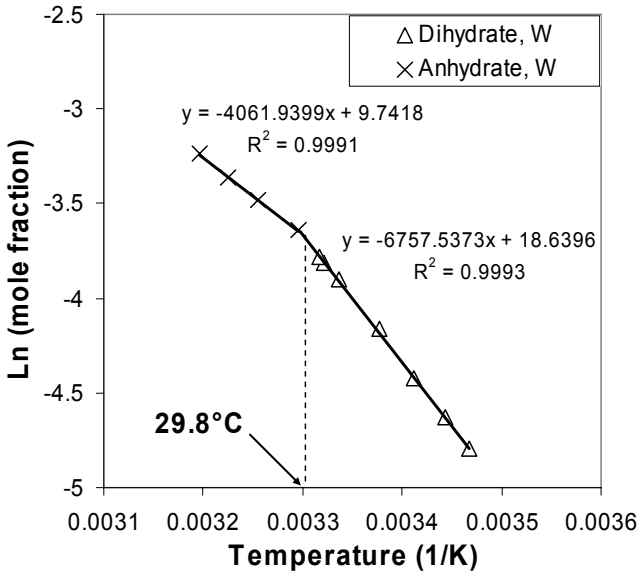

Figure 4-9. Van't Hoff plot of the solubility of sodium naproxen in pure water

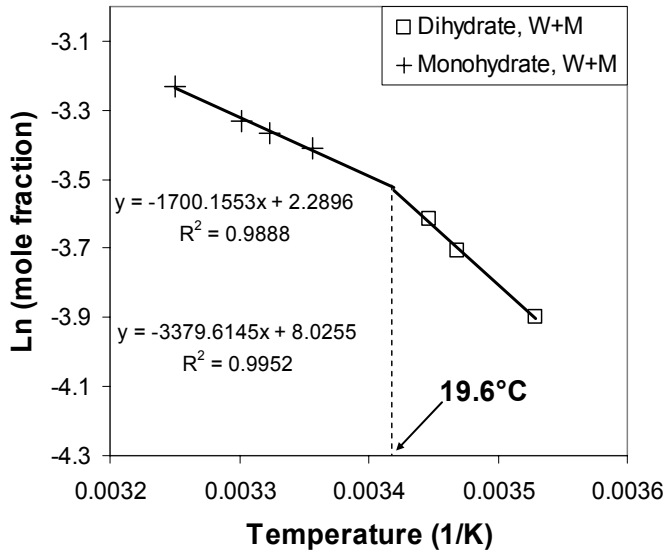

Figure 4-10. Van't Hoff plot of the solubility of sodium naproxen in the mixture of water and methanol

4.4.4 Relationships among heats of solution and heat of dehydration

The heat of solution is important in understanding the behavior of many pharmaceutical compounds. For example, Urakami et al. (2002)[48] used heat of solution and successfully estimated transition temperatures for polymorphic pairs in pharmaceuticals. Terada et al. (2000) clarified the quantitative relationship between initial dissolution rates and the heats of solution of drug substances.[49] Suryanarayanan and Mitchell (1986) estimated the energy of activation for rehydration from the heat of solution of calcium gluceptate.[50] The characterization of pharmaceutical compounds often relies on the relationship of the heat of solution to the solubility of a specific compound. For example, the heat of solution was calculated from the van't Hoff relationship for pseudopolymorphic systems of glutethimide, theophylline and succinyl sulfathiazole by shefter et al. (1963).[51] Suryanarayanan and Mitchell (1985)[52] also calculated the heat of solution of calcium gluceptate hydrate from the slope of a van't Hoff plot (i.e., a plot of log mole fraction *vs.* the reciprocal of absolute temperature).

An alternative method to measure the heat of solution is by solution calorimetry. Through this method, a small amount of compound is dissolved at a given temperature and heats evolved or absorbed are measured. Solution calorimetry though, is relatively less accessible than other methods such as thermogravimetric analysis (TGA) and differential scanning calorimetry (DSC) in the characterization of pharmaceutical compounds.

In this section, a method was developed to estimate the heat of solution using the heat of dehydration from DSC measurements. The method is useful when a species is unstable in solution, making it difficult to measure its solubility. In such cases, obtaining

crystal samples from the solution is not possible and heats of solution cannot be obtained from van't Hoff plot.

The following development shows how the enthalpy of solution for hydrated sodium naproxen may be predicted from that for the anhydrous sodium naproxen using the heat of dehydration for the dihydrated sodium naproxen. The approach utilizes the thermodynamic cycle shown in Figure 4-11. The temperature at which dissolution takes place is T_s, while the temperature at which dehydration occurs is T_d.

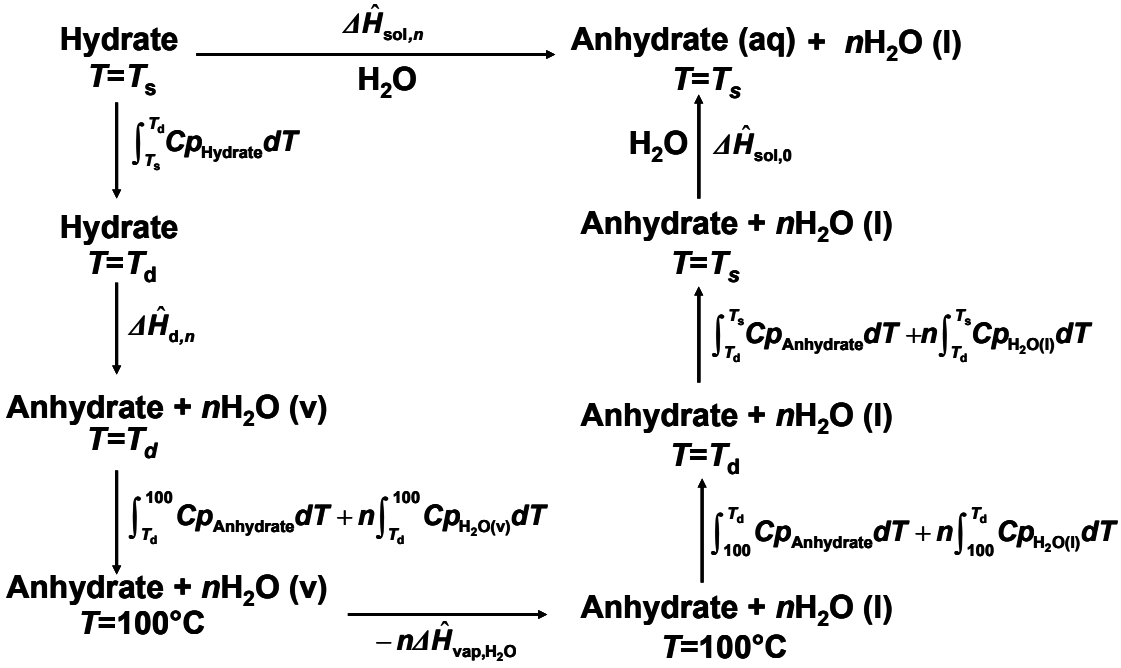

$$\Delta\hat{H}_{sol,n} = \Delta\hat{H}_{d,n} - n\Delta\hat{H}_{vap,H_2O} + \Delta\hat{H}_{sol,0} + n\int_{T_d}^{100}(Cp_{H_2O(v)} - Cp_{H_2O(l)})dT + \int_{T_s}^{T_d} Cp_{Hydrate}dT - \int_{T_s}^{T_d} Cp_{Anhydrate}dT - n\int_{T_s}^{T_d} Cp_{H_2O(l)}dT$$

Figure 4-11. Alternative paths in which dihydrated sodium naproxen is dissolved in water

The heats of solution of the anhydrate and the dihydrate in the thermodynamic cycle were obtained from van't Hoff plot for each pseudopolymorph in Figure 4-9 and Figure 4-10. The linearity of the plots indicates that the heats of solution were constant over the conditions at which the data were obtained.

The heat capacities of the anhydrous and the hydrated compounds (the monohydrate and the dihydrate) are required to use the result of the thermodynamic cycle in Figure 4-11, but these are not always available. The assumption used here that the heat capacity of the dihydrate is approximately the sum of those of the anhydrate and water can be justified from the report by Khankari et al. (1992)[53] that most pharmaceutical hydrates have water molecules present in liquid-like structures in the hydrates. Therefore,

$$\int_{T_s}^{T_d} Cp_{\text{Hydrate}} dT \approx \int_{T_s}^{T_d} Cp_{\text{Anhydrate}} dT + n\int_{T_s}^{T_d} Cp_{\text{H}_2\text{O(l)}} dT \tag{4-13}$$

Consequently, the equation to estimate the heat of solution of the dihydrate becomes

$$\Delta\hat{H}_{\text{sol},n} = \Delta\hat{H}_{\text{d},n} - n\Delta\hat{H}_{\text{vap,H}_2\text{O}} + \Delta\hat{H}_{\text{sol},0} + n\int_{T_d}^{100^\circ\text{C}} (Cp_{\text{H}_2\text{O(v)}} - Cp_{\text{H}_2\text{O(l)}}) dT \tag{4-14}$$

The heat of dehydration at T_d can be determined in DSC measurements in which a hydrated form of a species loses water from its structure and the water is vaporized. If we let the species be represented by A, the process and associated enthalpy change are as follows:

$$\text{A} \cdot n\text{H}_2\text{O(s)} \rightarrow \text{A(s)} + n\text{H}_2\text{O(v)} \qquad \text{at } T = T_s \tag{4-15}$$

$$\Delta\hat{H}_{\text{d},n} = \hat{H}_{0(\text{s})} + n\hat{H}_{\text{H}_2\text{O(v)}} - \hat{H}_{n(\text{s})} \tag{4-16}$$

where $\hat{H}$ is the specific enthalpy relative to a common set of reference states, n denotes the number of associated water molecules in a unit cell, the subscript d stands for dehydration and subscripts n and 0 mean hydrated and anhydrous forms, respectively.

Strictly speaking, dehydration in the DSC occurs over a range of temperature; in the present work, we chose the point at which an endotherm reached minimum as the dehydration temperature, T_d. For the dihydrated sodium naproxen, there were two overlapping endothermic peaks and consequently, two temperatures (60.7°C and 82.2°C) at which an endotherm reached minimum (Kim and Rousseau, 2004).[54] The average of these two values (71.45°C) was used in the present work as the dehydration temperature for the dihydrated sodium naproxen.

Using the heat of solution of anhydrous sodium naproxen (33.8 kJ/mol), which was evaluated from the van't Hoff plot in Figure 4-9, the heat of vaporization of water (2261 J/g of water) at 100°C (Stark and Wallace, 1976),[55] the heat capacities of water in liquid state (4.186 J/g °C) and in vapor state (2.009 J/g °C) and the heat of dehydration evaluated from DSC data (108.6 kJ/mol) in Chapter 3, the heat of solution of the dihydrated species can be estimated as 58.7 kJ/mol. There is a 4.4% difference between the estimated value and the value determined from the dihydrate portion of the van't Hoff plot in Figure 4-9 (56.2 kJ/mol).

The same approach can be applied to the heats of solution of sodium naproxen in the mixture of water and methanol. Dihydrated species transformed to monohydrated sodium naproxen in the mixture. A new variable, *m*, is defined to represent the hydrated form with lower degree of hydration than *n*. The more general equation for prediction of heat of solution from the heat of dehydration is as follows:

$$\Delta\hat{H}_{\mathrm{sol},n} = \Delta\hat{H}_{\mathrm{d},n\to m} - (n-m)\Delta\hat{H}_{\mathrm{vap,H_2O}} + \Delta\hat{H}_{\mathrm{sol},\,m} + (n-m)\int_{T_d}^{100^\circ\mathrm{C}} (Cp_{\mathrm{H_2O(v)}} - Cp_{\mathrm{H_2O(l)}})dT \,. \tag{4-17}$$

The dehydration temperature of the dihydrated sodium naproxen to the monohydrated species is 60.7°C for the first water removal in Chapter 3. However, the heat of dehydration of the dihydrate to the monohydrate is not clear because two endothermic peaks overlapped. In Chapter 3, the heat of dehydration for the dihydrate to the anhydrate is 376.8 J/g dihydrate and that for the monohydrate to the anhydrate is 207.3 J/g monohydrate. Since the units for two enthalpies are different simple subtraction of 207.3 from 376.8 does not result in the heat of dehydration of the dihydrate to the monohydrate. Thus, two heats of dehydration should be converted to those with the same unit. In Chapter 3, the way to convert the unit for the heat of fusion was derived. This method can be applied to convert the unit for the heat of solution.

$$\Delta\hat{H}_{\mathrm{sol},0} = \frac{w_n}{w_0}\Delta\hat{H}_{\mathrm{sol},n} = \left(\frac{1}{1-x_{\mathrm{H_2O},n}}\right)\Delta\hat{H}_{\mathrm{sol},n} \tag{4-18}$$

where w is the mass of the samples, $x_{\mathrm{H_2O},n}$ is the mass fraction of water in the indicated species. $x_{\mathrm{H_2O},n}$ was determined by TGA and 0.06832 for the monohydrate and 0.12957 for the dihydrate were reported by Kim and Rousseau.[54] The converted heats of dehydration of the monohydrate and the dihydrate are 222.5 J/g anhydrate and 432.9 J/g anhydrate, respectively. Now, the heat of dehydration of the dihydrate to the monohydrate is determined by subtracting 222.5 J/g anhydrate from 432.9 J/g anhydrate and reconverted to the heat of solution with the unit of J/g dihydrate, resulting in 183.1 J/g dihydrate.

Using the heat of solution of the monohydrated sodium naproxen (14.1 kJ/mol), which was evaluated from the van't Hoff plot in Figure 4-10, the heat of solution of the dihydrated species in aqueous solution containing 64 mol% methanol can be estimated as

26.1 kJ/mol. There is a 7.1% difference between the estimated value and the value determined from the dihydrate portion of the van't Hoff plot in Figure 4-10 (28.1 kJ/mol).

Khankari et al. (1992)[53] suggested that a hydrated species may first be transformed to an intermediate state before a transformation to a final stable form. Such an intermediate state was assumed to have a lattice structure that is different from both of the pseudopolymorphs.

A generalized description of the phenomena and the associated enthalpy changes in DSC may be represented as

$$\mathrm{A}\cdot n\mathrm{H_2O(s)} \rightarrow \mathrm{A}^*\mathrm{(s)} + n\mathrm{H_2O(l)} \qquad \text{at } T = T_\mathrm{d} \tag{4-19}$$

$$\Delta\hat{H}^*_{\mathrm{d},n} = \hat{H}_{0^*\mathrm{(s)}} + n\hat{H}_{\mathrm{H_2O(l)}} - \hat{H}_{n\mathrm{(s)}} \tag{4-20}$$

$$\mathrm{A}^*\mathrm{(s)} \rightarrow \mathrm{A(s)} \qquad \text{at } T = T_\mathrm{d} \tag{4-21}$$

$$\Delta\hat{H}_{\mathrm{trans}} = \hat{H}_{0\mathrm{(s)}} - \hat{H}_{0^*\mathrm{(s)}} \tag{4-22}$$

$$\mathrm{H_2O(l)} \rightarrow \mathrm{H_2O(v)} \qquad \text{at } T = 100^\circ\mathrm{C} \tag{4-23}$$

$$\Delta\hat{H}_{\mathrm{vap,H_2O}} = \hat{H}_{\mathrm{H_2O(v)}} - \hat{H}_{\mathrm{H_2O(l)}} \tag{4-24}$$

where subscript 0^* represents a polymorph of the anhydrous form. When the hydrate with n water molecules or the anhydrous species is dissolved, the processes and enthalpy changes are given by

$$\mathrm{A}\cdot n\mathrm{H_2O(s)} \rightarrow \mathrm{A(aq)} + n\mathrm{H_2O(l)} \tag{4-25}$$

$$\Delta\hat{H}_{\mathrm{sol},n} = \hat{H}_{0\mathrm{(aq)}} + n\hat{H}_{\mathrm{H_2O(l)}} - \hat{H}_{n\mathrm{(s)}} \tag{4-26}$$

$$\mathrm{A(s)} + n\mathrm{H_2O(l)} \rightarrow \mathrm{A(aq)} + n\mathrm{H_2O(l)} \tag{4-27}$$

$$\Delta\hat{H}_{\mathrm{sol},0} = \hat{H}_{0\mathrm{(aq)}} - \hat{H}_{0\mathrm{(s)}} \tag{4-28}$$

where $\Delta\hat{H}_{sol}$ is the heat of solution.

Grant and Higuchi (1990)[22] showed that the heat of hydration $\Delta\hat{H}_H$ can be expressed in terms of the heats of solution of the anhydrate and the hydrate.

$$\Delta\hat{H}_H = \Delta\hat{H}_{sol,0} - \Delta\hat{H}_{sol,n} \tag{4-29}$$

Combining this result with that of Equations 4-26, 4-28, 4-16 and 4-24 makes clear that the heat of hydration and the heat of dehydration as measured by DSC, differ by the heat of vaporization of water; that is,

$$\Delta\hat{H}_H = n\Delta\hat{H}_{vap,H_2O} - \Delta\hat{H}_{d,n} - n\int_{T_d}^{100}(Cp_{H_2O(v)} - Cp_{H_2O(l)})dT \tag{4-30}$$

4.4.5 Crystal habit of pseudopolymorphs of sodium naproxen

As mentioned earlier, dihydrated sodium naproxen in pure water has needle-like crystals, which made it difficult to take liquid samples from the equilibrium cell. That is because the needle-like crystals form networks and the captured solution by the networks is not easily sucked through a needle by a syringe. Crystal photographs are shown in Figure 4-12. Thin and long crystals are placed in the center of the figure. Part of the figure looks dark because of the networks.

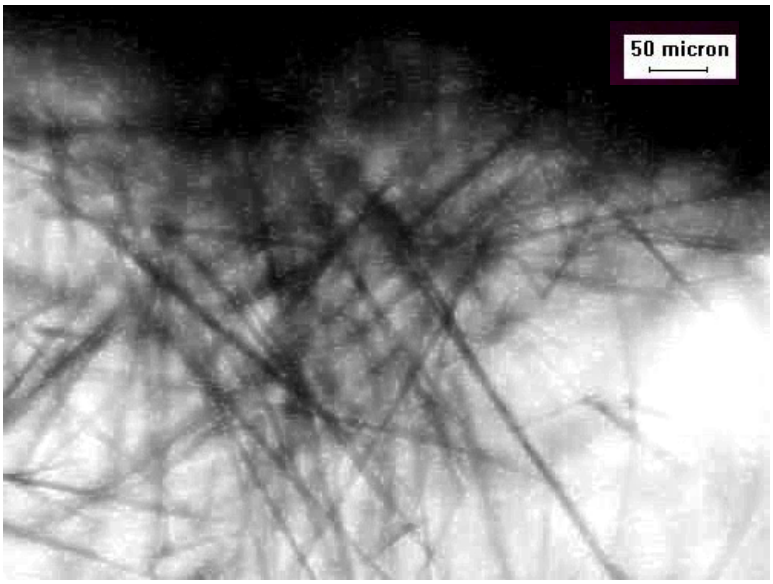

Figure 4-12. Photomicrographs of dihydrated sodium naproxen in pure water at 23°C

Dihydrated sodium naproxen in the mixture of water and methanol also formed needle-like crystals as shown in Figure 4-13. However, the aspect ratio is much smaller than that for the dihydrate in pure water and the crystals do not form networks.

Monohydrated crystals in the mixture in Figure 4-14 are much bigger than the dihydrated crystals and the needle-like form no longer exists. As mentioned earlier, since crystals with the shape in Figure 4-14 did not form networks, which caused difficulty in taking samples from the cell, the temperature range investigated for the solubility of sodium naproxen in the mixture was wider than that in pure water.

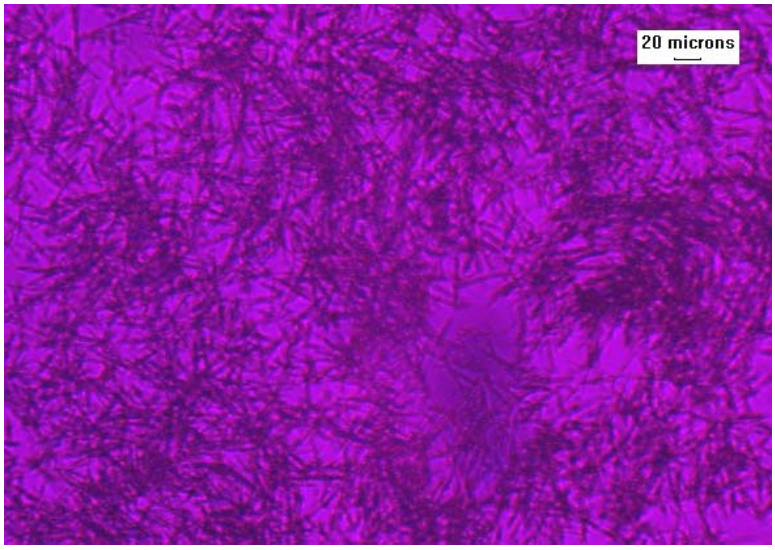

Figure 4-13. Photomicrographs of dihydrated sodium naproxen in aqueous solution containing 64 mol% methanol at 10°C

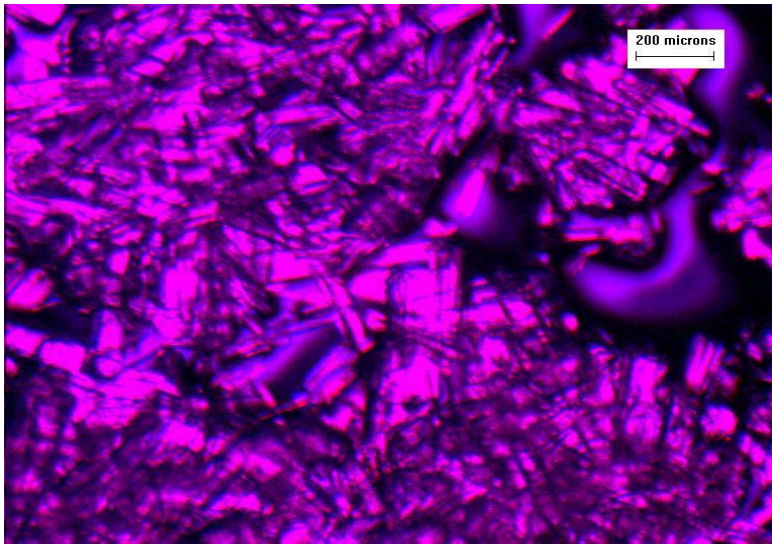

Figure 4-14. Photomicrographs of monohydrated sodium naproxen in aqueous solution containing 64 mol% methanol at 25°C

4.5 CONCLUSIONS

The solubilities of sodium naproxen were measured, using an equilibrium cell with solution compositions determined by HPLC. In aqueous solutions containing 64 mol% methanol, it was observed that a pseudopolymorphic transition of sodium naproxen between the dihydrate and the monohydrate occurred at 19.6°C. However, in pure water, according to the study on solubilities of sodium naproxen by Mendéz del Río (2004)[45] and Kim et al.[56], the transition between the dihydrated form and the anhydrous one was observed at 29.8°C, implying that the monohydrated form cannot be recovered from pure water. Therefore, it can be concluded that adjusting solvent compositions is one possible method to control the formation of pseudopolymorphic forms of pharmaceutical interest.

A new thermodynamic cycle to estimate the heat of solution using the heat of dehydration was developed. This method was successfully applied to calculate the heats of solution of pseudopolymorphs of sodium naproxen, giving good agreements between the calculated heat of solution and the experimental heat of solution.

The thermodynamic cycle has very interesting thermodynamic implication. For the enantiotropic system, if two pseudopolymorphic forms exist and Form I has a lower degree of hydration than Form II, Form I is more stable over a higher temperature range above the transition temperature and Form II over a lower temperature range. This relationship has not been explained theoretically. By rearranging Equation 4-17, the difference between the heats of solution of two pseudopolymorphs can be derived.

$$\Delta\hat{H}_{\mathrm{sol},n} - \Delta\hat{H}_{\mathrm{sol},\,m} = \Delta\hat{H}_{\mathrm{d},n\to m} - (n-m)\Delta\hat{H}_{\mathrm{vap,H_2O}} + (n-m)\int_{T_d}^{100^\circ\mathrm{C}} (Cp_{\mathrm{H_2O(v)}} - Cp_{\mathrm{H_2O(l)}})dT \tag{4-30}$$

Since *m* is less than *n* by definition, $\Delta\hat{H}_{\text{sol},\,m}$ and $\Delta\hat{H}_{\text{sol},n}$ are the heats of solution of Form I and Form II, respectively. On the right-hand side of Equation 4-30, the integral term is relatively small and the first term is always greater than the second. Therefore, the quantity on the right-hand side is always positive and, consequently, the heat of solution of Form I is always smaller than that of Form II. The smaller heat of solution means a lower slope of the solubility curve in van't Hoff plot. Therefore, it can be concluded that, for the enantiotropic system, a pseudopolymorph with a lower degree of hydration is more stable over a higher temperature range above the transition temperature.

CHAPTER 5

CRYSTAL STRUCTURE OF ANHYDROUS SODIUM NAPROXEN, $C_{14}H_{13}O_3Na$

Crystal structures are providing very important information to understand the chemical and physical properties of organic compounds. Different polymorphs and pseudopolymorphs of pharmaceutical compounds may be generated during processing steps such as crystallization, lyophilization, wet granulation, aqueous film-coating or spray-drying, and through storage in humid environments.[57] The pseudopolymorphs differ in properties such as melting points, crystal shape, dissolution kinetics and other important ways.

The structure of naproxen[34] has been determined previously and the structure of the monohydrated sodium salt[11] is also known. However, the structure of the anhydrous form of the sodium salt has not previously been determined. The present work was undertaken to determine the structure of anhydrous sodium naproxen and its relationship to that of the monohydrate.

5.1 CRYSTALLIZATION OF SINGLE CRYSTALS

Sodium naproxen was supplied by Albemarle Corp. It was used without further purification in obtaining the crystals studied. Single crystals of anhydrous sodium naproxen were prepared by slow evaporation of a saturated solution in methanol at room temperature as shown in Figure 5-1. After the crystals were grown, they were washed with cyclohexane to inhibit powder generation on the surface of the crystals.

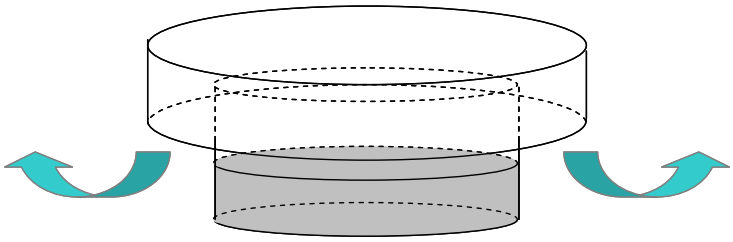

Figure 5-1. Schematic diagram of slow evaporation

5.2 RESULTS AND DISCUSSION

The asymmetric unit of anhydrous sodium naproxen contains two independent molecules, denoted A and B as shown in Figure 5-2. There are significant differences between the torsion angles O1a-C12a-C11a-C13a (-10.4(3) º) of molecule A and O1b-C12b-C11b-C13b (-37.7(3) º) of molecule B as depicted in Figures 5-3a and 5-3b. The difference in the torsion angles seems to be due to interactions between carboxyl O and Na.

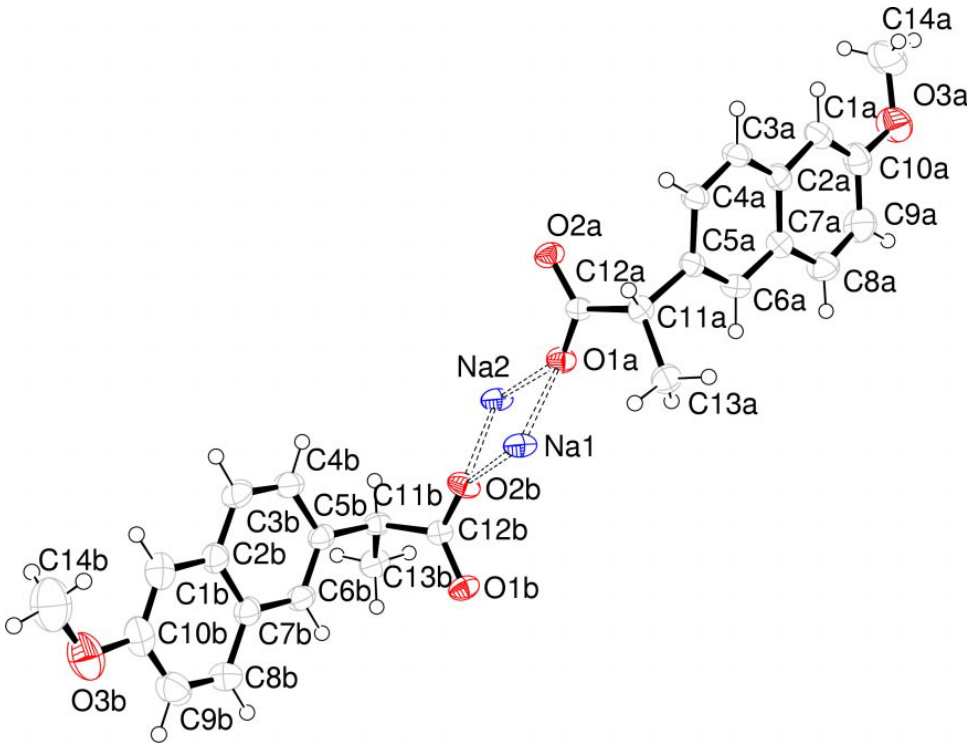

Figure 5-2. A perspective drawing of two independent molecule A and B of anhydrate of sodium naproxen (50% probability ellipsoids)

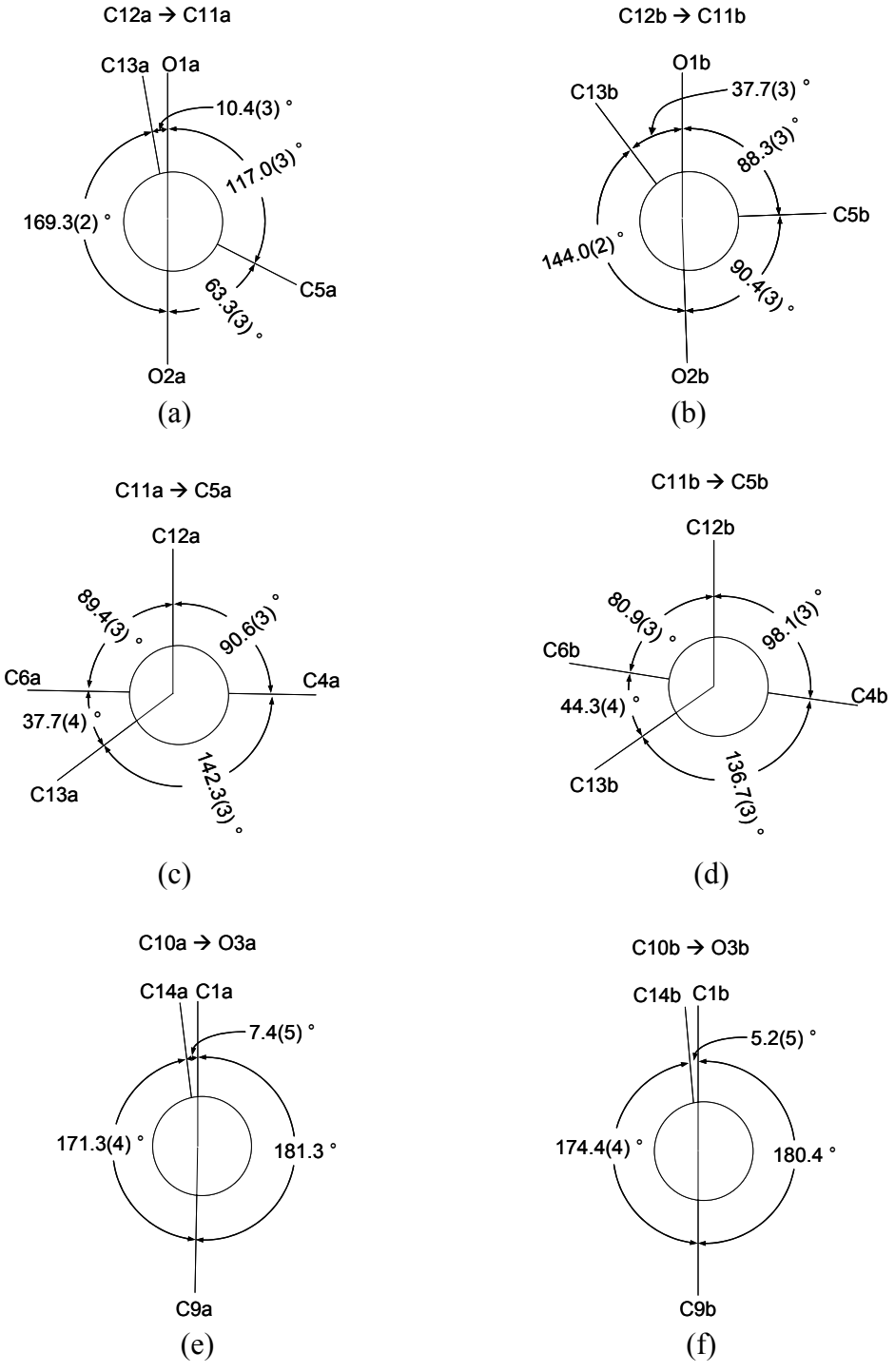

Figure 5-3. Newman projections of anhydrous sodium naproxen along the bonds of (a) C12a–C11a, (b) C12b–C11b, (c) C11a–C5a, (d) C11b–C5b, (e) C10a–O3a, and (f) C10b–O3b

A torsion angle around the bond between a chiral center (C11) and a naphthyl group (C5) is also flexible. In the anhydrate the torsion angle of C13–C11–C5–C6 is 37.7(4) º for molecule A and 44.3(4) º for molecule B as shown in Figures 5-3c and 5-3d while in the monohydrate the corresponding torsion angle is 11.5 º.

The methoxy group in each molecule A and B is essentially coplanar with the naphthyl ring bringing about an enlargement of the C1a–C10a–O3a and C1b–C10b–O3b angles and narrowing of the C9a–C10a–O3a and C9b–C10b–O3b angles (Table 5-1). A similar effect was previously reported and attributed to some degree of conjugation between O in the methoxy group and the benzene ring, giving rise additionally to some shortening of the C-O bond.[58]

The molecular geometry in the anhydrous material was compared to that in the monohydrate. The bond lengths and bond angles of the methoxy group for the corresponding atoms are very similar to one another. However, the torsion angle of -4.1° for the methoxy group in the monohydrate is slightly smaller than those found in the anhydrous material (C1a–C10a–O3a–C14a = -7.4(5) º in molecule A, C1b–C10b–O3b–C14b = -5.2(5) º in molecule B as shown in Figure 5-3e and 5-3f, respectively).

Both the anhydrous and monohydrated salts crystallize in space group, $P2_1$. However, the monohydrate has only one ion pair in the asymmetric unit, whereas the anhydrous material has two anions and two cations. The removal of water leads to a slight change in packing and crystal volumes. In order to compare the crystal volumes, the volume of the monohydrate was doubled since $Z' = 2$ for the anhydrous material. The unit-cell volume of the anhydrous material is smaller than the doubled unit cell volume of

the monohydrate by 11.33%. The change in packing and crystal volumes is presumably driven by changes in sodium coordination as the water is removed.

In the anhydrous material, the Na^+ ion is four-coordinate (Table 5-1). It has four nonequivalent Na-O bonds that involve the carboxyl groups of four different naproxen anions. However, in the monohydrate the Na^+ has five Na-O interactions involving four carboxyl oxygen atoms in three naproxen molecules and an oxygen atom from a water molecule. The removal of water from the monohydrate cause a slight change in packing as the carboxyl groups now have to satisfy the coordination needs of the sodium.

Summary of crystallographic data is tabulated in Table 5-2.

Table 5-1. Selected geometric parameters (Å, °) for sodium naproxen

Angles		Torsion angles	
Na1-O1b^{i}	2.259 (2)	O3b-C10b-C1b	125.0 (4)
Na1-O2b	2.270 (2)	O3b-C10b-C9b	114.9 (3)
Na1-O1b^{ii}	2.290 (2)	C1a-C10a-O3a	125.3 (3)
Na1-O1a	2.394 (2)	O3a-C10a-C9a	114.4 (3)
Na2-O2a^{iii}	2.276 (2)		
Na2-O2a^{iv}	2.291 (2)		
Na2-O1a	2.328 (2)		
Na2-O2b	2.341 (2)		

Symmetry codes: (i) –x, y+1/2, -z; (ii) x, y+1, z; (iii) –x-1, y-1/2, -z; (iv) x, y-1, z

Table 5-2. Crystallographic Data and Refinement Details

Empirical formula	$C_{14}H_{13}NaO_3$
Color/shape	Colorless/plate
Formula weight	252.23
Temperature, K	298 (2)
Wavelength, Å	0.71073
Crystal system	Monoclinic
Space group	P2(1)
Unit cell dimensions	a = 9.969(3)
	b = 5.9346(16)
	c = 20.823(6)
	α = 90
	β = 102.025(6)
	γ = 90
Volume, Å ^{3}	1204.9(6)
Z	4
Density (calculated), Mg/m^3	1.417
Diffractometer/scan	Bruker D8 SMART/CCD area detector
θ range fro data collection, deg	2.5 to 27.4
Reflection measured	6886
Independent reflections	4036 [R_{int} = 0.035]
restraints / parameters	1 / 347
Goodness-of-fit on F2	1.048
Final R indices [I>2σ (I)]	R_1 = 0.0475, wR_2 = 0.1211
R indices (all data)	R_1 = 0.0543, wR_2 = 0.1245

CHAPTER 6

PROPAGATION OF SOLID-STATE TRANSFORMATIONS BY DEHYDRATION AND STABILIZATION OF PSEUDOPOLYMORPHIC FORMS OF SODIUM NAPROXEN

The importance of crystal hydrates has been recognized and addressed for several decades. This attention is due to the changes in physical and chemical properties (e.g., density, solubility, dissolution rate, and bioavailability) that are brought about with insertion of water molecules in the lattice structure.[2, 57]

Dehydration and/or rehydration of crystalline materials may depend on environmental conditions and processing. For example, Cox et al.[59] obtained the water content of cromolyn sodium as a function of relative humidity during hydration and dehydration, and Braga et al.[8] reported that a supermolecular salt $[Co^{III}(\eta^5\text{-}C_5H_5)_2]^+[Fe(\eta^5\text{-}C_5H_4CO_2H)(\ \eta^5\text{-}C_5H_4CO_2)]^-$ was transformed to the monohydrated species by grinding. Moreover, crystal dehydration can result in a variety of consequences, essentially all of which are related to the dehydrated species having a structure that is different from the hydrate. The differences go far beyond a simple removal of water from the lattice structure and correctly lead to the view that the dehydrated compound is a different crystalline species from the hydrate. For example,

the dehydration of crystalline cephradine dihydrate produces an amorphous solid that undergoes subsequent oxidation,[3] and the dehydrated compound of thiamine hydrochloride monohydrate retains its packing arrangement, but with lower density.[60]

Dehydration has been studied using thermogravimetric analysis (TGA), differential scanning calorimetry (DSC), and hot-stage microscopy (HSM) to characterize pharmaceutical compounds.[61, 62] Dehydration and rehydration have been carried out in sealed systems in which the relative humidity is controlled by saturated salt solutions in the container,[59] and dehydration kinetics has been studied by isothermal dehydration.[37, 40, 41]

Relatively large (120μm) monohydrated sodium naproxen crystals are produced using a patented process.[9] and their size is reduced during a drying process that yields commercially available anhydrous sodium naproxen. The present research was motivated by and focused on the mechanisms by which the size reduction occurred. In the present study, dehydrations of dihydrated powder samples and monohydrated single crystals were carried out. The relative stability of pseudopolymorphs of sodium naproxen was determined by the dehydration of the dihydrated powder samples. In the experiments of the dehydration of the monohydrated single crystals, it was observed that dehydration occurred anisotropically and the surface of dehydrated samples was covered with a lot of cracks. These observations were rationalized by considering the crystal lattice structure of the monohydrate. The study presented here also showed similarity and stabilization forces of crystal structures for the monohydrate and the anhydrate, providing an insight into how the lattice structure of the anhydrous crystalline species can be stable after the removal of water.

6.1 EXPERIMENTAL SECTION

6.1.1 Materials

Anhydrous sodium naproxen supplied by Albemarle Corporation was used for all the experiments without further purification or processing. Crystalline powders of the dihydrated sodium naproxen were produced as described in Chapter 3 and used for the experiment of dehydration of powder sodium naproxen dihydrate. Single crystals of monohydrated species for experiments of dehydration in an oven and a desiccator were recrystallized from a solvent containing 64.0 mol% methanol in water solution where sodium naproxen was dissolved.

6.1.2 Powder X-ray Diffraction (PXRD)

Crystals were analyzed and identified by powder x-ray diffraction (PXRD) analysis using Philips® PW3040-PRO automatic powder diffractometer with X'Pert Data Collector 2.0d software. Square aluminum holders with a recessed cavity that is 15 mm × 20 mm × 1.8 mm were used and about 1 to 2 g of crystals was required for an analysis. Each crystalline sample was ground to a fine powder with a mortar and pestle before it was placed into the sample holder. Copper Kα radiation was used. The radiation for Copper Kα1 is 1.541Å. A voltage and a current are 40 kV and 30mA, respectively. The PXRD patterns were made over a diffraction-angle (2θ) range of 3 to 40º, with a step size of 0.02º and a counting time of 1 second per step. X'Celerator was used and diffraction patterns were collected very quickly.

6.1.3 Thermogravimetric Analysis (TGA)

The loss of mass from sodium naproxen samples was analyzed with a TG/DTA 320 instrument (Seiko Instruments Inc.). Samples of mass 10 to 15 mg were heated from 20 ºC to 100 ºC in aluminum pans that were 5 mm in diameter. An empty aluminum pan was used as the reference. A heating rate of 10 ºC/min was employed with a nitrogen purging rate of 90 mL/min. Open pans without lids were used and prominent weight losses were observed.

6.1.4 Scanning Electron Microscopy (SEM)

After dehydration experiments, a surface of a dehydrated sample was investigated with a field emission SEM, Model S-800, Hitachi, Japan. The dehydrated crystal sample was attached to a round sample holder. The sample was coated with gold because it is nonconducting. A magnification ratio of 2000 and a voltage of 15keV were used.

6.1.5 Microscopy

Single-crystal samples were analyzed under a ML 9000 instrument made by MEIJI, Japan, with a 10X objective lens. The microscope was equipped with a Sony digital camera DKC-500 that converted the focused light into a digital signal. This signal was visualized by Image-Pro Plus version 4.5.

6.1.6 Visualization

Cerius^2 version 4.2, Accelrys, was used to visualize molecular structures of anhydrous and monohydrated sodium naproxen. The CIF file for sodium naproxen

anhydrate was imported and displayed on a screen. For the monohydrated species, crystal builder module was used. Average atom positions and thermal factors, unit cell constants and space groups from the study by Kim et al.[11] were entered into the crystal builder module and the resulting structure was explored for the present research. Visualizing parts of molecules was performed by highlighting only desired atoms and selecting "Show Only Selected Atoms" function in "Atom Visibility."

6.1.7 Dehydration of Crystalline Powders of Sodium Naproxen

Dihydrated crystalline samples produced by the procedure mentioned above were ground gently by a mortar and pestle and placed in a desiccator. Relative humidity (RH) was controlled at 0% with drierite, anhydrous $CaSO_4$, manufactured by W. A. Hammond Drierite Company, Xenia, Ohio. Small samples were taken from the desiccator at various times and analyzed with PXRD and TGA.

6.1.8 Dehydration of Single Crystals of Sodium Naproxen

Rapid dehydration of single crystals was performed in an oven. The temperature inside the oven was controlled at 80 ºC. For analysis of the crystal, it was taken from the oven and analyzed under the microscope. Since the evolution of the dehydration process of a given sample was to be observed, the analyzed sample was returned to the oven between analyses. At the conclusion of a drying experiment, the dried sample was coated with gold and analyzed by SEM. Slow dehydration of single crystals was also carried out in a desiccator in which RH was controlled at 0%.

6.2 RESULTS AND DISCUSSION

6.2.1 Dehydration of Dihydrated Sodium Naproxen

Dehydration results in the transformation of hydrated species to other pseudopolymorphic forms that have a lower degree of hydration. As a crystal loses water from its structure, the remaining units in the lattice may reposition themselves. We examined the course of dehydration of the dihydrate of sodium naproxen using the procedure described above. The experiment was intended to determine the relative stability of the pseudopolymorphs and whether or not one or more intermediate compounds were formed during the dehydration.

Figure 6-1 shows PXRD patterns of samples of sodium naproxen containing varying amounts of water, ranging from 0 to 12.49 wt%, in the crystal structure. Only three stable pseudopolymorphs (the anhydrate, monohydrate, and dihydrate) were observed in the present study; these contained 0, 6.72 and 12.49 wt% water, respectively.

Although PXRD patterns were obtained over a broad range, those in Figure 6-1 (below 15º) were sufficient to identify the three species and the route of dehydration. As shown by the dashed vertical lines superimposed on the figure, there were two peaks for each pseudopolymorph that were prominent and clearly separated, and that may be considered characteristic because they do not overlap peaks of other pseudopolymorphs. According to crystallographic data for the monohydrate[11] and the anhydrate (Chapter 5) of sodium naproxen, the chosen peaks for the monohydrate correspond to interplanar spacing of (*h*00) planes and the peaks for the anhydrate correspond to interplanar spacing of (00*l*) planes. For the dihydrate, Miller indices for peaks were not available because the

structure of the dihydrated sodium naproxen has not been determined. Peaks at 4.4º and 13.1º for the anhydrate result from diffractions of (001) and (003) planes while peaks at 4.2º and 12.6º for the monohydrate are from (100) and (300) planes. Characteristic peaks at 4.0º and 11.9º for the dihydrate are also observed in Figure 6-1.

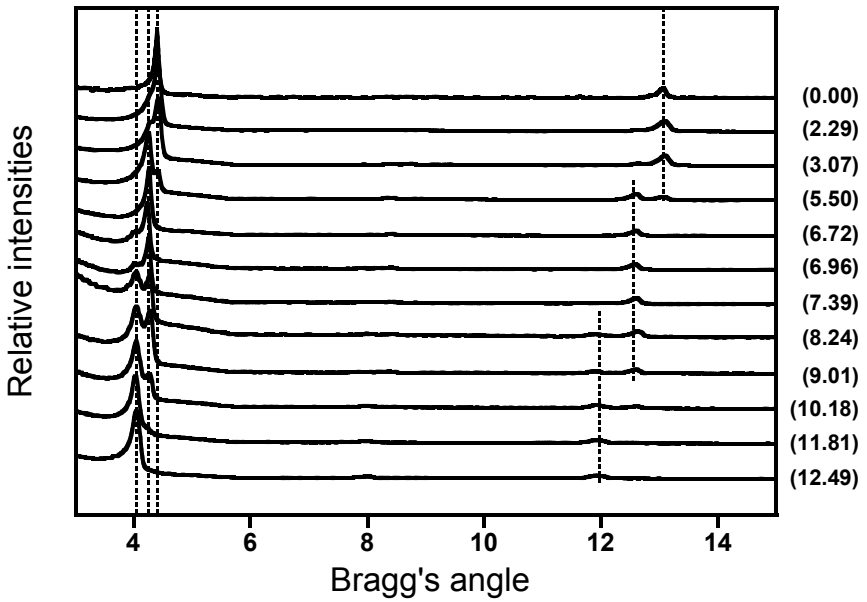

Figure 6-1. PXRD patterns of sodium naproxen samples containing varying amounts of water. The weight % water is shown to the right of the diagram. Samples were obtained by dehydration of dihydrated sodium naproxen in a desiccator

Figure 6-1 shows that as dehydrations occurred, the PXRD pattern evolved from that corresponding to one pure pseudopolymorph to another by first taking on the characteristics of a physical mixture of the two polymorphs. For example, the PXRD pattern of the sample with a water content of 9.01 wt% (which is between those of the dihydrate and monohydrate) has characteristic peaks corresponding to the dihydrate and the monohydrate; there are no indications of the formation of an intermediate structure as the dihydrate is transformed to the monohydrate. These data indicate that the sample analyzed was a simple mixture of the dihydrate and the monohydrate, which is unlike the case of cromolyn sodium[59] in which the lattice volume was slightly reduced without changing the orientation of the cromolyn sodium molecules as dehydration occurred.

The same behavior was exhibited by the sample that had a water content of 7.39 wt%; i.e., it showed peaks for the monohydrate and dihydrate and no others. Moreover, the characteristic peaks for the dihydrate were much smaller than those obtained with the sample that had a water content of 9.01 wt%. It can be concluded, then, that the relative amounts of the two pseudomorphs determine the relative intensity of the peaks found in samples having amounts of water between the dihydrate and the monohydrate. This behavior was also observed by Shefter et al.[40] with theophylline monohydrate.

TGA is commonly used to determine the water content of pharmaceutical hydrates, with the outcome of the analysis being a trace of the mass loss with respect to time or temperature, depending on the purpose of run. In Figure 6-2, TGA and dTG graphs are given for the samples of sodium naproxen that contain 7.39 wt% water (slightly more than would be in the monohydrate) and 9.01 wt% water (significantly more than would be in the monohydrate). The data in Figure 6-2a show a slight water

loss before the second mass loss from the monohydrate, while the data in Figure 6-2b represent two different and apparently independent dehydrations with the second mass loss corresponding to removal of water from the monohydrated species. Combining these results with those from the above powder x-ray diffraction analysis shows that the initial water loss in Figures 6-2a and 6-2b corresponds to that remaining from the dihydrate.

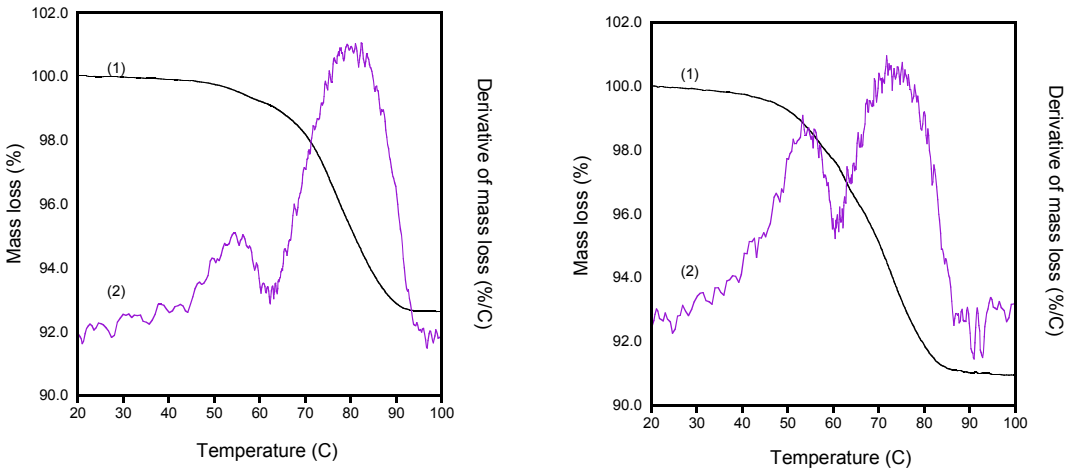

(a) (b)

Figure 6-2. Thermal analyses curves of (1) TGA and (2) dTG of samples with water content of (a) 7.39 wt% and (b) 9.01 wt%

The PXRD patterns in Figure 6-1 of samples containing an amount of water between the monohydrate (6.72 wt%) and the anhydrate (0 wt%) show behavior similar to that of samples between the dihydrate and the monohydrate. Namely, they showed peaks that are characteristic of the monohydrate and the anhydrate, rather new peaks that would result from the existence of an intermediate species. Again, the conclusion can be drawn that as dehydration of the monohydrate proceeded, intensities of peaks corresponding to the monohydrate diminished and peaks for the anhydrate appeared and became more significant, and there was no emergence and subsequent disappearance of peaks corresponding to one or more new species.

The above results show that the peaks corresponding to the anhydrate did not appear until those of the dihydrate completely disappeared. This observation implies that dehydration of the monohydrated crystalline powder started only after the dihydrated crystalline materials were totally dehydrated to the monohydrate. It can be concluded, then, that the monohydrated sodium naproxen is more stable than the dihydrated species, and that the anhydrate is more stable than the monohydrate. This conclusion is consistent with the study in Chapter 3 which showed that the dihydrate had a lower activation energy than the monohydrate and water in the dihydrate has very weak interactions with nearby molecules in the crystal lattice.

6.2.2 Dehydration of Single Crystals of the Monohydrated Sodium Naproxen

The progress of water removal was followed by observing the dehydration of single crystals of the monohydrated sodium naproxen. The outcome of this experiment helps explain why such dehydration results in destruction of the macroscopic crystal with drying. The experiment was carried out only with the monohydrated species because the available dihydrate crystals were thin, very long, and difficult to handle as discussed in Chapter 3.

The monohydrate single crystals were formed from a solvent containing 64.0 mol% methanol in water solution. Dehydration of single crystals was carried out by two protocols: (1) rapid dehydration in an oven and (2) slow dehydration in a desiccator. Figure 6-3 shows successive pictures of a sample that had been placed in an oven and observed every 10 minutes until the sample was completely dehydrated. Note that the initial sample was transparent, but a dark area denoting dehydration was propagated from the crystal edges to the center of the crystal; dehydration did not occur uniformly throughout the crystal body. Instead, there was a steady progression with a clear interface between the portion of the crystal that had been dehydrated and that which had not. Consequently, PXRD pattern of a sample which has two portions shows peaks corresponding to each portion.

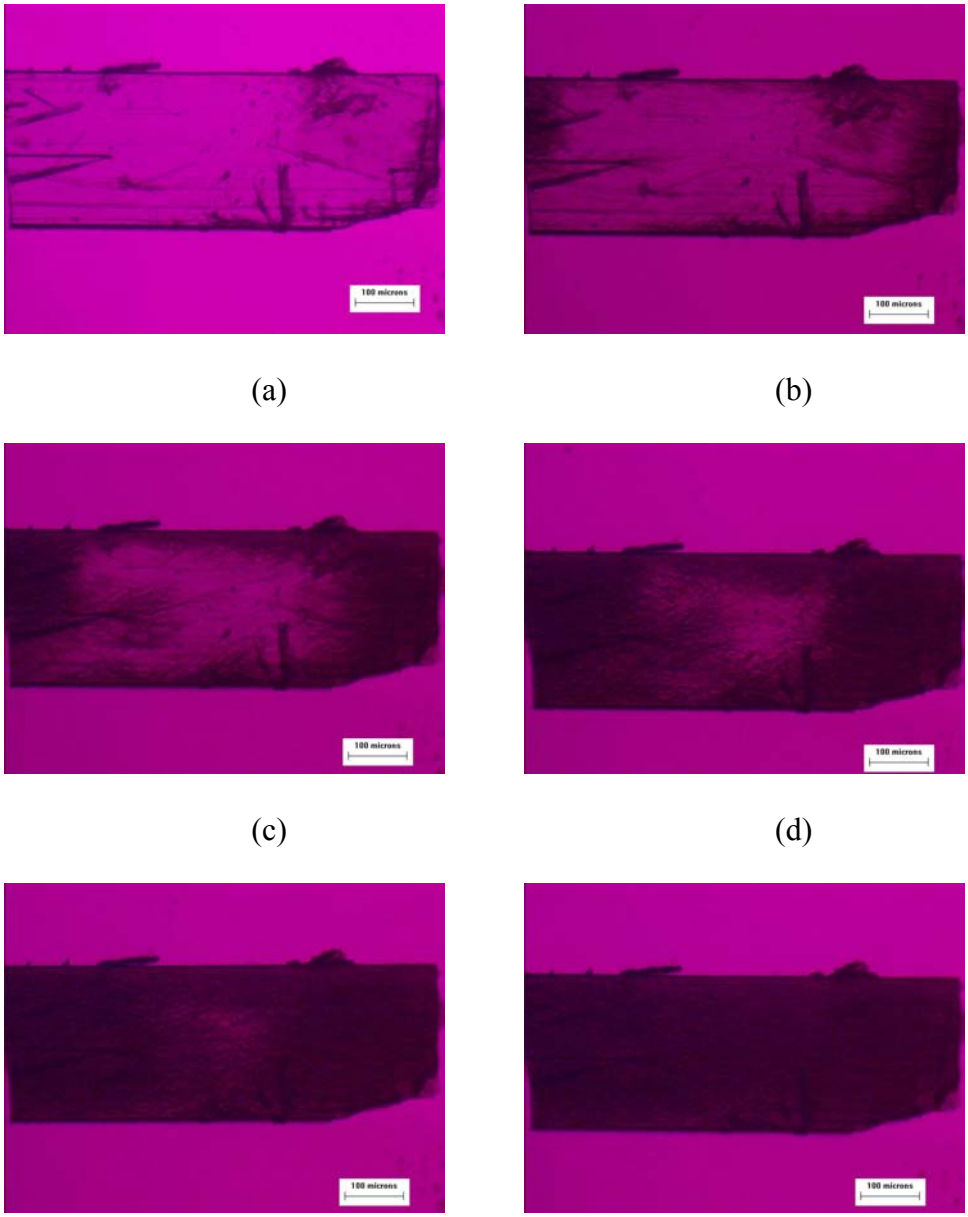

Figure 6-3. Photomicrographs of a single crystal that initially was monohydrated sodium naproxen before being rapidly dehydrated in an oven. The progress of the experiment is shown at (a) t = 0 minute, (b) t = 10 minutes, (c) t = 20 minutes, (d) t = 30 minutes, (e) t = 40 minutes and (f) t = 50 minutes. The scale mark in every graph is 100 micro meters long.

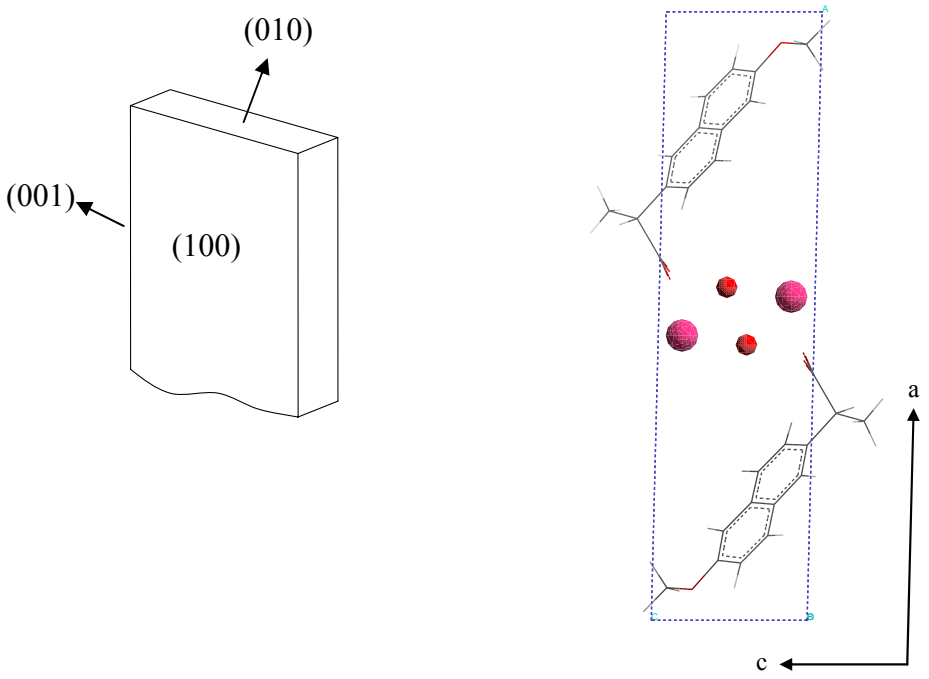

(a) (b)

Figure 6-4. (a) Miller indices of crystal faces and (b) a projection perpendicular to the $(0\bar{1}0)$ plane of the monohydrate of sodium naproxen showing water channels. In (b), sodium atoms and oxygen atoms in water are exaggerated for clarity and the larger circles represent sodium atoms and the smaller circles represent oxygen atoms in water.

The anisotropic dehydration in Figure 6-3 can be rationalized by considering the crystal lattice structure of the monohydrate in Figure 6-4. The crystal is dehydrated more rapidly along the *b*-axis and relatively slowly along the *c*-axis, and scarcely at all through (100) plane. This is consistent with our earlier reporting of a channel that allows movement of water molecules in monohydrated sodium naproxen in Chapter 3. Figure 6-4b clearly shows the water channel running along the *b*-axis and providing a path for movement of water out of the crystal, and resulting in the rapid dehydration of the single crystal along the *b*-axis. Water removal in the non-*b* directions can also be explained

from the lattice structure of the monohydrated sodium naproxen. Movement of water along the *c*-axis is blocked by sodium cations, making diffusion of water more difficult in that direction. Naproxen anions provide even greater obstacles to movement of water in the direction of the *a*-axis; it is much bulkier than sodium cations and, of course, they have large hydrophobic regions.

Figure 6-5 shows the progress of slow dehydration of monohydrated single crystals in a desiccator at ambient temperature. It had been thought that the slow dehydration of crystals may occur without a change in the crystal structure and, therefore, there would be no propagation of dark areas as samples dehydrated isotropically along the *b* and *c* axes. However, the PXRD pattern of the slowly dehydrated samples was identical to that of the anhydrous species. Slow dehydration also collapsed the lattice structure of the monohydrate, producing the anhydrous sodium naproxen; in other words, the outcome of slow dehydration in a desiccator was very similar to that from rapid dehydration an oven. Dehydration occurred most rapidly along the *b*-axis and water removal along the *a*-axis was almost non-existent. The most significant difference between rapid and slow dehydrations was the period of time required to dehydrate samples: 2 days in a desiccator, but only 50 minutes in an oven.

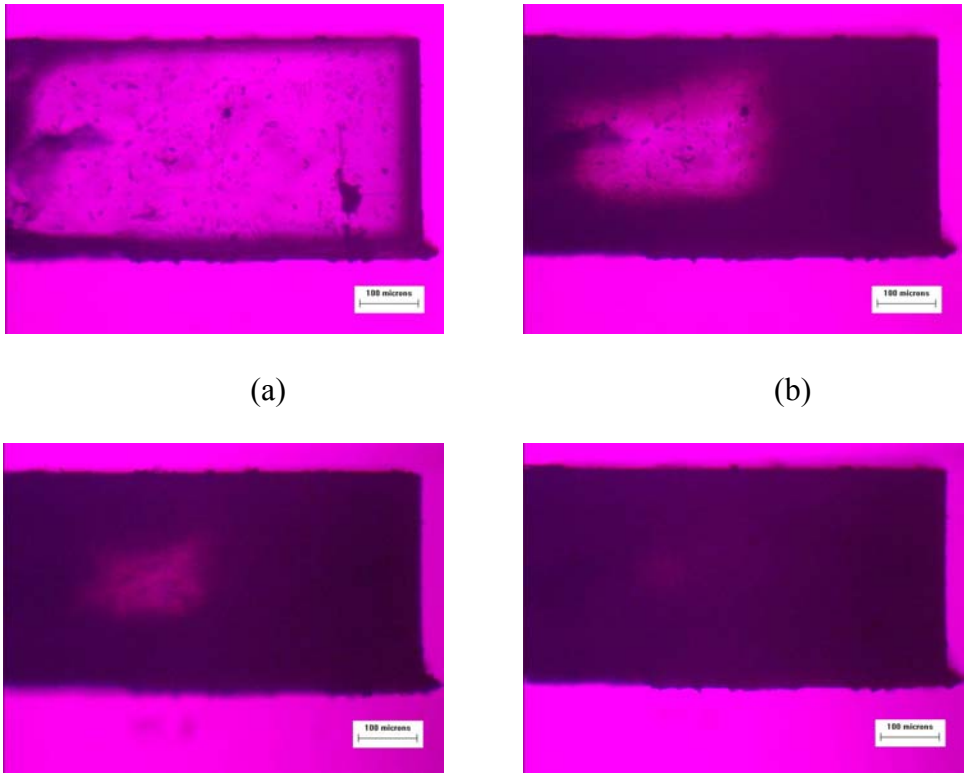

(a) (b)

(c) (d)

Figure 6-5. Photomicrographs of single crystals on monohydrated sodium naproxen slowly dehydrated in a desiccator. Progress of the experiment is shown at (a) t = 0 hour, (b) t = 24 hours, (c) t = 33 hours and (d) t = 42 hours.

Figure 6-6 shows an SEM photomicrograph of the surface of a dehydrated sample from rapid dehydration. The surface displays numerous cracks that made the dehydrated samples look dark under the microscope; note that these were aligned in the direction of *b*-axis. These cracks make the anhydrous sodium naproxen produced by dehydration very fragile and often result in the production of powder-like crystals.

The alignment of the cracks in Figure 6-6 can be explained by shrinkage of the unit cell as it is transformed from the monohydrate to the anhydrate. Table 6-1 provides a comparison of cell constants for the anhydrate and the monohydrate of sodium naproxen. Note that the greatest difference in cell constants is with the *c*-axis of the monohydrate, which is the *a*-axis of the anhydrate. That transition requires shrinkage of about 8.4 %, while the other transitions are a factor of 4 less significant. The significant shrinkage of interplanar spacing of (001) planes, which are normal to the *c*-axis of the monohydrate, generates stress and the cracks shown in Figure 6-6 are aligned along those planes.

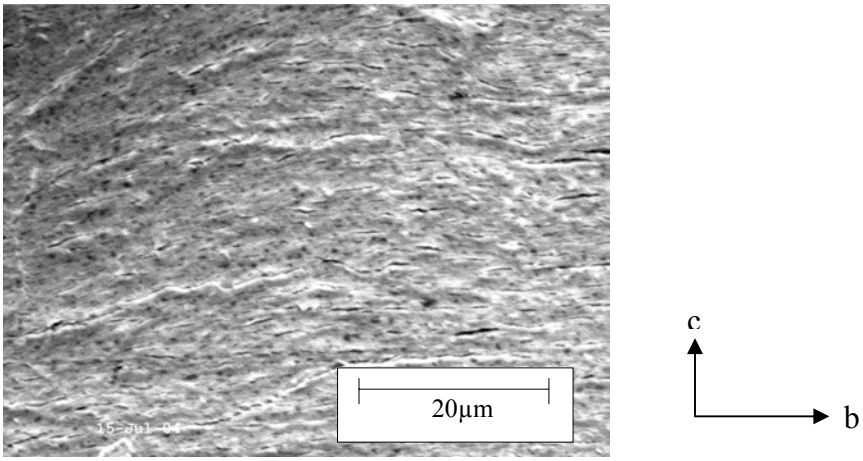

Figure 6-6. SEM analysis of a sample from rapid dehydration of the monohydrated sodium naproxen

Table 6-1. Shrinkage and expansion of cell constants by dehydration of the monohydrated sodium naproxen to the anhydrous species

Monohydrate[11]		Anhydrate (Chapter 5)[63]		Difference (%)[b]
Axis	Length(Å)[a]	Axis	Length(Å)[a]	
a	21.177(6)	*c*	20.823(6)	–1.672[c]
b	5.785(2)	*b*	5.9346(16)	+2.586[d]
c	5.443(2)	*a*	9.969(3)	–8.424[c]

[a] Lengths are means with their standard deviations.
[b] Values are calculated with means.
[c] Length of the axis is shrunk by dehydration.
[d] Length of the axis is expanded by dehydration.

6.2.3 Comparison of Structures and Stabilization Forces for Anhydrous and Monohydrated Sodium Naproxen

The removal of water results in changes in physical and energetic environments in the unit cell. Physically, spaces that were occupied by water are vacated upon dehydration, and they are filled with sodium cations and naproxen anions as the residual species rearrange in the unit cell that has a reduced cell volume. After water removal, hydrogen bonding no longer exists in the unit cell. Sodium cations and naproxen anions that fill the vacant spaces rearrange themselves into a new lattice without hydrogen bonds. This is unlike the case of crystalline cephradine dihydrate[3] in which the dihydrated cephradine is transformed to an amorphous solid by dehydration. In this section we describe the structural aspects that lead to the formation of the crystal lattice exhibited by the anhydrous crystalline species. The structure is stable, even though the hydrogen bonding associated with inclusion of water has been eliminated.

PXRD patterns of three pseudopolymorphs in Figure 6-1 show different peak positions and intensities, clearly showing differences in lattice structures. Both the anhydrous and the monohydrated crystals of sodium naproxen crystallize in space group $P2_1$ and the monoclinic crystal system. The volume of the unit cell for the anhydrate, 1204.9($Å^3$), is almost double the volume of the monohydrate, 666.61($Å^3$). The anhydrate has two anions and two cations in the asymmetric unit and totally four anions and four cations in the unit cell, whereas the monohydrate has only one ion pair in the asymmetric unit and totally two ion pairs in the unit cell. Therefore, the *c*-axis in the monohydrate was doubled when it was compared to *a*-axis in the anhydrate in Table 6-1.

Comparison of the lattice structures of the monohydrate and anhydrate pseudopolymorphs of sodium naproxen reveals similarities. Figure 6-7 uses the shorthand notation defined in Figure 6-7a to show diagrams of the unit cells for the monohydrate along *b*- and a-axes (Figures 6-7b and 6-7c, respectively), and for the anhydrate along the *b*-and c-axes (Figures 6-7d and 6-7e). Only the two oxygen atoms in the carboxyl group, four covalent bonds from the two oxygen atoms to the naphthyl group, a sodium atom, and an oxygen atom in the water of hydration are shown in Figures 6-7c and 6-7e to prevent bulky naproxen anions from obscuring the location of sodium anions and water molecules. This makes it easy to see clearly the arrangement of carboxyl groups, water molecules and sodium cations. In diagrams providing a view perpendicular to the $(0\bar{1}0)$ plane (Figures 6-7b and 6-7d), naproxen anions are aligned at similar angles. Water molecules and sodium cations in the monohydrate and sodium cations in the anhydrate are located between carboxyl groups. A simple adjustment of the non-water molecules of the monohydrate (Figure 6-7c) leads to the structure of the anhydrate (Figure 6-7e).

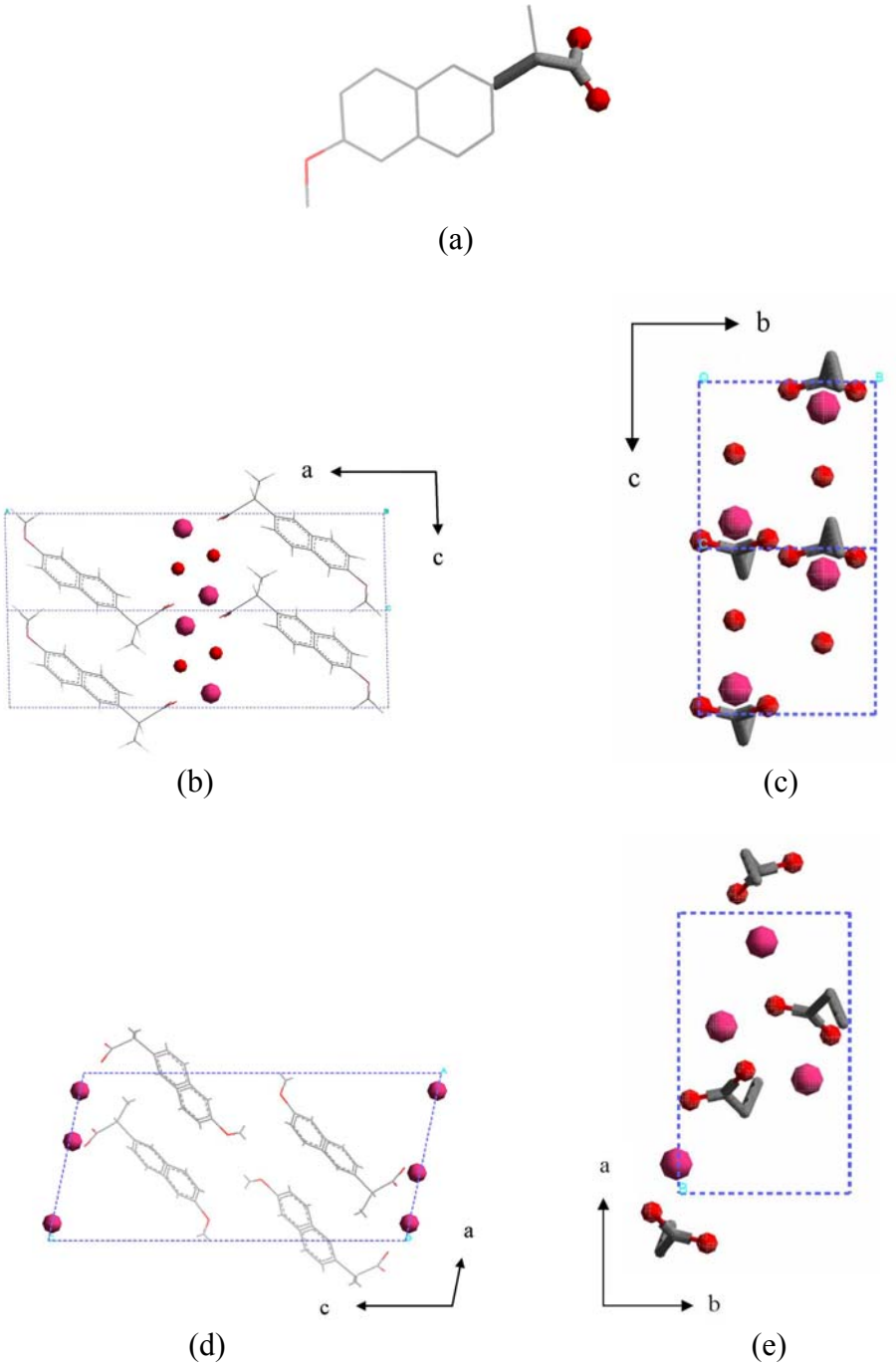

Figure 6-7. (a) Sodium naproxen with the sodium and hydrogen atoms omitted, (b) and (c) projections perpendicular to the $(0\,\bar{1}\,0)$ plane and the $(\bar{1}\,00)$ plane of the monohydrate, respectively, (d) and (e) projections perpendicular to the $(0\,\bar{1}\,0)$ plane and the $(00\,\bar{1})$ plane of the anhydrate, respectively. In (a), two oxygen atoms and four covalent bonds are exaggerated for emphasis. For clarity, only this portion of the molecule is depicted in (c) and (e). In (b) and (d), only sodium atoms and oxygen atoms in water are exaggerated. In (b), (c), (d) and (e), the larger circles represent sodium atoms and the smaller circles represent oxygen atoms.

As pointed out earlier, the *a*-axis in the monohydrate has the longest cell dimension, and it corresponds to the *c*-axis in the anhydrate, which is the longest in that species (see Figures 6-7b and 6-7d). This difference in nomenclature is because selection of the coordinate system is quite arbitrary, but it is restricted to the right-hand convention. The *b*-axis in $P2_1$ is the unique axis and cannot be altered. Consequently, the *c*-axis of the monohydrate corresponds to the *a*-axis in the anhydrate (Figures 6-7c and 6-7e). These dimensions were given and compared in Table 6-1.

The stabilization forces for packing in anhydrous and monohydrated sodium naproxen were found to be different. The dominant forces to stabilize the packing of the monohydrated sodium naproxen are hydrogen bonds between hydrogen in water and oxygen in the carboxyl group as well as an interaction of the sodium with the oxygen in water (Figure 6-8a). There is also the interaction between the sodium atom and the carboxyl oxygen atom (Figure 6-8b). Lengths of the electrostatic bonds between sodium and oxygen are listed in Table 6-2. Even though an oxygen atom in water is a little far from a sodium cation, 3.210Å, the sodium cation is surrounded by six oxygen atoms that form an octahedral cage with the sodium atom located in the cage. Cameron et al.[64] showed a typical view of sodium atoms in octahedral cages.

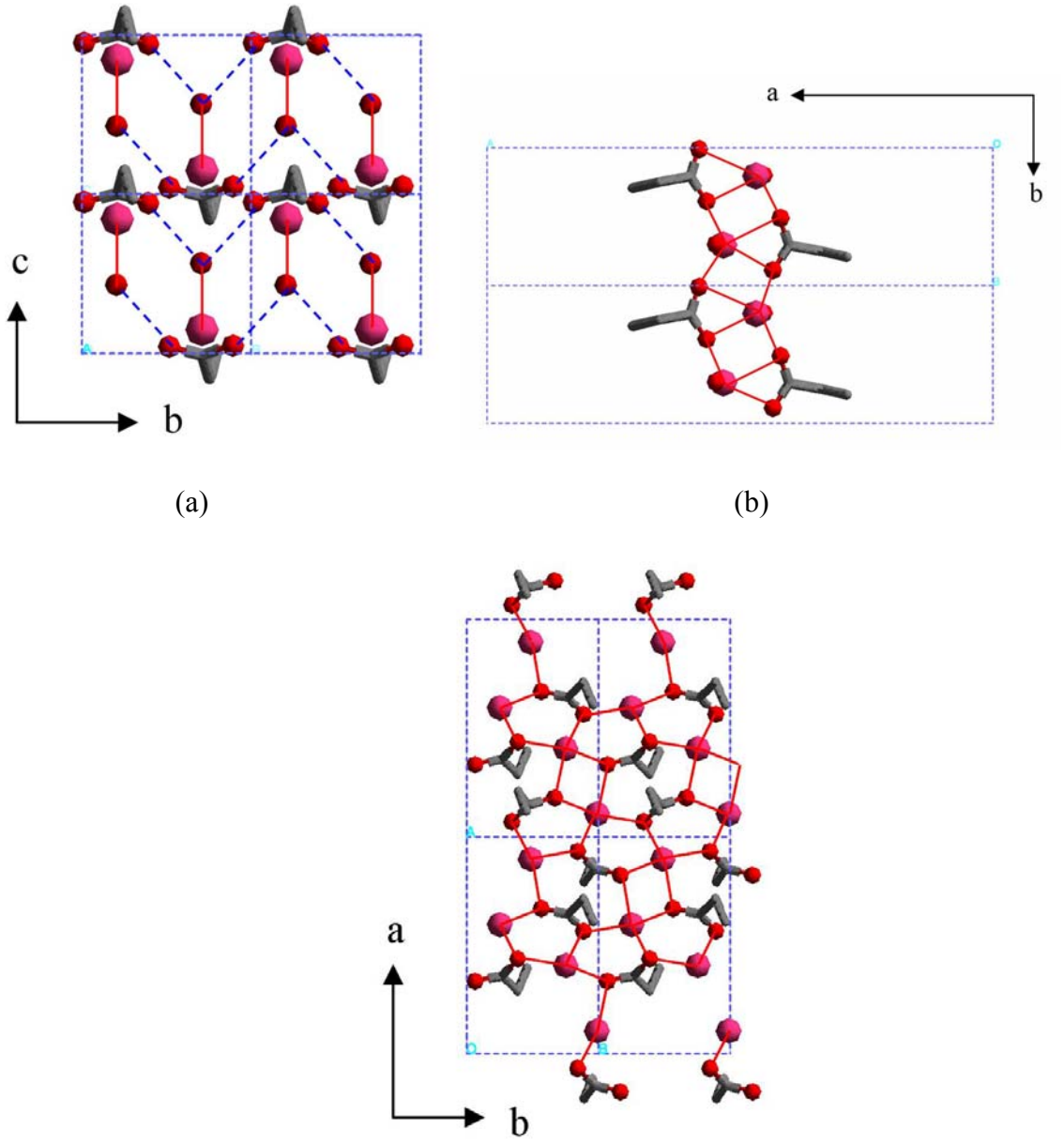

(a) (b)

(c)

Figure 6-8. Planar projections of the unit cell of the monohydrate of sodium naproxen: perpendicular to (a) the (100) plane, (b) the (001) plane, and (c) the $(00\bar{1})$ plane. Only a small portion of sodium naproxen was depicted using the definition in Figure 6-7a. The larger circles represent sodium atoms and the smaller circles represent oxygen atoms; solid red lines and dotted blue lines between atoms represent the Na–O type interactions and hydrogen bonds, respectively.

As pointed out earlier, the removal of water molecules from the unit cell of the monohydrate causes a change in packing structure leading to a reduction in the unit cell volume. Furthermore, the hydrogen bonds that existed in the monohydrate no longer exist, and the interactions between sodium and oxygen atoms in the carboxyl groups become the dominant force stabilizing the packing of the anhydrate. The sodium atom has four different Na–O interactions with carboxyl oxygen atoms of four different sodium naproxen molecules.

Table 6-2. Distances between Na and O by the Na–O type interactions

Pseudopolymorphs	Anhydrate[63]		Monohydrate[11]
	1[a]	2[a]	
Distance (Å)	2.259 (2)	2.276 (2)	2.272[b]
	2.270 (2)	2.291 (2)	2.328[b]
	2.290 (2)	2.328 (2)	2.375[b]
	2.394 (2)	2.341 (2)	2.690[b]
			2.273[c]
			3.210[c]

[a] The anhydrate has two independent sodium atoms in a unit cell.
[b] Bond distances are between a sodium cation and oxygen atoms in three different carboxyl groups.
[c] Bond distance is between a sodium cation and oxygen in water.

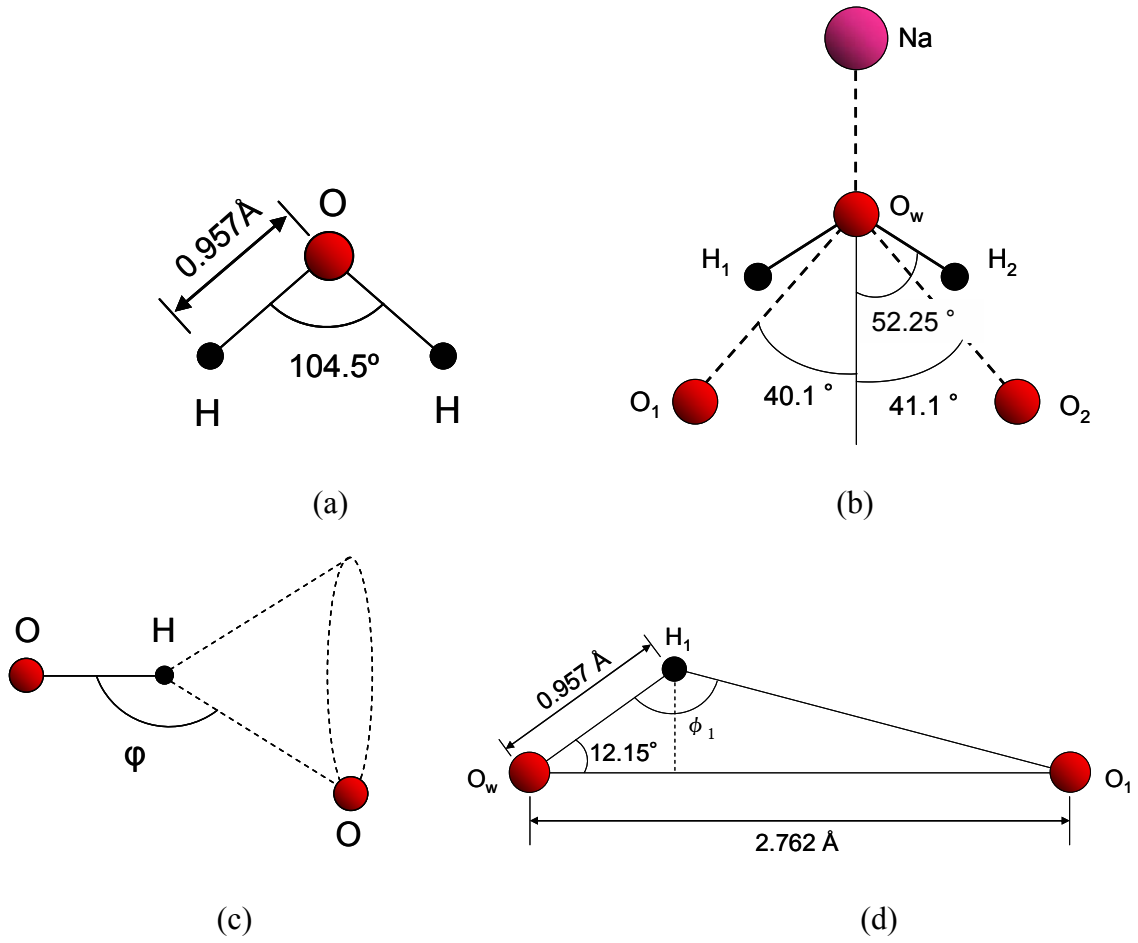

Figure 6-9. (a) Geometry of free water, (b) placement of hydrogen atoms in water, (c) the definition of hydrogen bond angle and (d) bond length and angle by hydrogen bonds

Table 6-3. Comparison of bond lengths and angles by hydrogen bonds

	Determined Structure		Calculated Values		Statistical Value[65]
	1	2	1	2	
O…O (Å)	2.762	2.841	-	-	2.7667 (0.0700)
H…O (Å)	-	-	1.837	1.911	1.8181 (0.0774)
Φ (°)	-	-	161.6	163.3	167.1 (6.5)

A more complete understanding of the structural forces stabilizing the monohydrated sodium naproxen can be obtained by examining the hydrogen bonds in the unit cell of this species. As shown in Table 6-3, the bond lengths between oxygen in water and oxygen in carboxyl groups compared favorably with values from the literature.[65] Figure 6-9 shows how water molecules were located and the corresponding bond angles and distances between hydrogen bond donors and acceptors. Since the location of hydrogen atoms was not determined by X-ray diffraction, it was necessary to place them intuitively around each oxygen atom in water. A free water molecule with an O–H bond length of 0.957Å and an H–O–H bond angle of 104.5º was introduced (Figure 6-9a).[2] Hydrogen atoms were located near oxygen with the assumption that they were symmetric with respect to the Na–O_w axis shown in Figure 6-9b. The assumption was verified by the symmetric positions of O_1 and O_2 along the Na–O_w axis, as determined from measurements of the angles of NaO_wO_1 (139.9º) and NaO_wO_2 (138.9º) and bond distances of O_w–O_1 (2.762Å) and O_w–O_2 (2.841 Å). It was also assumed that $H_1$and H_2 were on the $O_wO_1O_2$ plane because, according to the measurement of the angle (3.4º) of intersection of the O_1O_2Na plane and the $O_1O_2O_w$ plane, Na, O_w, O_1 and O_2 are roughly placed on a plane. After a triangle, $\Delta O_wH_1O_1$ (Figure 6-9d), was constructed, the hydrogen bond and the angle that represents linearity of hydrogen bonds (Figure 6-9c) could be calculated in Figure 6-9d. These values were compared to statistical data in Table 6-3. The average value of H···O from neutron data is 1.8181Å (0.0774Å). The mean O–H···O angle (ϕ) is 167.1º (6.5º) based on 74 inter- and intra-molecular neutron data. The hydrogen bond lengths and the angles were quite reasonable in comparison with the calculated values and the statistical data.

6.3 CONCLUSIONS

The course of dehydration of dihydrated sodium naproxen was followed with powder X-ray diffraction and thermal gravimetric analysis. Samples that were partially dehydrated, meaning that their water content was between that of the dihydrate and the monohydrate, contained only crystalline material whose structure was that of the dihydrate or the monohydrate. In other words, there was no intermediate structure or pseudopolymorph formed. Furthermore, the anhydrous species was observed only after complete disappearance of the dihydrate. It can be concluded from this observation that the monohydrated sodium naproxen is more stable than the dihydrate.

The slow dehydration of single crystals of monohydrated sodium naproxen was observed through optical microscopy. Crystal dehydration occurred at different rates from the surfaces towards the center of the crystals. Dehydration along the *b*-axis of the lattice structure was most rapid because of the existence of channels that facilitate transport of water molecules along that axis in the monohydrate. SEM analysis showed the formation of large cracks aligned along the *b*-axis in the dehydrated crystals. The alignment of the cracks was explained by significant shrinkage (8.4 %) along the *c*-axis as a result of the dehydration. These cracks made the anhydrous crystals that were produced from the monohydrated species very brittle and, eventually, such crystals became powder-like.

The unit cell for the sodium naproxen anhydrate contains twice the number of naproxen ions and its volume, 1204.9($Å^3$), is almost double the volume of the

monohydrate, 666.61(Å^3). Both anhydrous and monohydrated crystals of sodium naproxen crystallize in the space group, $P2_1$, and monoclinic crystal system.

Water molecules in the monohydrate play an important role in stabilizing the crystal packing of the monohydrate. Each water molecule in the monohydrate is connected by hydrogen bonds to two different naproxen anions and to a sodium cation by Na–O type interaction. On the other hand, a sodium cation in the anhydrate has four different Na–O interactions with carboxyl oxygen atoms of four different naproxen anions which stabilize the crystal packing of the anhydrate.

CHAPTER 7

STRUCTURE PREDICTION OF ANHYDROUS SODIUM NAPROXEN VIA MOLECULAR MODELING

The lattice structure of a crystalline species provides fundamental knowledge which gives researchers a good insight to understand the properties of materials. Single-crystal X-ray diffraction is undoubtedly the most powerful technique for structure determination, and it is used widely and routinely to determine structures of crystalline species. However, many important crystalline solids cannot be prepared in the form of single crystals of sufficient size and quality for single-crystal X-ray diffraction. In such cases, only powder X-ray diffraction patterns are available and it is essential that powder X-ray diffraction patterns contain the same amount of structural information as single X-ray diffraction. In the last decade, very intensive studies have been carried out on crystal structure determination from power X-ray diffraction patterns. Reviews about crystal structure determination from powder diffraction data have been made by several authors.[66-68]

Crystal structure determination from powder diffraction data has three subdivided steps: (1) determination of lattice parameters and assignment of space group, (2) structure solution, and (3) structure refinement. Lattice parameters and space group are essential

prerequisite and they are determined in the very first step. Autoindexing programs such as ITO[69], TREOR[70] and DICVOL[71] are available to obtain lattice parameters from powder X-ray diffraction pattern. The space group is assigned by identifying the conditions for systematic absences in the indexed powder diffraction data. In the second step, an initial structural model is derived either directly or independently from powder diffraction pattern. If the initial model is good enough to represent the true structure, structure refinement can be performed to obtain a high quality structure. Structure refinement is fairly routine and, usually, the Rietveld refinement technique[72] is used. Currently, structure solution is an active research area.

Depending on the way to generate initial structures in the step of structure solution, structure determination from powder pattern is divided into two categories, the traditional approach and the direct-space approach. In the traditional approach, extraction of single-crystal X-ray diffraction pattern-like information from powder pattern is required. If peak intensities of individual peaks are extracted successfully, crystal structure solution techniques for single-crystal diffraction data such as direct methods and the Patterson method are used. However, three-dimensional information in single-crystal X-ray pattern is collapsed into one-dimensional space and, consequently, considerable overlap of peaks in power pattern is unavoidable, resulting in ambiguities in extracting the intensities of individual peaks.

In the direct-space approach, trial crystal structures are generated in three-dimensional direct space independently from experimental powder X-ray diffraction pattern.[73-75] Quality of each trial structure is assessed by the *R* factor R_p which is usually used in the Rietveld refinement.

$$R_P = \frac{\sum |y_{io} - y_{ic}|}{\sum |y_{io}|} \tag{7-1}$$

where F is the structure factors. y_{io} is the observed profile and y_{ic} is the calculated profile. The strategy for structure solution in the direct-space approach is to find the trial structure that has the lowest possible R factor and, technically, any global optimization technique such as generic algorithm and Monte-Carlo method can be employed. However, effort to search trial solutions in minimum energy state has rarely been made in this field.

In the present study, structure determination of the anhydrous sodium naproxen from powder X-ray diffraction pattern was carried out by molecular mechanics to generate trial structures in direct space. Cell constants of anhydrous sodium naproxen were determined from powder X-ray diffraction pattern by using DICVOL91. Initial structures in the step of structure solution were generated from the structure of monohydrated sodium naproxen and trial structures for Rietveld refinement were obtained by energy minimization. Since the anhydrous sodium naproxen was obtained by dehydration of the monohydrated species generation of the initial structure from the structure of the monohydrated sodium naproxen was considered reasonable as structural similarity between the anhydrate and the monohydrate was described in Chapter 6. The trial structures obtained by energy minimization were refined by using the Rietveld refinement technique.

7.1 SOFTWARE TO ASSIST IN SOLVING STRUCTURES FROM POWDER X-RAY DIFFRACTION PATTERN

Powder X-ray diffraction pattern collected on the sample of interest is analyzed step by step to obtain data required to determine the structure of the sample from the powder pattern. First of all, searching peak position is carried out to determine unit-cell parameters and space group. It is then required to run programs to find cell constants from searched peak positions. Cares should be taken to deal with many data generated on each step. Fortunately, software for each step is available on-line and in this chapter, three programs are introduced.

7.1.1 PowderX

PowderX was developed to process conveniently the powder X-ray data.[76] It has following major functions and feathers.

(1) It runs under Window with user-friendly graphical interfaces.

(2) It has many useful functions such as data smoothing, background subtraction, α_2 elimination, peak search, indexing.

(3) It can read data in many different formats used by diffractometers from Mac Science, Rigaku, Siemens, Philips as well as two columns ASCII file (2θ versus intensity).

(4) It can write output files in 9 different formats, which can be used directly as input data files for other plotting program, whole-pattern fitting and Rietveld refinement (GSAS, RIETAN, DBWS) programs.

This program was used in the present study to smooth powder patterns and search peak positions. PowderX has 4 different smoothing methods such as *Adaptive Smoothing*, *Savitzky-Golay Smoothing*, *Fourier Filtering* and *Binomial Smoothing*. First, *Adaptive Smoothing* was recommended for most cases. This method can eliminate noises while it keeps the profile shapes. Point number and noise level can be selected or input. If the powder pattern is too smooth, the point number and the noise level should be reduced and if the pattern is needed to be more smoothed, the variables should be increased. Second, *Savitzky-Golay Smoothing* is basically a least square fitting of the data using polynomials. Point number and the order of polynomial can be selected. The point number must be larger than the order of the polynomial used. Also, the point number times the step width should be approximately equal to the full width at half maximum. For the polynomial, usually, 2 or 3 are used. Third, *Fourier Filtering* uses Fourier transform to smooth the data. This method is useful to reduce noises with the high frequency. Last, in *Binomial Smoothing*, data smoothing was done using binomial coefficients as weight factors. Only one parameter is needed for this method.

For the peak search, PowderX has 5 options such as *Simple Peak*, *2nd Derivative*, *Test*, *Zero Convolution* and *Manual Pick* and first 4 methods are automatic peak-searching methods. First, *Simple Peak* finds peaks with intensity larger than user defined intensity threshold and with maximum intensity among a number of points. Two parameters are required to use this method, the number of points and intensity limit (in percentage). This method is useful when there are no serious peak overlaps in the powder pattern. It has the advantage to give most accurate peak area and FWHM. However, the peaks on the shoulder cannot be detected by this method. Second, *2nd*

Derivative finds peaks based on the fact that the second order derivative shows a minimum at a peak position. This is the most popular peak-search method for powder X-ray analysis. Three parameters are used to run this method, the number of points and intensity limit and derivative limit. Third, *Test* is a new way to find peaks developed by the author of PowderX. Fourth, *Zero Convolution* uses a designed discrete function to find local minima. This method requires three parameters, the number of points, intensity limit and area limit. If shoulder peaks are expected, *2nd Derivative* and *Zero Convolution* are the best choices. Last, Manual Peak can be used in the whole diffraction angle range or the small range of the powder pattern.

7.1.2 Autoindexing programs

Once peak positions are determined from the previous step it is ready to determine cell parameters from the peak positions. There are three popular autoindexing programs, ITO[69], TREOR[77] and DICVOL[71]. All of them are included in a program, CRYSFIRE which is developed by Robin Shirley.[78] It runs eight of the principal powder-indexing programs under MS-DOS, taking their input data either from a dataset or by manual input. It can be downloaded from the web site, http://www.ccp14.ac.uk/tutorial/crys/.

Three popular autoindexing programs mentioned above has been reviewed very clearly.[68] The programs ITO and TREOR are especially dependent on accurate low-angle data, because the peak positions at the low angle range play an important role in the indexing strategies, whereas for DICVOL, data errors play an independent role in the diffraction angle. Several non-systematic absences can make it impossible to find a

solution with ITO, but are of much less importance for DICVOL or TREOR. Since ITO introduces a general triclinic approach to the indexing problem it can be expected that ITO will sometimes solve triclinic problems that cannot be solved by DICVOL and TREOR which use relatively strong restrictions in the triclinic tests. DICVOL and TREOR sometimes distinguish a possible impurity peak whereas DICVOL cannot identify such peak.

7.1.3 GSAS - Rietveld refinement

A method of the least-squares refinement which minimizes the difference between the experimental and the simulated powder patterns was proposed in the late 1960s.[72] At first, this method was applied to powder patterns collected by using constant wavelength neutrons, rather than X-rays, because of the simpler peak shape of the Bragg reflections. However, it has been extended to a wide range of solid-state problems.

The Rietveld method is a powerful tool, but it is limited by the same drawback that affects powder methods in general: the loss of information that arises from the compression of the three-dimensional information into a single dimension. It is also important to notice that the Rietveld method requires a good starting model to obtain the final structure successfully.

GSAS (General Structure Analysis System), a program which implements the Rietveld method, was used in this study. It has been developed over a period of decades by Allen C. Larson and Robert B. Von Dreele[79]. The GSAS package contains approximately fifty programs and each of these programs is designed for specific types of tasks or types of crystallographic calculations. The majority of the programs require

minimal or no user input. The only program in the GSAS package that requires extensive user interaction is name EXPEDT, an acronym for experiment editor. The GSAS package is quite sophisticated, because a lot of options are available. The alternative method to execute commands and control options in GSAS is a program, EXPGUI.[80] This is a graphical user interface (GUI) editor for GSAS experiment (.EXP) files and shell which allows all the other GSAS programs to be executed with a GUI. In the present study, EXPGUI was used to control three main programs, POWPREF, GENLES and LIVEPLOT, in GSAS.

(1) POWPREF prepares powder diffraction data for subsequent least squares analysis.

(2) GENLES is a least squares refinement program. It constructs a single full least squares matrix and vector using multiple data sets. A mixture of powder diffraction and single crystal data for a given structural problem can thus be processed simultaneously.

(3) LIVEPLOT draws the experimental and the simulated patterns and the difference between two patterns together.

7.2 RESULTS AND DISCUSSIONS

7.2.1 Determination of cell parameters from powder pattern

Powder X-ray diffraction pattern was obtained from anhydrous sodium naproxen by using Philips® PW1800 automatic powder diffractometer with APD 3720 analysis software. The output file, which was the extension of rd, from the analysis was input to PowderX. Diffraction pattern collected on anhydrous sodium naproxen is shown in Figure 7-1 and it was smoothed as shown in Figure 7-2. The option of *Adaptive Smooth* was used and values for parameters to smooth peaks are listed in Table 7-1.

Table 7-1. Values for parameters in each task

Task	Option	Parameters	Values
Smoothing Peaks	Adaptive Smooth	Select Points	7
		Noise Level	100
Searching Peaks	2nd Derivative	Select Points	7
		Intensity Limit (%)	1
		Derivative Limit (%)	10

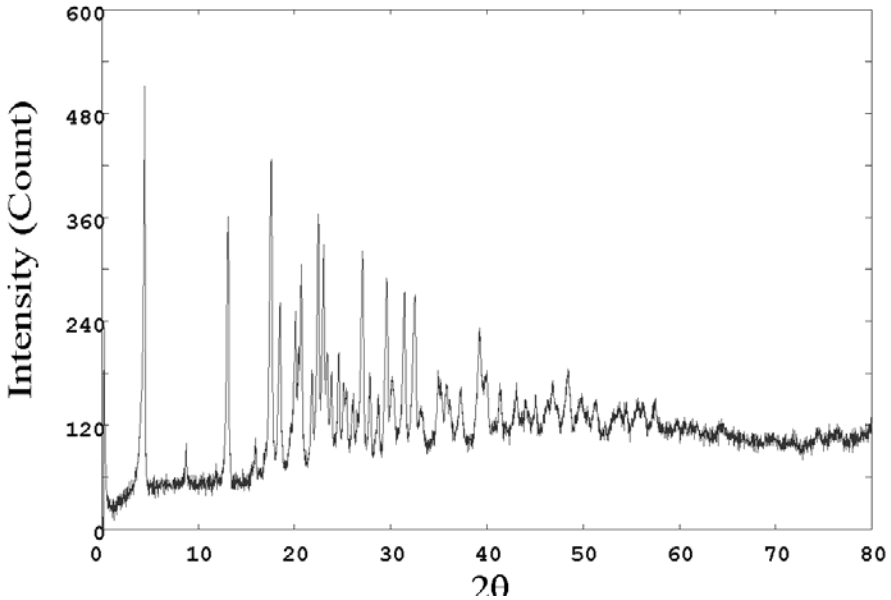

Figure 7-1. Powder X-ray diffraction pattern for anhydrous sodium naproxen from Philips® PW1800

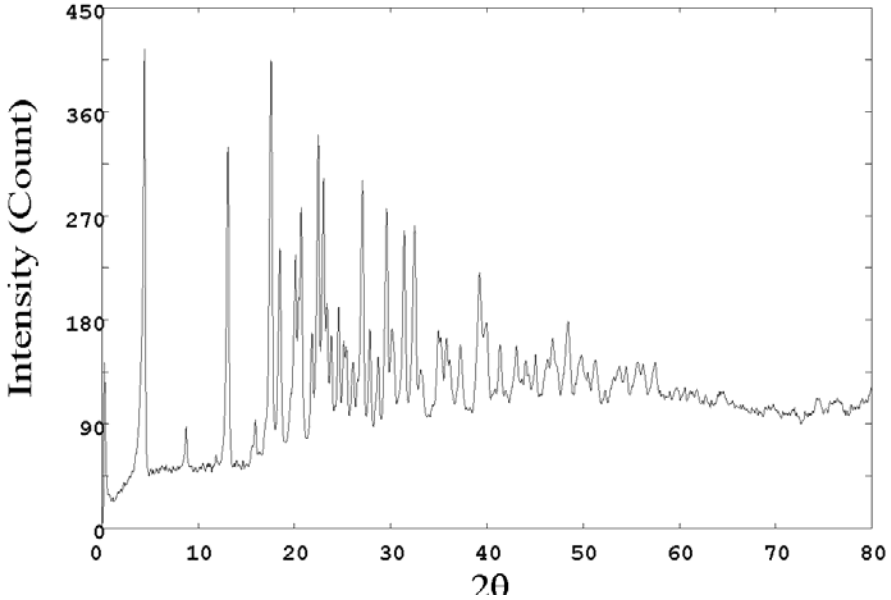

Figure 7-2. Powder pattern after smoothing peaks

Peaks were searched from the powder pattern after peak smoothing had been carried. 2nd Derivative method was used and the parameters for the method were listed in Table 7-1. Searched peaks are listed in Table 7-2 and 2θ or d-space (Å) was entered into CRYSFIRE to create a dataset for determination of cell parameters from the peaks.

Table 7-2. Peaks searched by 2nd Derivative method in PowderX

2Theta	d (A)	Height	Area	FWHM
4.431	19.92656	416.5	3726.5	0.18
8.766	10.07925	87.6	696.4	0.16
13.109	6.74802	330.5	3498.4	0.22
17.587	5.03875	404.8	4709.9	0.24
18.496	4.79295	242	2622.1	0.22
20.119	4.40995	236.6	2365.6	0.2
20.465	4.33607	199.4	1385.2	0.14
20.715	4.28429	277.7	2727.5	0.2
21.838	4.06645	168.6	1854.2	0.22
22.481	3.95157	339.9	4041.8	0.24
23.029	3.85889	303	3322.5	0.22
23.392	3.79982	195.1	1922.8	0.2
23.846	3.72849	166.2	1820.2	0.22
24.618	3.61326	191.2	2459.7	0.26
25.145	3.53865	161.9	1604.4	0.2
25.412	3.5021	157	1555.2	0.2
26.118	3.40906	143.3	2110.4	0.3
27.076	3.29055	301.2	3862.9	0.26
27.856	3.20016	171.4	2204.5	0.26
28.705	3.10742	147.8	1772.8	0.24
29.586	3.01679	277.2	3591	0.26
31.426	2.84429	257.3	3331.2	0.26
32.493	2.75322	261.7	4074.2	0.32
34.959	2.56447	170.9	1874.4	0.22
39.239	2.29408	220.9	3746.6	0.34

Determination of cell parameters was carried by using DICVOL. Zero correction was – 0.08° which was determined by comparison of the experimentally obtained powder X-ray diffraction pattern with the simulated powder pattern for monohydrated sodium naproxen. DICVOL needs an error tolerance which is an estimate of the typical absolute plus/minus error bounds on observed 2θ values. For the present study, default value, 0.03°, for the error tolerance was used. Also, default values, 0 and 6000 $Å^3$, for minimum and maximum cell volumes were used.

Table 7-3. Cell parameters searched by DICVOL in CRYSFIRE

Crystal system	Case	a	b	c	beta	M_{20}	F_{20}
Cubic Tetragonal Hexagonal	No Solution						
Orthorhombic	1	60.94492	20.54451	3.62956	-	5.0	10.2
Monoclinic	1	20.2746	4.3035	17.7330	92.337	5.4	11.0
	2	20.8693	5.9416	9.9875	102.066	17.9	31.0
	3	21.1763	5.9406	9.9866	105.403	17.1	29.1
	4	24.9458	5.9395	9.9871	125.099	18.1	31.0
	5	25.7009	5.9399	9.9865	127.411	17.4	29.8
	6	24.9536	5.9404	9.9867	125.101	17.3	29.5

Cell parameters searched by DICVOL are listed in Table 7-3. No solution was found in cubic, tegragonal and hexagonal crystal systems. A set of cell parameters for the orthorhombic crystal system was searched. However, the figure of merits for the solution is not big enough to believe that the cell parameters represent the unit cell of anhydrous sodium naproxen. For the monoclinic crystal system, six solutions are found

and, except for the case 1 in Table 7-3, every solution has figures of merit[a] higher than 17.0 and 29.0 for M_{20} and F_{20}, respectively. Case 2 and case 4 which are highlighted in Table 7-3, seem to be the most correct solutions according to the figures of merit because it has the highest figures of merit. The difference between the case 2 and the case 4 is the cell dimension for *a*-axis. If there's no information about the unit cell for anhydrous sodium naproxen both sets of cell parameters should be considered feasible for further analysis. However, a closer look at the packing diagram of monohydrated sodium naproxen gave an insight to choose a set, the case 2, with the second highest figures of merit. Figure 7-3 depicted the unit cell for the monohydrated sodium naproxen. The length of the longest axis is 21.177Å and it can be assumed that the space for a sodium cation and a naproxen anion has approximately the longest length of 10.5Å. The longest axis in the case 4 is 24.9458Å and, if this case is correct, there is too much empty space between naproxen anions. However, physically, anhydrous sodium naproxen is produced by dehydration of the monohydrated species and the space, where two water molecule were located per unit cell, between two naproxen anions may become either closer than or approximately similar to the space in the monohydrate. Therefore, the longest cell dimension, 20.8693Å, in the case 2 is more reliable and it was chosen for the next step to determine the structure of the anhydrous sodium naproxen.

[a] Criteria for the physical plausibility of the indexing.

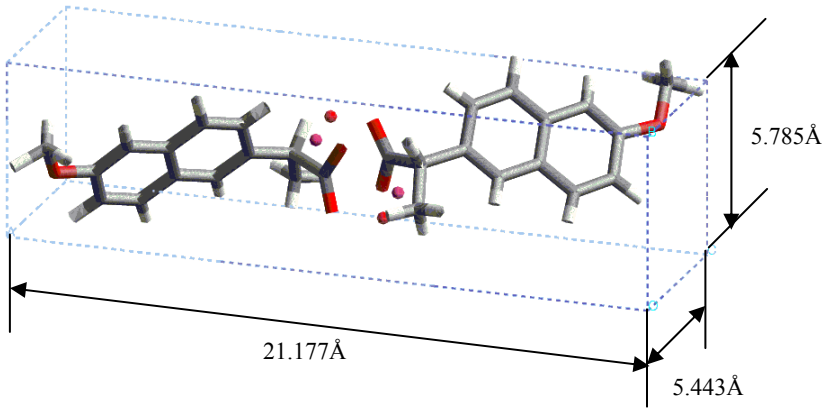

Figure 7-3. Dimension of a unit cell for monohydrated sodium naproxen

7.2.2 Determination of force fields for energy minimization

Energy minimization for structural determination requires proper force fields which are a critical key to successful final structures. When proper force fields were searched root-mean-square (RMS) deviation was used as a criterion to show how proper the force fields are. RMS is defined as follows:

$$RMS = \sqrt{\frac{\sum_{i=1}^{n}\left(\left(x_0 - x_f\right)^2 + \left(y_0 - y_f\right)^2 + \left(z_0 - z_f\right)^2\right)_i}{n}} \tag{7-2}$$

where x, y and z are the coordinates of atom i , n is the total number of atoms and subscripts 0 and f represent initial and final positions before and after energy minimization, respectively. Positions of every atom in the unit cell for monohydrated sodium naproxen were used as an initial model. The final positions of atoms were obtained by energy minimization with a force field of interest. If parameters in a force field mimics the inter-atomic forces in the unit cell well the final atomic positions are

very close to the initial positions, resulting in small RMSs. Therefore, the smaller RMS is the more proper the force field is.

Several forcefields in cerius2® for organic compounds with metal ions are available and they are listed in Table 7-4 including van der Waals parameters for sodium ion. First of all, since forcefield parameters in COMPASS forcefield are not in the ASCII format which can be edited easily, COMPASS is ignored to use. Second, Amber forcefield has a lot of missing bond terms for the monohydrated sodium naproxen. When those missing terms were ignored, the minimized structure was totally different from the determined structure. Therefore, Amber forcefield was also ignored to use. Now, CVFF and PCFF are left to test.

Table 7-4. Forcefield available in Cerius2 and comparison

FF	File Name in Cerius2	in Ascii Format?	Charge?	VdW	Na	
					R^* (Å)	ε (kcal/mol)
CVFF	cvff_950_1.01	Yes	Yes	LJ12-6	2.1298	1.6071
PCFF	pcff_300_1.01	Yes	Yes	LJ9-6	3.9624	0.738
Amber	amber2.01	Yes	No	LJ12-6	3.144	0.5
COMPASS	compass	No	Yes	LJ9-6	-	-

PCFF forcefield includes parameterized atom-type charges while the charge for sodium atom is zero. When energy minimization was carried out with the charges in the forcefield the minimized model was unreasonable. So, the Gasteiger method was employed to assign charges into atoms. And, Ewald sum was used for non-bonded terms such as van der Waals term and electrostatic term and conjugate gradient minimization method was used. The results are listed in Table 7-5. For the case 1, crystalline

superlattice structure of the monohydrated sodium naproxen was used without any other constraint as an initial model while the case 2 used SPC/E charges(Q_H = 0.4238e and Q_O = -0.8476e)[81] for water molecules as well as the crystalline superlattice structure of the monohydrate. As shown in Table 7-5, RMS with PCFF is over 0.9 and sometimes it's around 2.0. The discrepancy was not enough to use the PCFF force field for the further study.

Table 7-5. RMS by energy minimization with PCFF force field

Case No.	Structures	Variables In Cell Constants	RMS
1	Crystalline Superlattice	-	0.972852
		a, b, c and β	1.928688
2	Crystalline Superlattice with SPC/E charges	-	0.926377
		a, b, c and β	1.595093

Table 7-6. RMS by energy minimization with CVFF force field

Case No.	Structures	Variables In Cell Constants	RMS
1	Crystalline Superlattice	-	0.139236
		a, b, c and β	0.578712
		a, b, c α, β and γ (resulting in α = γ = 90°)	0.749785
2	Crystalline Superlattice with SPC/E charges	-	0.192415
		a, b, c and β	0.432823
		a, b, c α, β and γ (resulting in α = γ = 90°)	0.441474
3	Crystalline Superlattice with SPC/E charges and the SPC/E structure	-	0.418153
		a, b, c and β	1.265335
		a, b, c α, β and γ (resulting in α = γ = 90°)	1.008382
4	Crystalline Superlattice with SPC/E charges, & vdW parameters for O	-	0.136226
		a, b, c and β	0.24782
		a, b, c α, β and γ (resulting in α = γ = 90°)	0.252583

Last, CVFF force field was tested in hoping that RMS between the initial structure and energy-minimized structure is small. This forcefield also includes parameterized atom-type charges and the charge for sodium atom is still zero. So, the Gasteiger charge assign method was employed. And, Ewald sum was also used for non-bond terms such as van der Waals term and electrostatic term and conjugate gradient method was used for energy minimization.

RMS without allowing cell constants to change in the case 1 in Table 7-6 was less than 0.14 Å and it seems CVFF force field has very good force parameters to mimic the inter-atomic forces in the unit cell for the monohydrate. CVFF force field was further tried to calculate RMSs with allowing cell constants to change and, unfortunately, RMSs were over 0.57 Å. Compared with Amber and PCFF, CVFF produced lower RMS deviations. However, further trials were required to reduce RMS deviations.

First effort was made on parameters of water moleculesin CVFF. A water model[81], extended simple point charge (SPC/E) model, has been successfully adopted in molecular simulations of dilute solutions[82], aqueous solutions[83, 84]. SPC and SPC/E models have tetrahedral geometry in which angles between electron pairs (and therefore the angle for the bond H-O-H) are 109.0°. The bond length between O and H in water is 1Å. Partial charges for O and H in SPC/E model are –0.8476e and +0.4238e, respectively, while charges for O and H in SPC are –0.82e and +0.41e, respectively. The van der Waals parameters of A and B for oxygen in water in the format of Equation 2-29 in Chapter 2 are $3.428\,(\text{kJ/mol})^{1/12}$ Å and $3.7122\,(\text{kJ/mol})^{1/6}$ Å, respectively.

In the case 2 in Table 7-6, point charges from SPC/E (-0.8476e for oxygen and 0.4238 for hydrogen) were assigned to O and H in water after the Gasteiger estimates

were used to assign charges. Even though, when cell constants were fixed during energy minimization, the RMS deviation was slightly higher than the case 1 in Table 7-6, it was still below 0.2Å. However, when cell constants were not fixed and they were allowed to vary during minimization, RMS deviations were lower than 0.5Å and better than the case 1.

In the case 3 in Table 7-6, tetrahedral geometry as well as charges of SPC/E was applied to water molecules in the monohydrate. And, water molecules are defined as rigid bodies to prevent them from changing in their geometry such as a bond length (1.0Å) and a bond angle (109°) during minimization. As shown in Table 7-6, the RMS became larger over 1.0Å. The geometry for SPC and SPC/E is too idealized structure of water to represent real water molecules. Actually, because the two non-bonding electron pairs in water remain closer to the oxygen atom, they exert a stronger repulsion against the two covalent bonding pairs, effectively pushing the two hydrogen atoms closer together. The result is a distorted tetrahedral arrangement in which the H-O-H angle is getting closer. Free water in vapor state has an OH bond length of 0.957Å and an HOH angle of 104.52°. In addition, the water molecules in crystal structures should be more non-ideal due to interactions with other atoms surrounding water molecules, implying that the tetrahedral arrangement for water molecules is not acceptable for the present case. Therefore, the RMS with the tetrahedral geometry became worse than the cases 1 and 2.

The case 4 in Table 7-6 employed van der Waals parameters of SPC/E for water. Van der Waals parameters for oxygen of water in CVFF were 3.5532 Å and 0.1554 kcal/mol for R^* and ε, respectively, and they were replaced with 3.5532 Å and 0.6502 kcal/mol obtained from the SPC/E model. RMS deviations in the case 4 were less than

the case 2 by using charges for hydrogen and oxygen and van der Waals parameters for oxygen from SPC/E.

Next effort to reduce RMSs was made on sodium ions. According to literature surveys, two different sets of Lennard-Jones parameters for sodium ions were found and listed in Table 7-7. These two sets of parameters were applied to the case 4 in Table 7-6, showing that the case 2 in Table 7-8 has better RMSs than other cases in Tables 7-6 and 7-8.

Table 7-7. VdW parameters for sodium ion (Na^+)

Potential	*σ/nm* (*R*/Å*)[a]	*ε/kJ mol⁻¹* (*ε/kcal mol⁻¹*)[b]	application	reference
LJ12-6	0.1897 (2.12931)	1.6100 (0.38333)	Dilute solutions[82]	Chandrasekhar et al.[85]
LJ12-6	0.235 (2.63779)	0.5439 (0.1295)	Aqueous solutions[83] Zeolite[86]	Smith and Dang[87]

Table 7-8. RMS by energy minimization with vdW parameters for sodium from literatures

Case No.	*σ/nm* (*R*/Å*) For Na^+	*ε/kJ mol⁻¹* (*ε/kcal mol⁻¹*) For Na^+	Variables In Cell Constants	RMS
1	0.1897 (2.12931)	1.6100 (0.38333)	-	0.202254
			a, b, c and β	0.383353
			a, b, c α, β and γ (resulting in α = γ = 90°)	0.388482
2	0.2350 (2.63779)	0.5439 (0.1295)	-	0.116261
			a, b, c and β	0.183504
			a, b, c α, β and γ (resulting in α = γ = 90°)	0.188162

[a] $R^* = 2^{1/6}\sigma$

[b] $1\,kcal/mol = \frac{1}{4.2} kJ/mol$

7.2.3 Generation of initial structures for structure solution

In this chapter, the way to generate the trial structures of anhydrous sodium naproxen from the structure of monohydrated species is presented.

Anhydrous sodium naproxen can be produced by dehydration of monohydrated sodium naproxen. Simple removal of water by dehydration drives the monohydrate to transform to the anhydrous species. Therefore, structural similarity between two species can be speculated. This idea is an important clue to generate an initial guess of the structures of the anhydrous sodium naproxen. The most reliable cell constants for the anhydrate were chosen in Section 7.2.1 and listed in Table 7-9 including the cell constants for the monohydrate. Since the volume of the unit cell for the anhydrate is almost double the volume of the monohydrate, as shown in Table 7-9, the initial structure for the anhydrate was generated by doubling unit cells of the monohydrate. Doubling unit cells of the monohydrate was carried out by displaying two unit cells and generating crystalline superlattice which belongs to P1 space group. The P1 space group[a] is usually used in molecular modeling because it makes simulations easier. Then, water molecules were removed from the doubled unit cell and determined cell constants of the anhydrate were used as cell constants for the doubled unit cell.

[a] No symmetry exists in the P1 space group. Therefore, every atom and/or molecule in the unit cells is independent from each other.

Table 7-9. Comparison of cell constants for the anhydrate to the monohydrate

	Monohydrate[11]	Anhydrate[a]
a	21.177	20.8693
b	5.785	5.9416
c	5.443	9.9875
β	91.41	102.066
volume	666.61	1211.05
crystal system	monoclinic	monoclinic

When cell constants determined from powder X-ray diffraction pattern were assigned to the doubled unit cell without water molecules, two initial guesses were generated shown in Figure 7-4 and 7-5. If the unit cell with the determined cell constants uses the same coordinate system as that for the unit cell of the anhydrate the determined cell constants, *a*, *b*, *c* and *β*, are corresponding to the cell constants, *a*, *b*, *c* and *β*, in the monohydrate, respectively, and the generated unit cell (Model 1) of the anhydrous sodium naproxen is shown in Figure 7-4. Another initial guess (Model 2) was generated because the coordinate system is quite arbitrary. As used in the first guess, longest axis is *a*-axis, *b*-axis is a unique axis, *c*-axis is automatically the remaining axis and *β* is 102.066°. However, different coordinate system results in totally different edge angle, 77.934°, which is corresponding to *β* in Model 1.

[a] Cell constants of the anhydrate determined from powder X-ray diffraction pattern in Section 7.2.1.

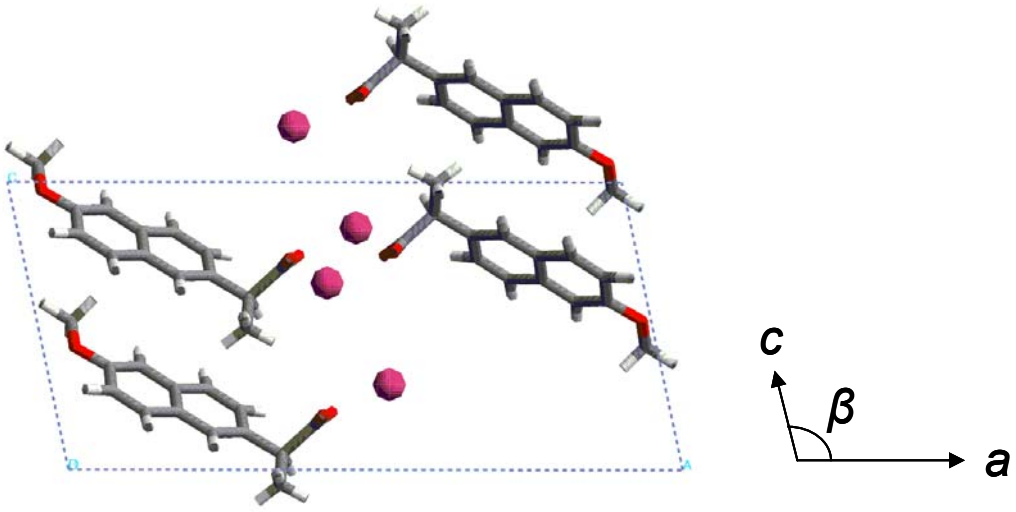

Figure 7-4. Model 1 which uses the same coordinate system as the monohydrated sodium naproxen

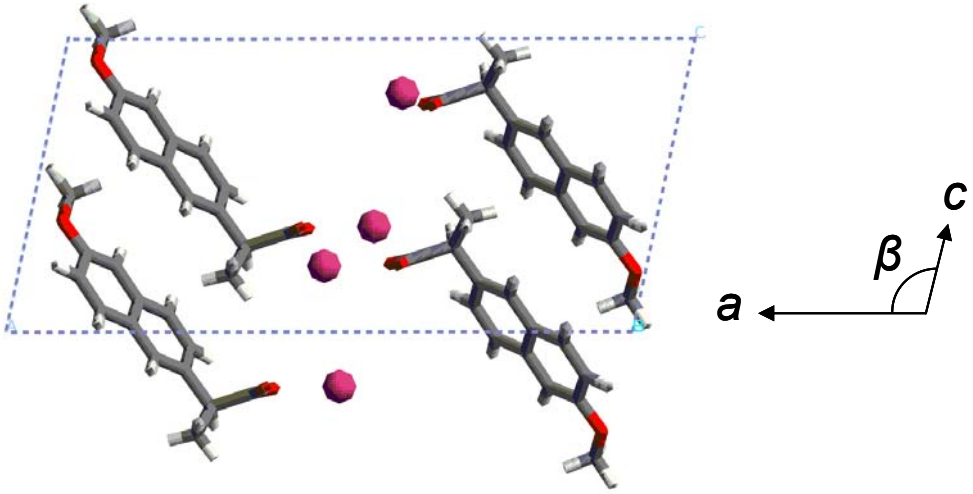

Figure 7-5. Model 2 which has different coordinate system from the monohydrate

7.2.4 Energy minimization to obtain trial structures for refinement

Usually, global optimization algorithms with the target function of R-factor have been used to obtain trial structures in the direct-space approach. However, if good initial guesses, whose structures are very close to final structure, for structure solution are obtained, local optimization algorithm is quite useful to produce trial structures for the Rietveld refinement in the step of the structure refinement. In the present study, the target function is not R-factor but total energy of crystal structures. In order to calculate total energy, force fields are required and the way to find force fields for the system of sodium naproxen was presented in Section 7.2.2. And, two initial guesses were obtained from the structure of monohydrated sodium naproxen.

First of all, energy minimization was carried out on Model 1 in Figure 7-4 and Model 2 in Figure 7-5. When energy minimization was performed, the Gasteiger method was employed to assign charges into atoms. And, Ewald sum was used for non-bonded terms such as van der Waals term and electrostatic term and smart minimization method, which is an option of energy minimization, was used. The minimized structure from Model 1 has lower energy, -606.036 kcal/mol, than that from Model 2, -599.65 kcal/mol. After energy minimization, finding space group symmetry was performed. Both minimized structures from Model 1 and Model 2 belong to $P2_1$ space group. And, the simulated powder X-ray diffraction patterns from energy-minimized structures were compared with the experimental powder X-ray pattern for the anhydrate in Figure 7-6 and they showed big discrepancy between the experimental powder pattern and the simulated powder X-ray patterns.

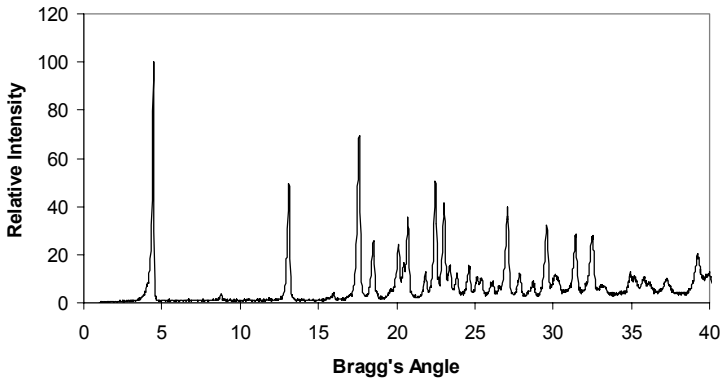

(a)

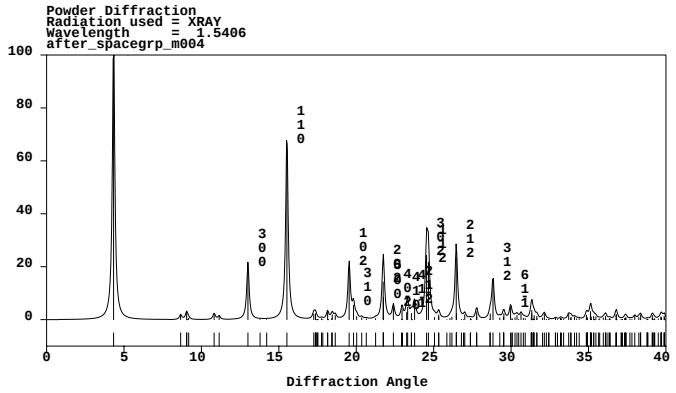

(b)

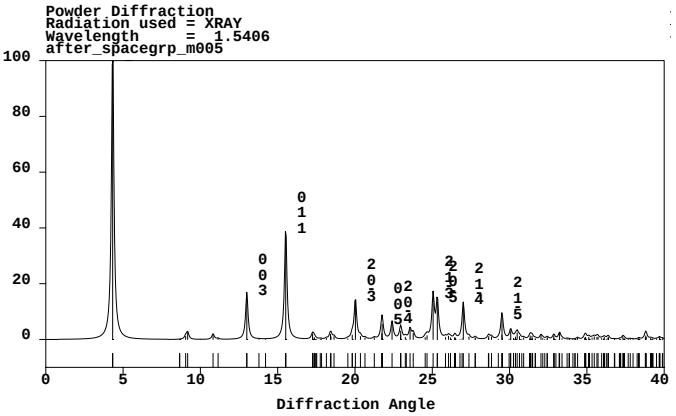

(c)

Figure 7-6. Powder X-ray diffraction patterns of (a) the anhydrous sodium naproxen, (b) Model 1 and (c) Model 2

More efforts were made to improve the simulated structures of anhydrous sodium naproxen. Three degrees of freedom, χ, φ and ψ, on the naproxen anion has been reported by Bednarek et al.[35] and they are defined in Figure 7-7.

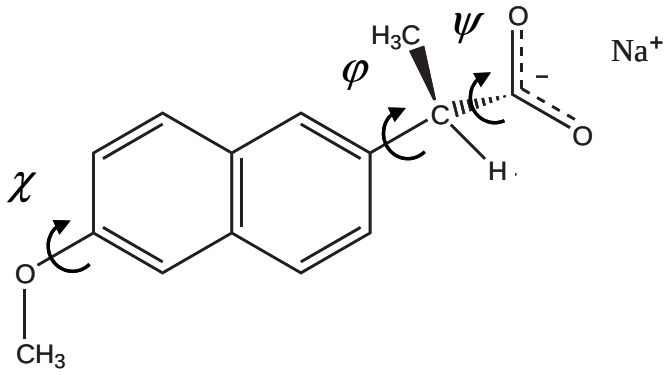

Figure 7-7. Definition of torsion angles in sodium naproxen

At first, the torsion angle, χ, for the methoxy group was examined in monohydrated sodium naproxen[11] and naproxen[34] and they show that the methyl group is almost on the plane of the naphthyl group. Furthermore, according to the dependency of potential energy of naproxen anion on χ obtained from the semiempirical AM1 calculation,[35] there is a very deep energy well at a certain angle of χ which is corresponding to the orientation of the methoxy group in the monohydrated sodium naproxen and naproxen. Therefore, searching conformers along χ was not carried out.

The other torsion angle, ψ, was directly related with the carboxyl group which has hydrogen bonds with water molecules and electrostatic forces with sodium cations in the monohydrated sodium naproxen. They are very significant forces to stabilize the monohydrate. In the anhydrous sodium naproxen, water molecules were removed and minimization was performed. During the minimization, the proper orientation for sodium

cations and oxygen atoms in carboxyl groups might be obtained because the electrostatic forces between oxygen in carboxyl groups and sodium cations are the major forces to stabilize the anhydrous sodium naproxen. Therefore, conformers were not searched along ψ at this moment.

The last torsion angle considered is φ. If, as mentioned earlier, oxygen atoms in carboxyl groups have proper relative orientation with sodium cations, φ determines the orientation of whole naphthyl group in the naproxen anion. Since the naphthyl group is a bulky and rigid part in the naproxen anion, rotating naphthyl group by changing φ may require overcoming a higher energy barrier. Furthermore, according to the dependency of potential energy of the naproxen anion on φ obtained from semiempirical AM1 calculation and *ab initio* RHF calculation using 3-21G* basis set,[35] several energy wells were observed along φ and huge energy barriers between energy wells were also observed from the *ab initio* RHF calculation. These energy barriers may not be overcome by local energy minimization, resulting in wrong structures. Therefore, examination of φ was carried out to find better structures whose simulated power X-ray patterns are closer to the experimental powder pattern than the structures obtained by only energy minimization from Model 1 and Model 2. The minimized structures from Model 1 and Model 2 are depicted in Figure 7-8.

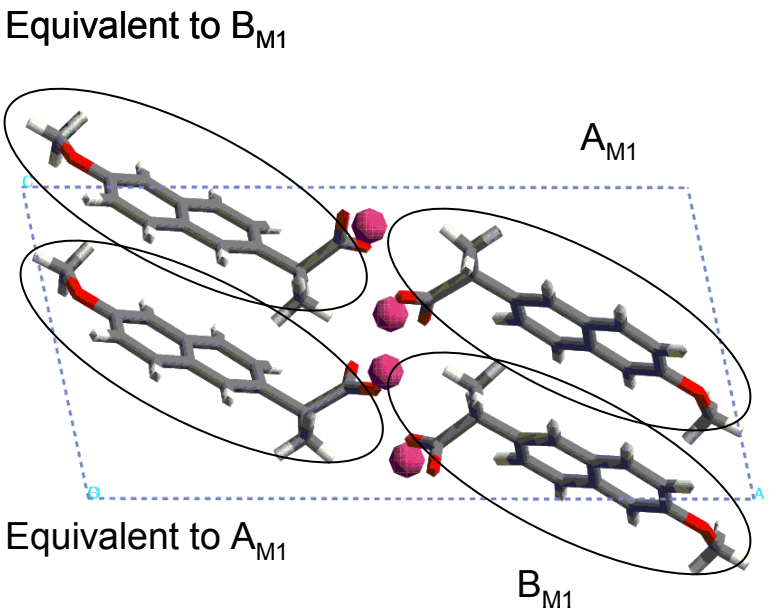

(a)

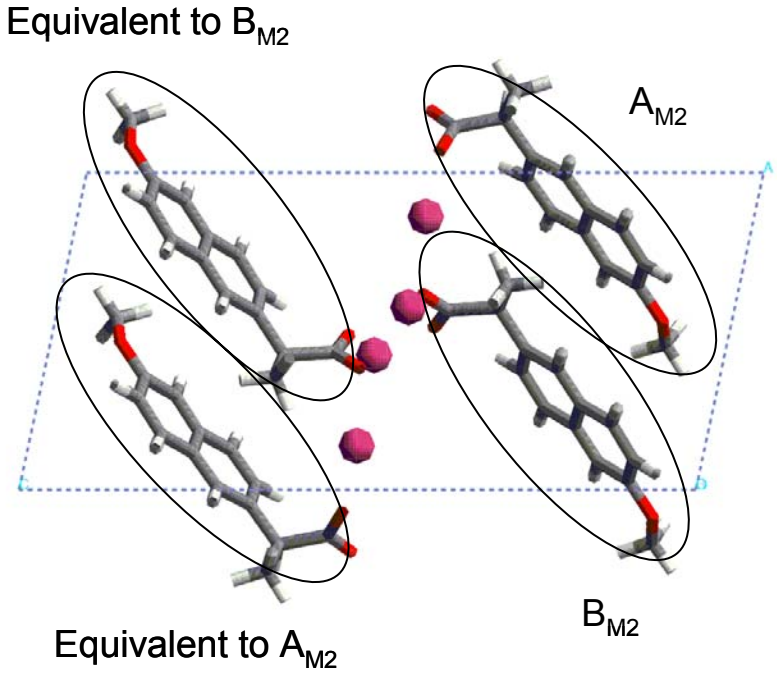

(b)

Figure 7-8. Minimized structures and definitions of A and B molecules in (a) Model 1 and (b) Model 2

Figure 7-8 shows the molecules, A and B, in the minimized structures from Model 1 and Model 2. Torsion angle, φ, in each molecule, A and B, was rotated separately. Then, energy-minimization was performed on every structure. When torsion angle was rotated, carboxyl group, the chiral center and methyl group attached to the chiral center were fixed and only naphthyl group and methoxy group attached to the naphthyl group were rotated along the bond between the chiral center and the naphthyl group. The results from energy-minimization were listed in Table 7-10.

Efforts to improve trial structures have a better structure in Model 2 and the structure has the lowest energy so far. Simulated powder X-ray diffraction pattern on the structure in the lowest energy state was calculated (Figure 7-9) and compared to the experimental powder X-ray diffraction pattern (Figure 7-6a) of the anhydrous sodium naproxen. The simulated and experimental powder patterns show a good agreement and the structure was chosen as a trial structure for the Rietveld refinement.

Table 7-10. Results from energy minimization of the minimized structures of Model 1 and Model 2

Rotation angle (°)	Molecules in Minimized Model 1		Molecules in Minimized Model 2	
	A_{M1} (kcal/mol)	B_{M1} (kcal/mol)	A_{M2} (kcal/mol)	B_{M2} (kcal/mol)
0	-606.036	-606.036	-599.465	-599.465
20	-606.036	-606.036	-599.465	-599.465
40	-596.168	-571.168	-617.506	-592.946
60	-596.168	-571.168	-617.506	-592.946
80	-591.129	-592.306	-599.828	-599.828
100	-596.168	-	-	-599.465
120	-595.293	-601.515	-594.630	-599.465
140	-595.293	-597.528	-594.630	-593.912
160	-595.293	-597.528	-594.630	-593.912
180	-595.293	-597.528	-594.630	-593.912
200	-595.293	-597.528	-594.630	-593.912
220	-591.730	-595.894	-576.963	-588.191
240	-595.501	-583.941	-594.530	-588.191
260	-595.501	-576.419	-599.465	-603.667
280	-576.527	-	-	-
300	-576.527	-	-	-578.078
320	-606.036	-606.036	-599.465	-599.465
340	-606.036	-606.036	-599.465	-599.465

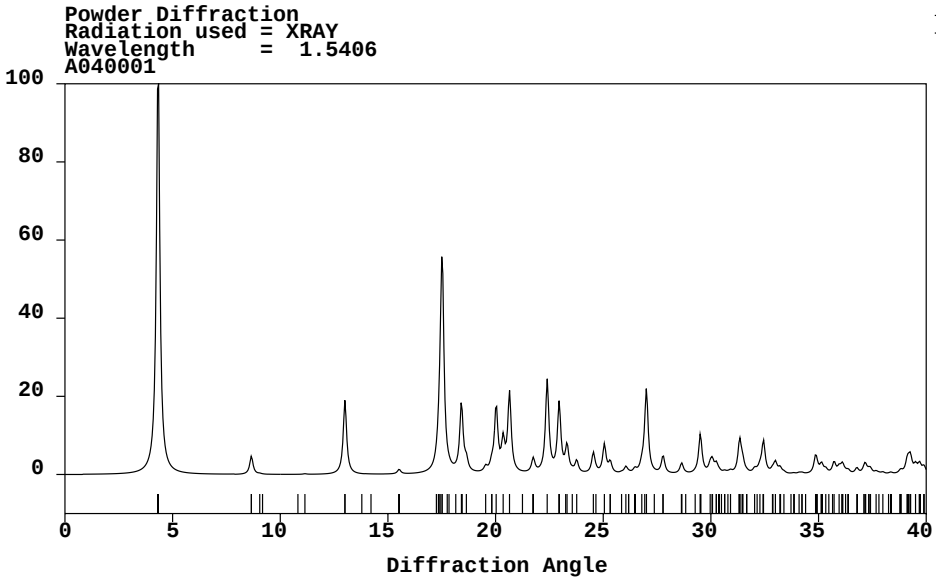

Figure 7-9. Simulated powder X-ray diffraction pattern of the structure in the lowest energy state in Table 7-10

7.2.5 Structure refinement

A trial structure was refined by the Rietveld method. There are a lot of parameters to adjust to fit the simulated power X-ray diffraction pattern to the experimental pattern. However, since there is no general guideline to reach the final structure trial and error is a way to get the final structure by the Rietveld method. In the present study, EXPGUI to control GSAS was used.[88] The input files to GSAS were generated by Cerius[2] from the trial structure which was searched in the previous section. The refinement result was depicted in Figure 7-10 with 0.1255 of R_p[a] and the parameter values for the final structure were listed in 7-11. Zero was set as -0.08 which was determined from powder X-ray diffraction pattern and used to determine cell constants using DICVOL. However, the zero was not refined any more. A Gaussian was used as a profile function. This function is typically not ideal for x-ray data. However, since the simulated pattern agreed reasonably well with the experimental profile, further optimatization was not performed. Based on the results from the Rietveld refinement, it was concluded that the refined structural model is a reasonable representation of the crystal structure for anhydrous sodium naproxen. Note that the differences between the experimental pattern and the simulated pattern were significant for the strong long angle peaks. These discrepancies could probably be reduced by optimizing the S/L and H/L parameters in the model for low angle peak asymmetry.

[a] 0.1955 of wR_p was also obtained from GSAS

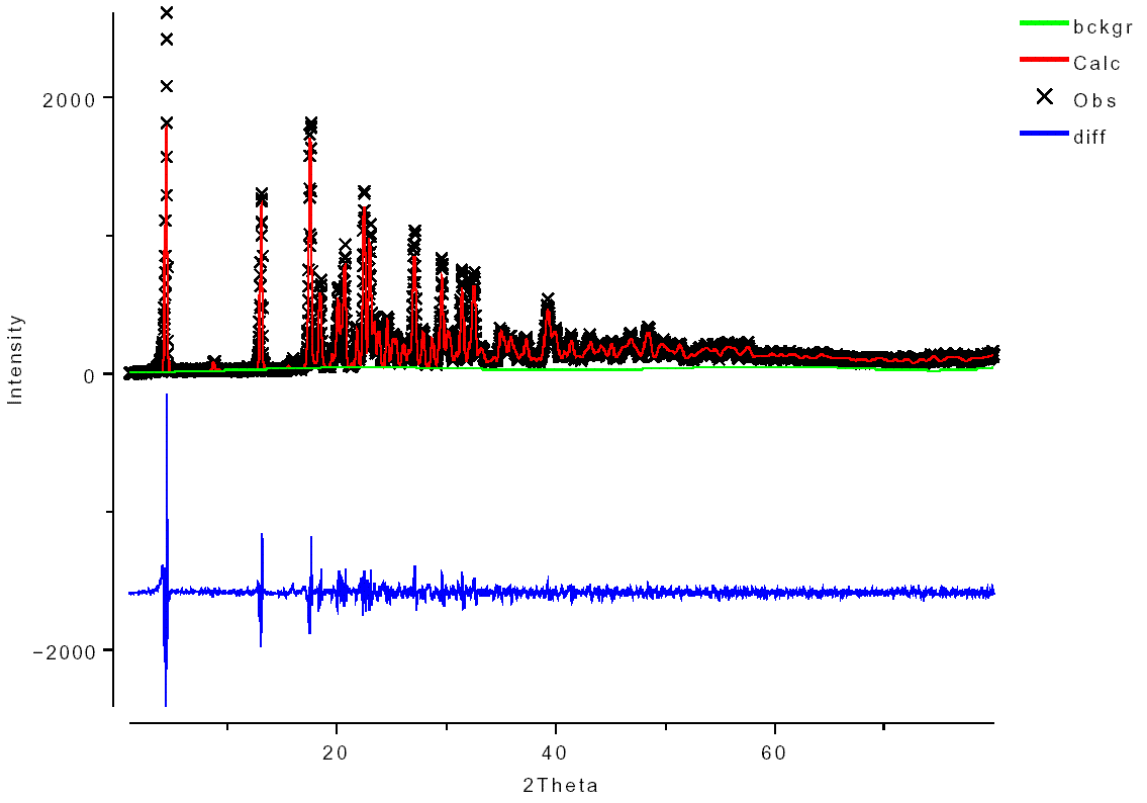

Figure 7-10. Output from the Rietveld refinement and the difference between the observed experimental pattern and simulated pattern

Table 7-11. Parameter values for the final structure of anhydrous sodium naproxen

Categories	Parameters	Values
LS Controls	Convergence Criterion	0.01
	Marquardt Damping	1.00
	Extract Fobs	on
	Extraction Method	F(calc) Weighted
Phase	Refine Cell	on
	Damping (Cell)	0
	a	9.965781
	b	5.927991
	c	20.780291
	α	90
	β	102.0313
	γ	90
	Fefinement Flags (X, U)	on
Histogram	Background Function Type	2 - cosine fourier series
	Number of terms of background function	10
	Damping(Background Function)	0
	Refine wave	off
	wave	1.53944498
	Refine zero	off
	zero	-0.08
	Refine POLA	off
	POLA	0.5
	Refine Abs./Refl.	off
Scaling	Refine Scale Factor	on
	Scale	0.50056
Profile	Damping (Profile)	0
	GU	on
	GU	0.239359E+04
	GV	on
	GV	-0.286322E+03
	GW	on
	GW	0.839626E+02
	asym	on
	asym	-0.843488E+00
	F1	off
	F2	off

7.3 CONCLUSIONS

Structure determination from powder X-ray diffraction pattern for anhydrous sodium naproxen was carried out successfully. Laboratory X-ray source was used to collect data on the anhydrous sodium naproxen. Smoothing profiles and searching peaks were performed by PowderX. DICVOL91 which is implemented in CRYSFIRE was used to determine Cell constants. A trial structure was constructed by energy-minimization of initial guesses from the structure of the monohydrated sodium naproxen. The trial structure was input to GSAS and the Rietveld refinement was carried out to obtain a final structure.

When the trial structure was constructed by energy-minimization, the crystal structure of the monohydrated sodium naproxen was employed as an initial guess based on the assumption that, since the anhydrous species is generated by dehydration of the monohydrate, the structural similarity exists between the anhydrate and the monohydrate. From the success of structure determination in the present study, it can be concluded that the structural similarity is proved and it can be an important key to structure determination of pseudopolymorphic forms from known structures. Furthermore, the simulations predict that the transition of the monohydrate to the anhydrous status occurs via a simple shifting and contraction of the lattice in response to the water removal. This is consistent with the shrinkage of the unit cells of the monohydrate by dehydration.

CHAPTER 8

CONCLUSIONS AND RECOMMENDATIONS

8.1 CONCLUSIONS

The present research was performed mainly on crystallization and solid-state transformation of pseudopolymorphs of sodium naproxen in order to provide fundamental information concerning stability of the pseudopolymorphic forms. Since pseudopolymorphs have different physical and chemical properties, such information can be crucial in the development of new drugs.

The specific pseudopolymorph that can crystallize from solutions depends on conditions such as temperature, pressure and solvent composition. Understanding the role played by these variables in crystallization provides important knowledge that can be used to control the formation of pseudopolymorphs of pharmaceutical interest. Furthermore, since solid-state transformation occurs very frequently (intentionally and/or accidentally) during processes to produce drugs, understanding the mechanism of dehydration and the stability of pseudopolymorphs provides deep insights into non-solvent mediated transformation of pseudopolymorphs.

In experiments that were part of this research, sodium naproxen was recovered from pure water either as the anhydrous or the dihydrated form. The transition

temperature between regions where one of these two pseudopolymorphs was stable was 29.8°C; the dihydrated form was stable at temperatures below the transition temperature, while the anhydrous species was more stable above that temperature. The monohydrated sodium naproxen was not found in pure water. Clearly, the monohydrated species in pure water is unstable thermodynamically or stable over a very small temperature range, which probably would be in the neighborhood of 29.8°C. Crystallization of sodium naproxen from 64 mol% methanol in aqueous solutions was conducted. Temperature between the regions of greater stability for the pseudopolymorphic transition the dihydrated and the monohydrated sodium naproxen was 19.6°C; the dihydrated form was stable below 19.6°C, while the monohydrated species was more stable at higher temperatures. Therefore, changes in solvent compositions as well as temperature provide variables to control the formation of pseudopolymorphs of organic compounds.

The solubilities of sodium naproxen in 0 mol% and 64 mol% methanol in aqueous solutions were determined. From the data, the heats of solution of pseudopolymorphs of sodium naproxen were obtained by correlating the solubility data with the van't Hoff equation. The heats of solution were related to the heat of dehydration from DSC by the thermodynamic cycle developed in the present study. According to the cycle, for an enantiotropic system, a form with a lower degree of hydration always has the lower heat of solution than a form with a higher degree of hydration, implying that a form with a lower degree of hydration is more stable at higher temperatures.

The stability of three pseudopolymorphs of sodium naproxen was investigated by dehydration of dihydrated sodium naproxen at 0% relative humidity. The dihydrated form was transformed to the monohydrate and, finally, it became the anhydrous species.

Samples whose water content was between that of the dihydrate and the monohydrate gave powder X-ray diffraction patterns that corresponded to the two pseudopolymorphs, meaning that the samples were mixtures of the dihydrate and the monohydrate. Furthermore, the anhydrous species began to appear only after complete disappearance of the dihydrate. In other words, after all the dihydrated form in the mixtures was transformed to the monohydrate, the anhydrous species was produced by dehydration of the monohydrate. Therefore, it can be concluded that the monohydrate is more stable than the dihydrate and less stable than the anhydrate.

The stability of pseudopolymorphs of sodium naproxen is closely related to the difficulty of removing water molecules from the unit cells of the hydrated forms. Measuring the activation energy of transformation is a good way to see how difficult it is to remove water molecules from the unit cells. Isothermal TGA experiments were employed to obtain the activation energy. The activation energy of transformation of the dihydrate to the monohydrate is lower than that of transformation of the monohydrate to the anhydrate, implying that the former transformation can happen more easily than the latter. That is, the dihydrate is less stable than the monohydrate because transformation of the dihydrate is easier than that of the monohydrate.

Dehydration of single crystals of the monohydrated sodium naproxen was observed under an optical microscope. Anisotropic dehydration occurred, showing different dehydration rates along axes from surfaces toward the center of crystals. Dehydration along the *b*-axis of the unit cells of the monohydrate was most rapid because of the existence of channels that facilitate transport of water molecules along the *b*-axis in the monohydrate.

This research explained why powder-like crystals of the anhydrous sodium naproxen were produced by dehydration of hydrated forms. SEM analysis of the anhydrous species which was generated by dehydration of the monohydrated form showed the enormous cracks aligned along the *b*-axis. The alignment of the cracks was explained by significant shrinkage (8.4 %) along the *c*-axis as a result of the dehydration. These cracks made the anhydrous crystals that were produced from the monohydrated species very brittle and, eventually, such crystals became powder-like.

8.2 RECOMMENDATIONS

The following recommendations are offered for future work: (1) modification of crystal morphology by additives and different solvents and (2) study on mechanism of transformation between pseudopolymorphs in solutions.

(1) The shape of crystalline organic solids is an important factor in the design and operation of solid-liquid separation systems. Crystal morphology affects the efficiency of downstream processes such as filtering, washing, and drying, and influences material properties such as density and mechanical strength. The modification of morphology can be performed by adding additives or using different ratios and/or kinds of solvents. In this present study, the dihydrated sodium naproxen from mixtures of water and methanol has much smaller aspect ratio than that from in pure water. This result

shows a possibility of morphology modification by changing the solvent compositions.

(2) Study of polymorphic (or pseudopolymorphic) transformation is considered very important in the pharmaceutical field because the sudden appearance of a more stable polymorph, which had not been discovered at the early stage of pharmaceutical development, can cause loss of time and resources. Microscopic mechanisms of polymorphic transformations (or pseudopolymorphism) can provide deep insights into stabilization of metastable polymorphs. Sodium naproxen has transitions between pseudopolymorphs in pure water and water-methanol solutions. Especially, from the water-methanol solutions, needle-like crystals transformed to plate-like crystals reversibly. The mechanism of interconversion was not studied in this work, because it was out of scope. However, the study on the mechanism of interconversion will be a good research project with sodium naproxen in water-methanol mixtures.

APPENDIX A

FITTING OF KINETIC MODELS TO ISOTHERMAL TGA DATA OF SODIUM NAPROXEN

A.1 1ST WATER REMOVAL FROM THE DIHYDRATED SODIUM NAPROXEN

A.1.1 T = 24.0˚C

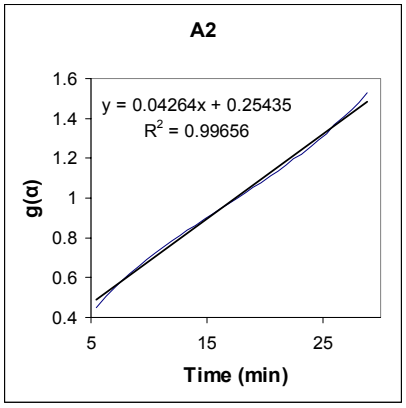

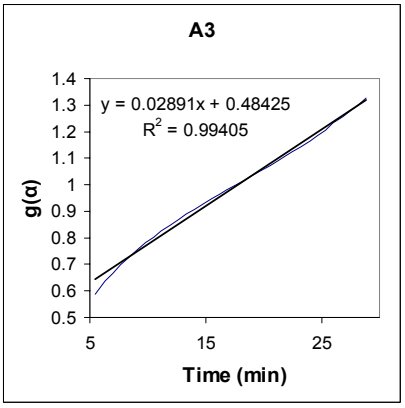

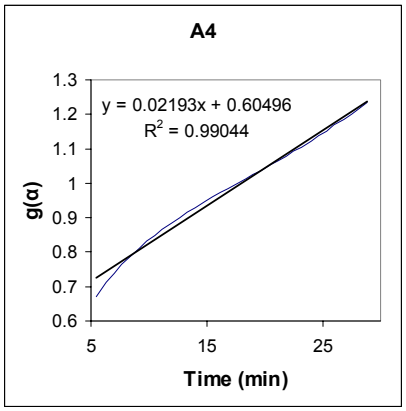
A4
y = 0.02193x + 0.60496
R2 = 0.99044
g(α)
Time (min)

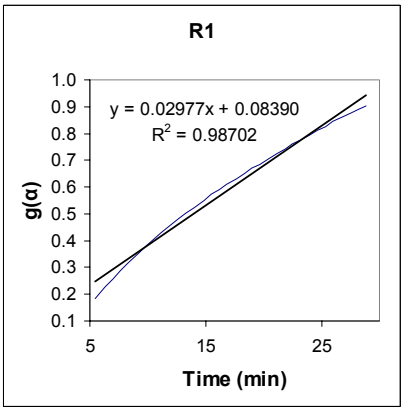
R1
y = 0.02977x + 0.08390
R2 = 0.98702
g(α)
Time (min)

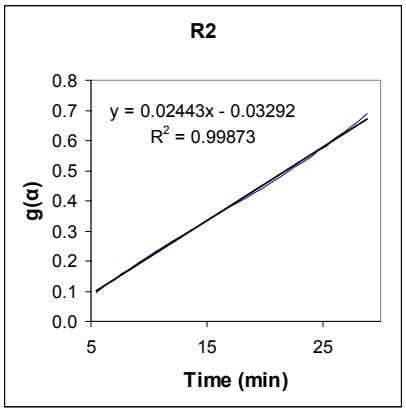
R2
y = 0.02443x - 0.03292
R2 = 0.99873
g(α)
Time (min)

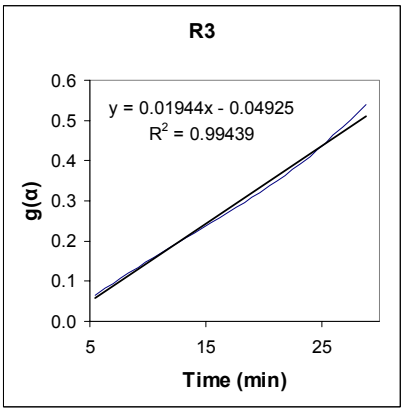
R3
y = 0.01944x - 0.04925
R2 = 0.99439
g(α)
Time (min)

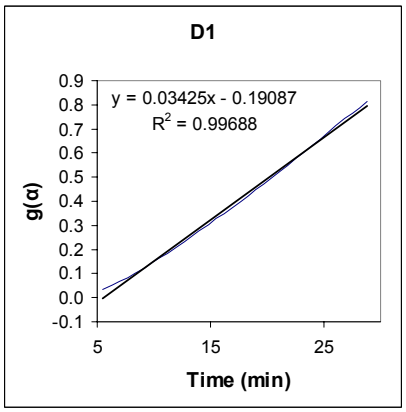
D1
y = 0.03425x - 0.19087
R2 = 0.99688
g(α)
Time (min)

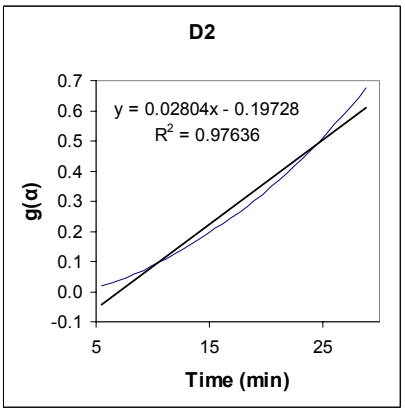
D2
y = 0.02804x - 0.19728
R2 = 0.97636
g(α)
Time (min)

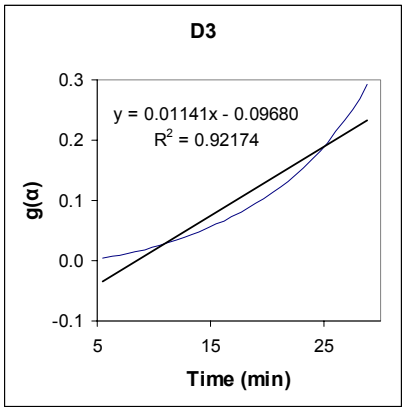
D3
y = 0.01141x - 0.09680
R2 = 0.92174
g(α)
Time (min)

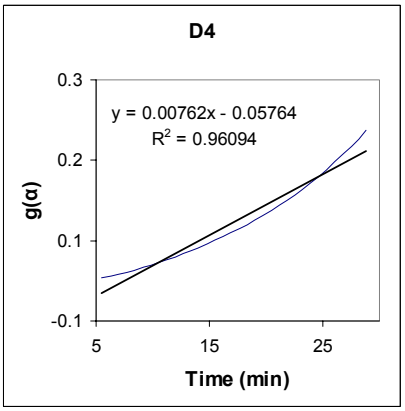
D4
y = 0.00762x - 0.05764
R2 = 0.96094
g(α)
Time (min)

A.1.2 T = 26.4˚C

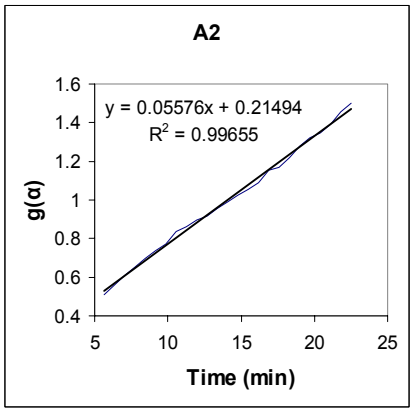
A2
y = 0.05576x + 0.21494
R2 = 0.99655
g(α)
Time (min)

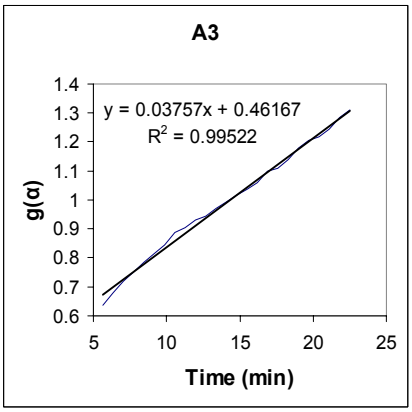
A3
y = 0.03757x + 0.46167
R2 = 0.99522
g(α)
Time (min)

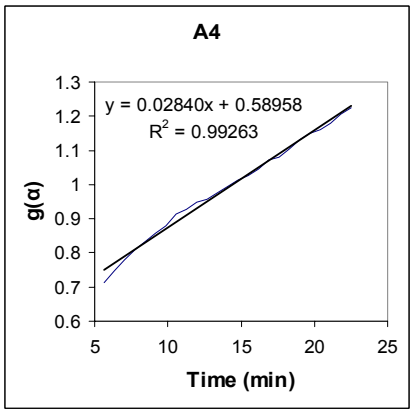
A4
y = 0.02840x + 0.58958
R2 = 0.99263
g(α)
Time (min)

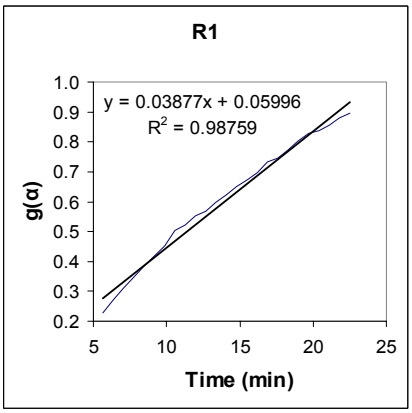
R1
y = 0.03877x + 0.05996
R2 = 0.98759
g(α)
Time (min)

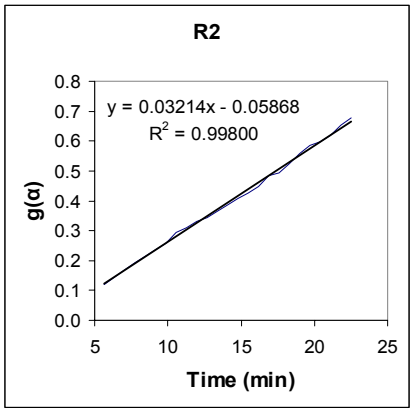
R2
y = 0.03214x - 0.05868
R2 = 0.99800
g(α)
Time (min)

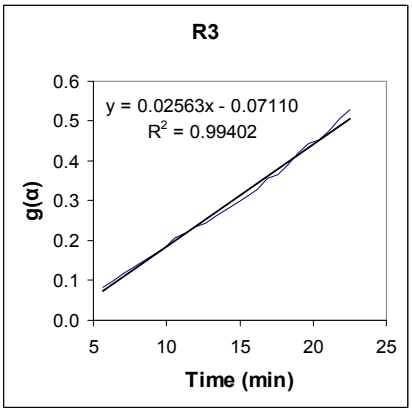
R3
y = 0.02563x - 0.07110
R2 = 0.99402
g(α)
Time (min)

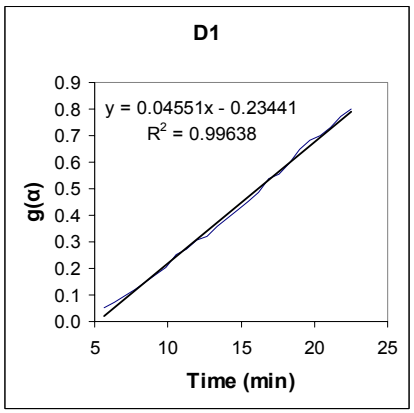
D1
y = 0.04551x - 0.23441
R2 = 0.99638
g(α)
Time (min)

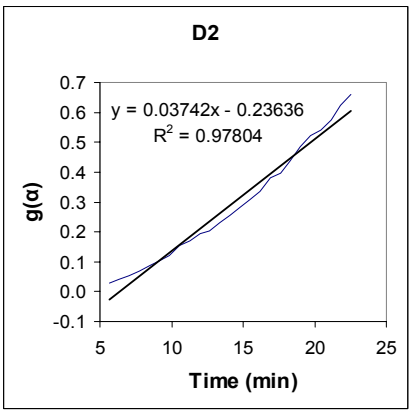
D2
y = 0.03742x - 0.23636
R2 = 0.97804
g(α)
Time (min)

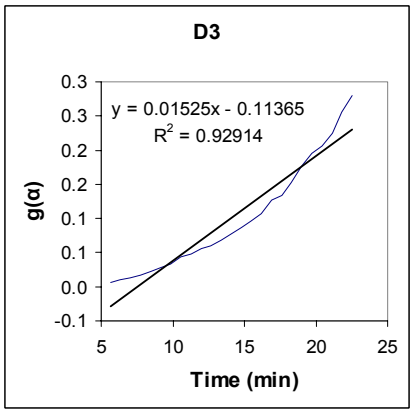
D3
y = 0.01525x - 0.11365
R2 = 0.92914
g(α)
Time (min)

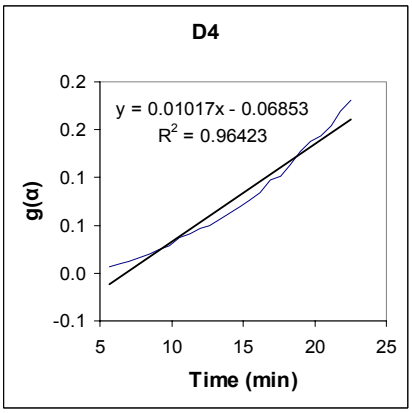
D4
y = 0.01017x - 0.06853
R2 = 0.96423
g(α)
Time (min)

A.1.3 T = 29.5˚C

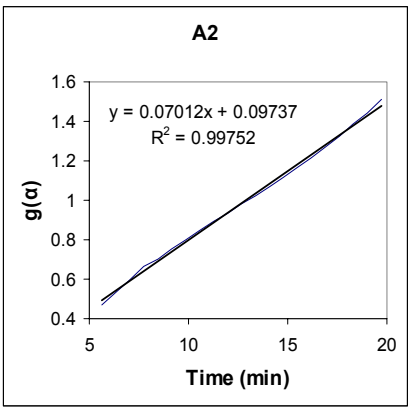
A2
y = 0.07012x + 0.09737
R2 = 0.99752
g(α)
Time (min)

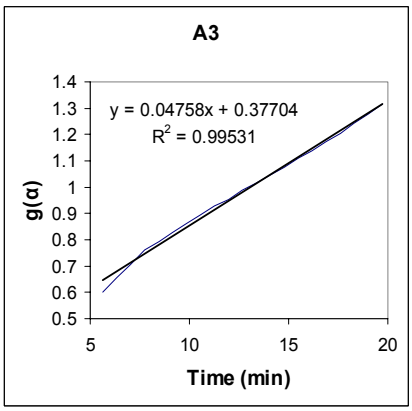
A3
y = 0.04758x + 0.37704
R2 = 0.99531
g(α)
Time (min)

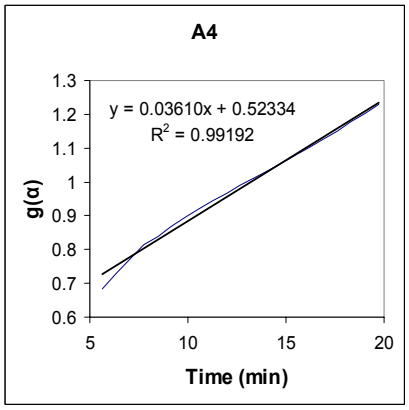
A4
y = 0.03610x + 0.52334
R2 = 0.99192
g(α)
Time (min)

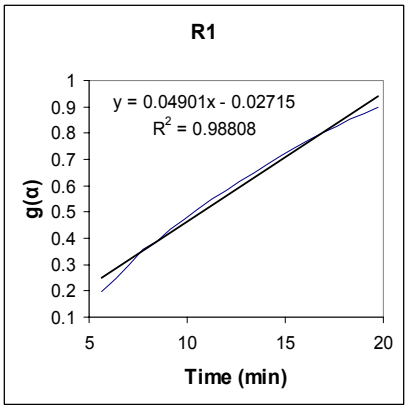
R1
y = 0.04901x - 0.02715
R2 = 0.98808
g(α)
Time (min)

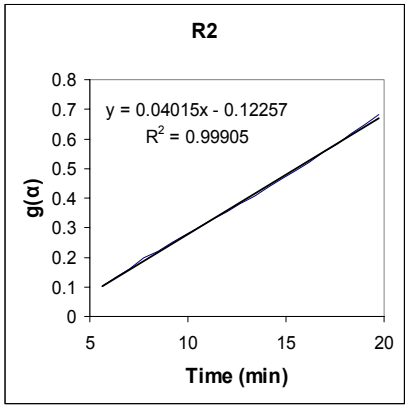
R2
y = 0.04015x - 0.12257
R2 = 0.99905
g(α)
Time (min)

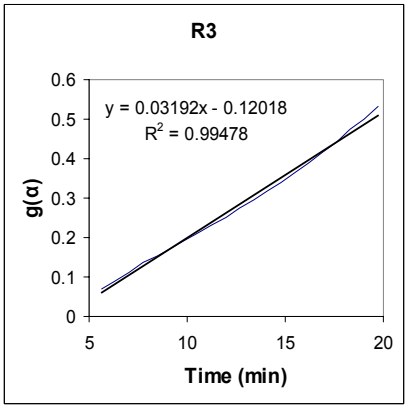
R3
y = 0.03192x - 0.12018
R2 = 0.99478
g(α)
Time (min)

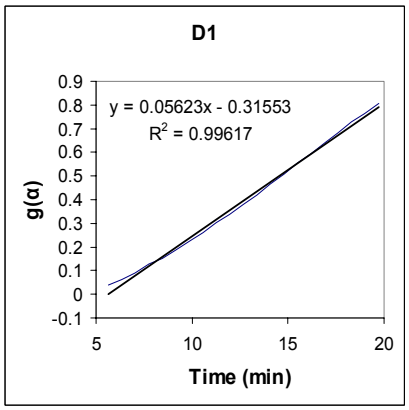
D1
y = 0.05623x - 0.31553
R2 = 0.99617
g(α)
Time (min)

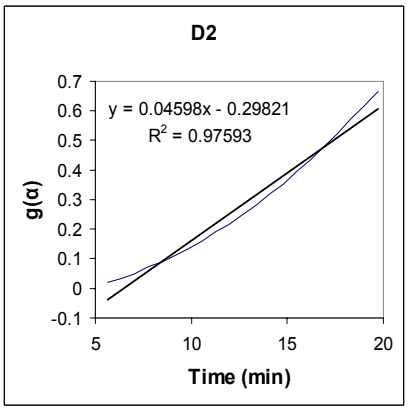
D2
y = 0.04598x - 0.29821
R2 = 0.97593
g(α)
Time (min)

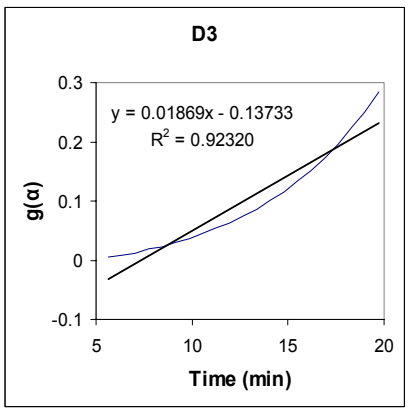
D3
y = 0.01869x - 0.13733
R2 = 0.92320
g(α)
Time (min)

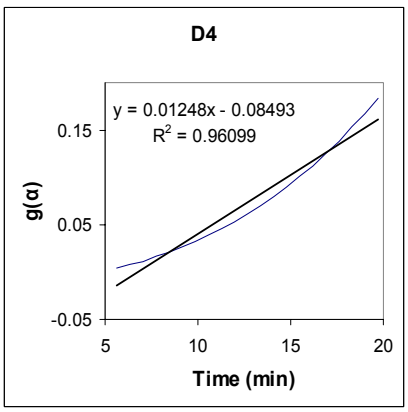
D4
y = 0.01248x - 0.08493
R2 = 0.96099
g(α)
Time (min)

A.2 2ND WATER REMOVAL FROM THE DIHYDRATED SODIUM NAPROXEN

A.2.1 T = 24.0˚C

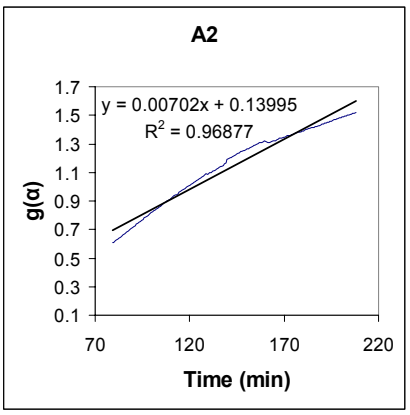

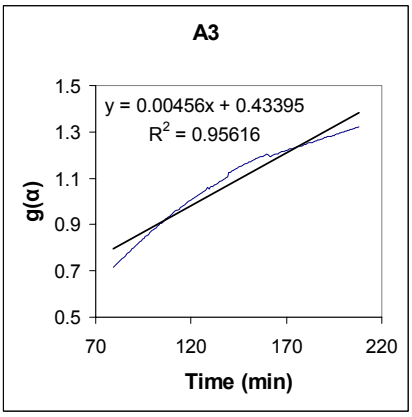

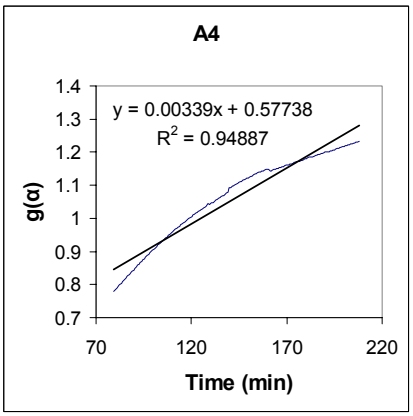

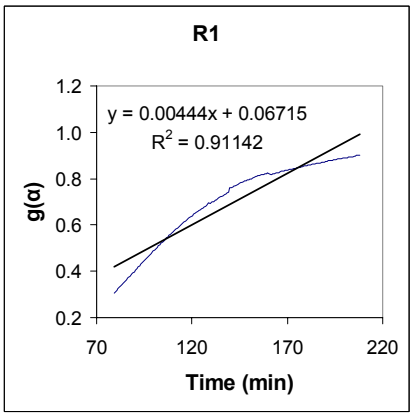

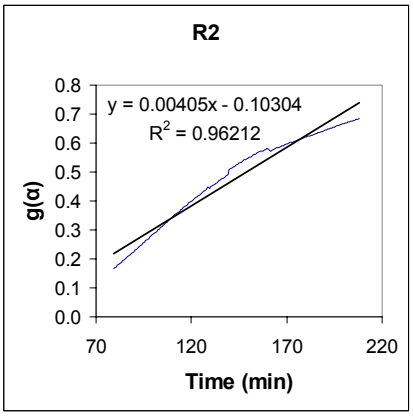
R2
y = 0.00405x - 0.10304
R2 = 0.96212
g(α)
Time (min)

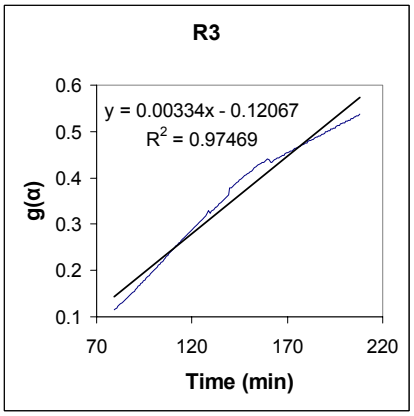
R3
y = 0.00334x - 0.12067
R2 = 0.97469
g(α)
Time (min)

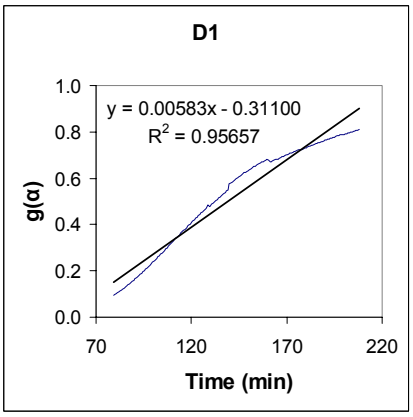
D1
y = 0.00583x - 0.31100
R2 = 0.95657
g(α)
Time (min)

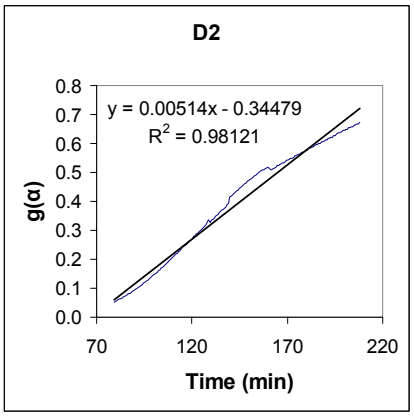
D2
y = 0.00514x - 0.34479
R2 = 0.98121
g(α)
Time (min)

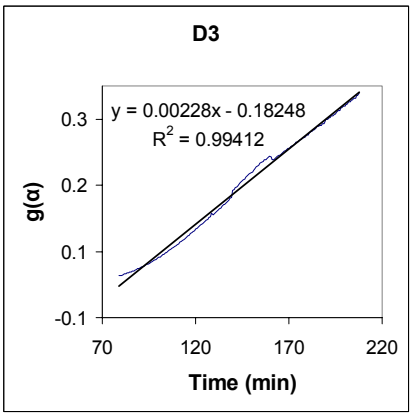
D3
y = 0.00228x - 0.18248
R2 = 0.99412
g(α)
Time (min)

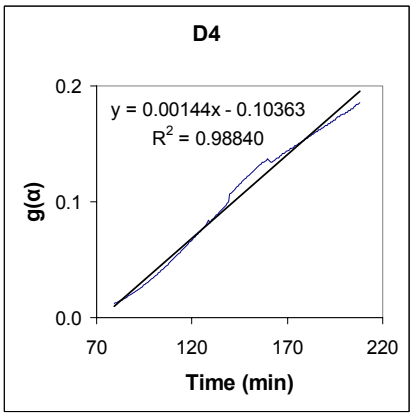
D4
y = 0.00144x - 0.10363
R2 = 0.98840
g(α)
Time (min)

A.2.2 T = 26.4˚C

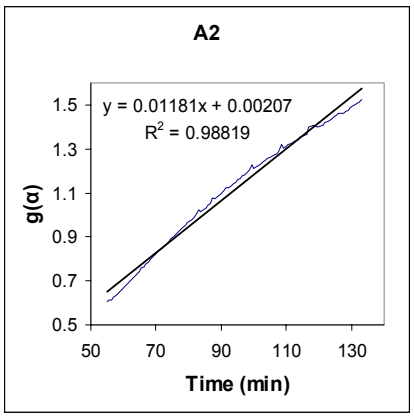
A2
y = 0.01181x + 0.00207
R2 = 0.98819
g(α)
Time (min)

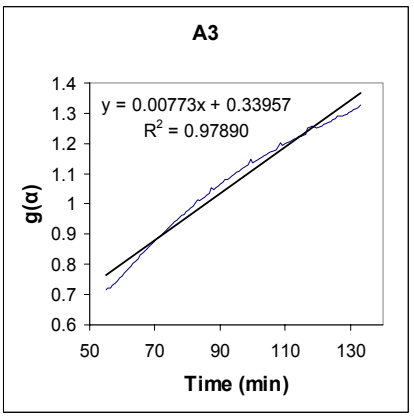
A3
y = 0.00773x + 0.33957
R2 = 0.97890
g(α)
Time (min)

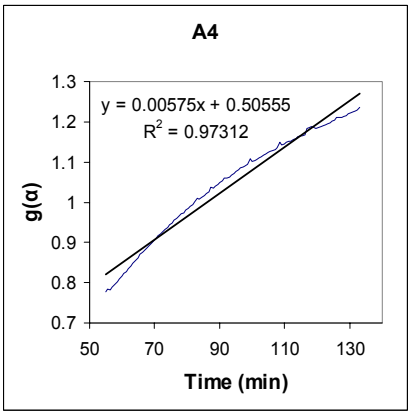
A4
y = 0.00575x + 0.50555
R2 = 0.97312
g(α)
Time (min)

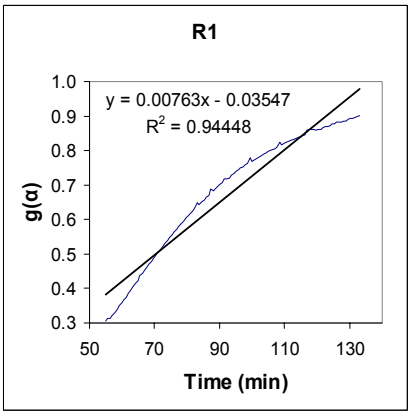
R1
y = 0.00763x - 0.03547
R2 = 0.94448
g(α)
Time (min)

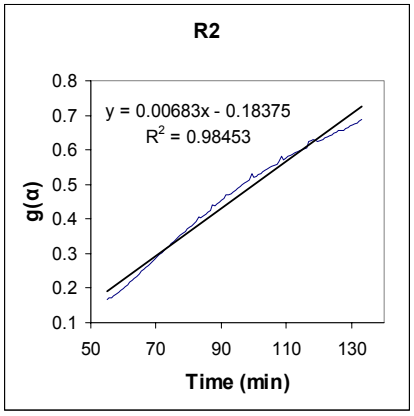
R2
y = 0.00683x - 0.18375
R2 = 0.98453
g(α)
Time (min)

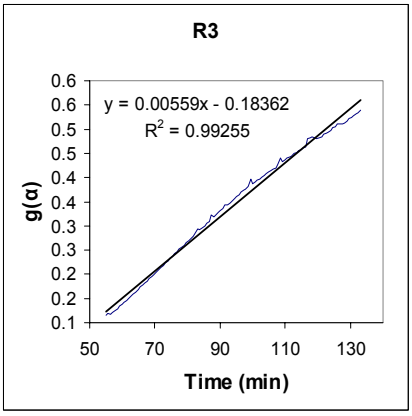
R3
y = 0.00559x - 0.18362
R2 = 0.99255
g(α)
Time (min)

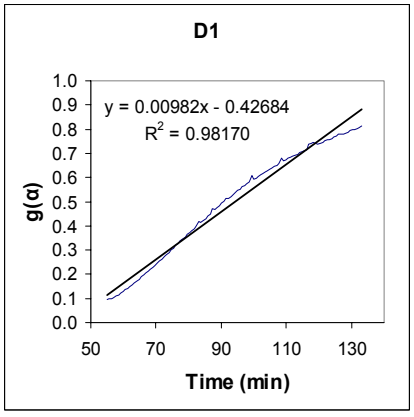
D1
y = 0.00982x - 0.42684
R2 = 0.98170
g(α)
Time (min)

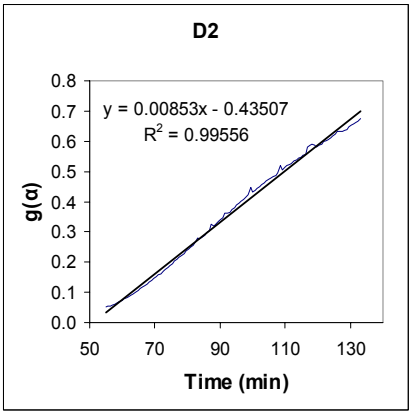
D2
y = 0.00853x - 0.43507
R2 = 0.99556
g(α)
Time (min)

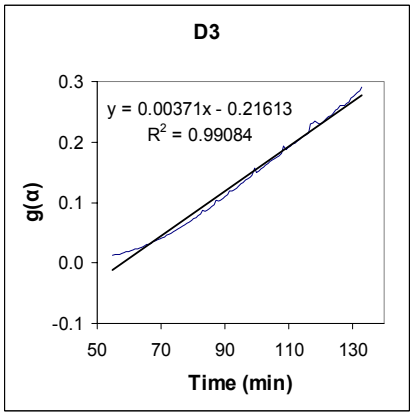
D3
y = 0.00371x - 0.21613
R2 = 0.99084
g(α)
Time (min)

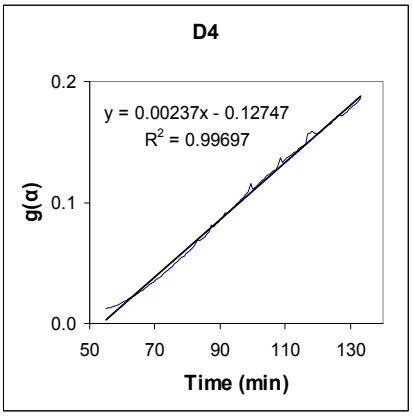
D4
y = 0.00237x - 0.12747
R2 = 0.99697
g(α)
Time (min)

A.3 1ST WATER REMOVAL FROM THE MONOHYDRATED SODIUM NAPROXEN

A.3.1 T = 24.1˚C

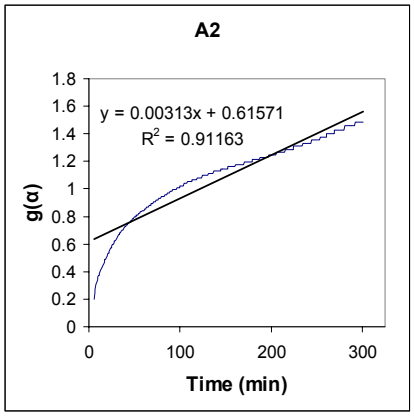

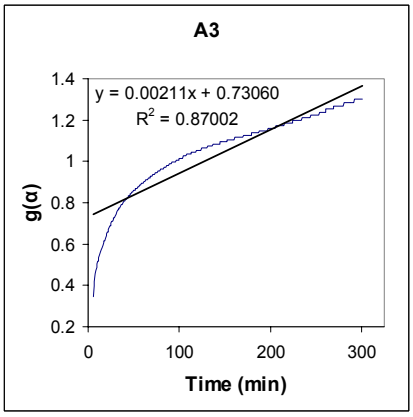

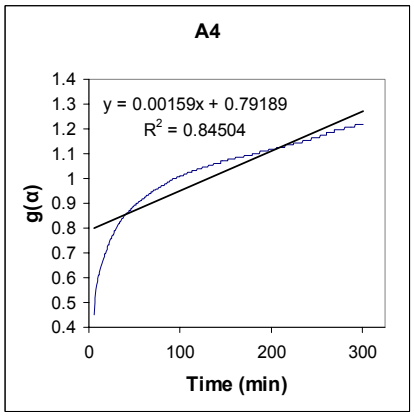

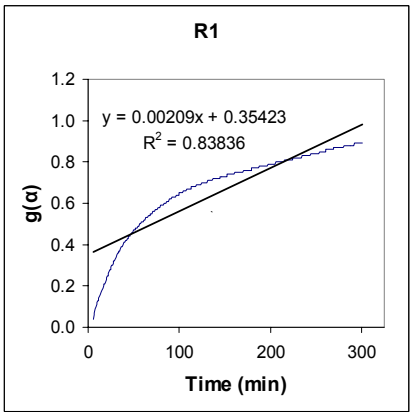

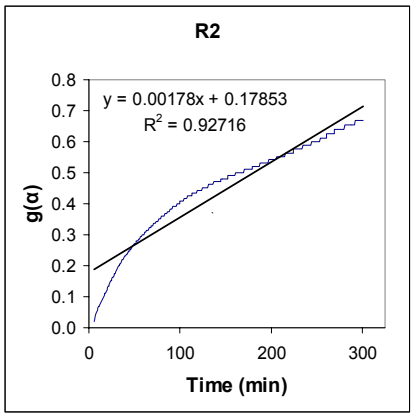
R2
y = 0.00178x + 0.17853
R2 = 0.92716
g(α)
Time (min)

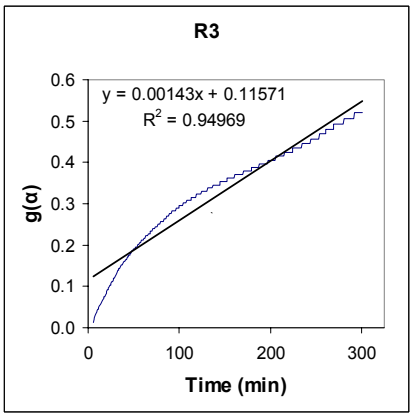
R3
y = 0.00143x + 0.11571
R2 = 0.94969
g(α)
Time (min)

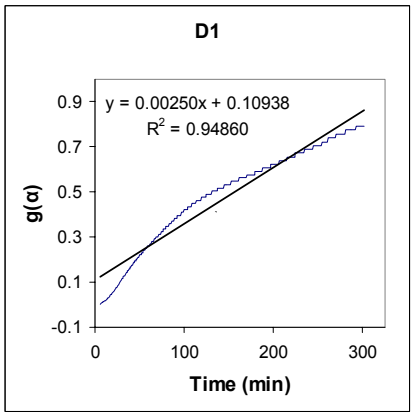
D1
y = 0.00250x + 0.10938
R2 = 0.94860
g(α)
Time (min)

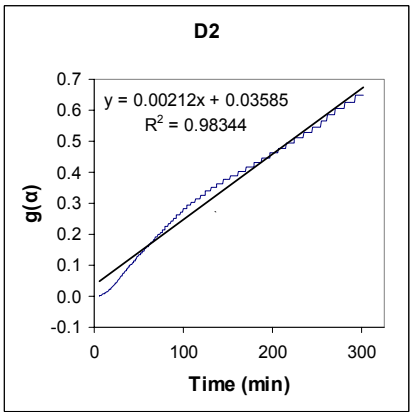
D2
y = 0.00212x + 0.03585
R2 = 0.98344
g(α)
Time (min)

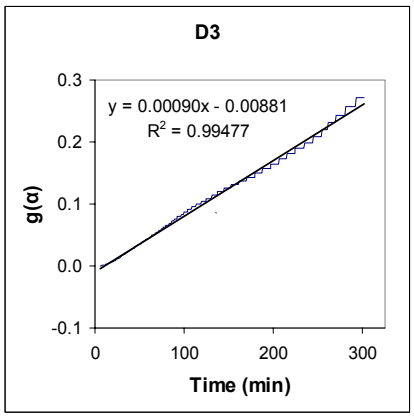
D3
y = 0.00090x - 0.00881
R2 = 0.99477
g(α)
Time (min)

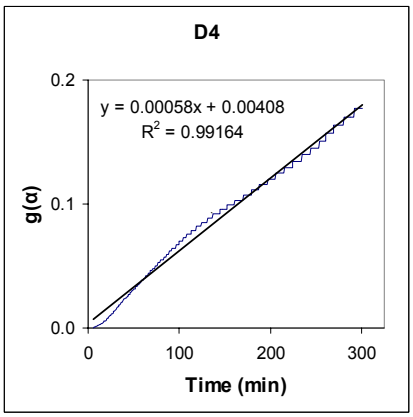
D4
y = 0.00058x + 0.00408
R2 = 0.99164
g(α)
Time (min)

A.3.2 T = 26.9˚C

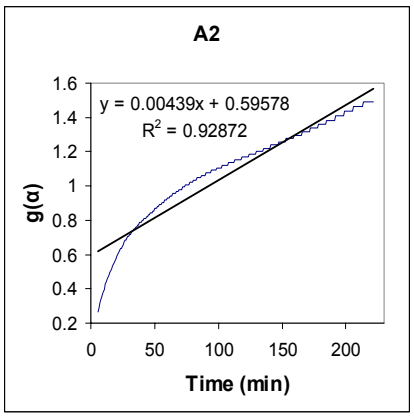
A2
y = 0.00439x + 0.59578
R2 = 0.92872
g(α)
Time (min)

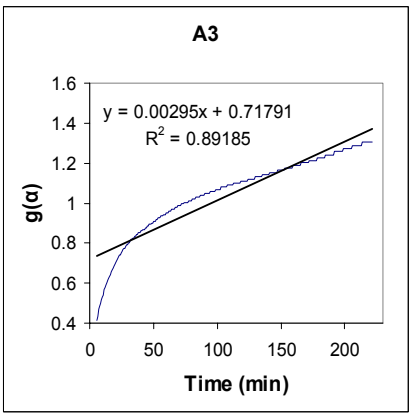
A3
y = 0.00295x + 0.71791
R2 = 0.89185
g(α)
Time (min)

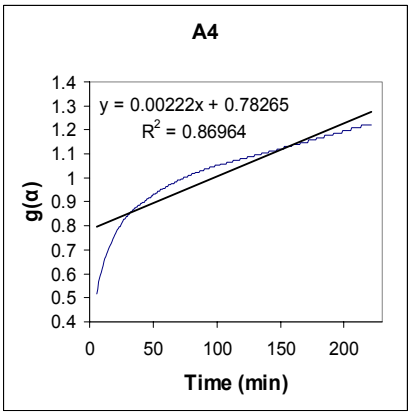
A4
y = 0.00222x + 0.78265
R2 = 0.86964
g(α)
Time (min)

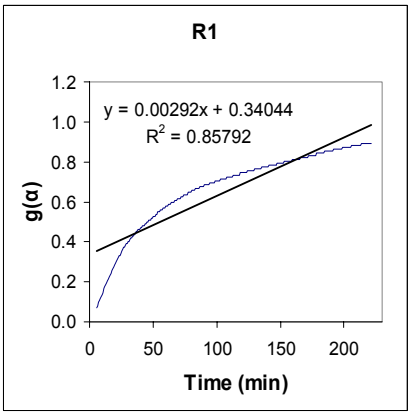
R1
y = 0.00292x + 0.34044
R2 = 0.85792
g(α)
Time (min)

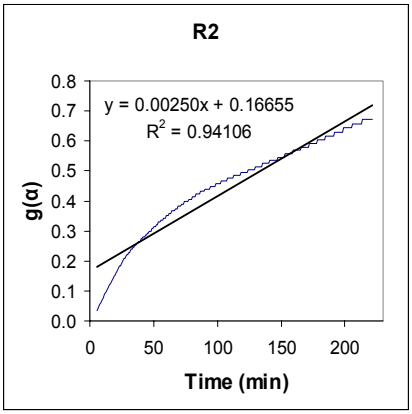
R2
y = 0.00250x + 0.16655
R2 = 0.94106
g(α)
Time (min)

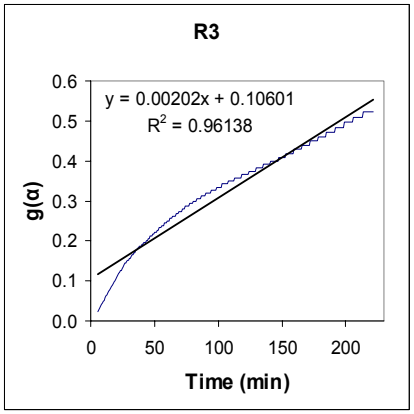
R3
y = 0.00202x + 0.10601
R2 = 0.96138
g(α)
Time (min)

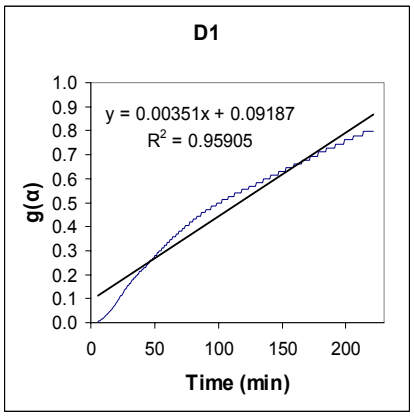
D1
y = 0.00351x + 0.09187
R2 = 0.95905
g(α)
Time (min)

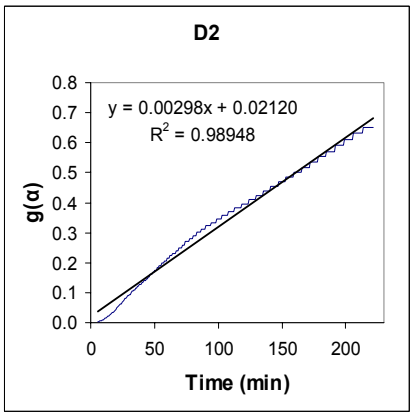
D2
y = 0.00298x + 0.02120
R2 = 0.98948
g(α)
Time (min)

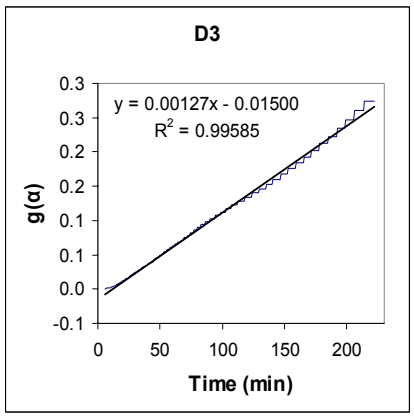
D3
y = 0.00127x - 0.01500
R2 = 0.99585
g(α)
Time (min)

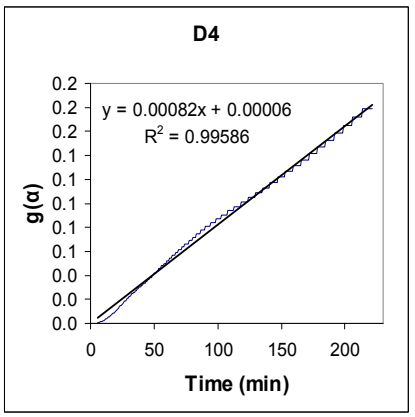
D4
y = 0.00082x + 0.00006
R2 = 0.99586
g(α)
Time (min)

A.3.3 T = 29.8˚C

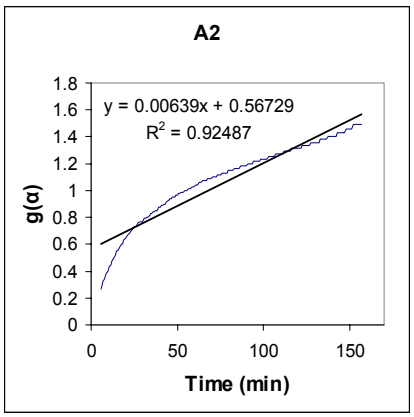
A2
y = 0.00639x + 0.56729
R2 = 0.92487
g(α)
Time (min)

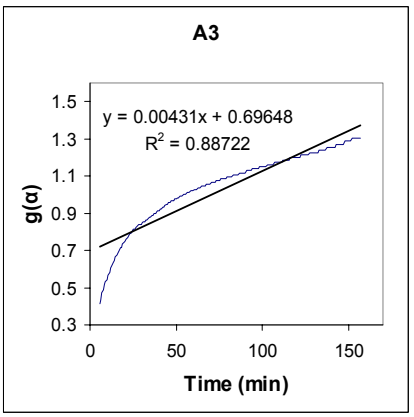
A3
y = 0.00431x + 0.69648
R2 = 0.88722
g(α)
Time (min)

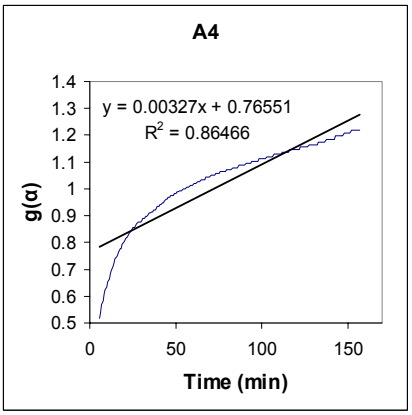
A4
y = 0.00327x + 0.76551
R2 = 0.86466
g(α)
Time (min)

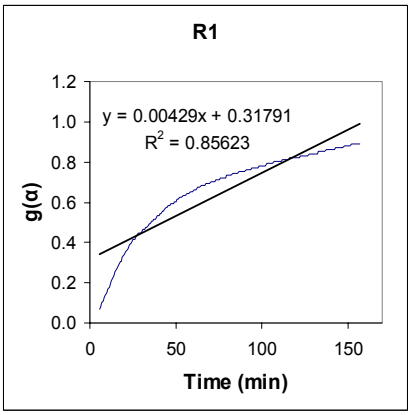
R1
y = 0.00429x + 0.31791
R2 = 0.85623
g(α)
Time (min)

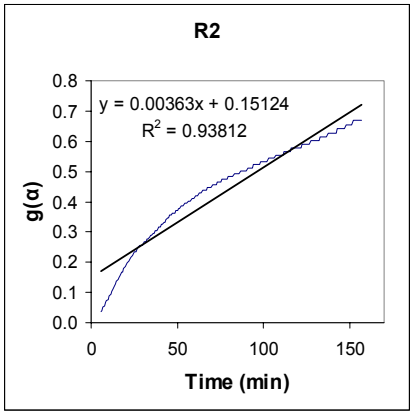
R2
y = 0.00363x + 0.15124
R² = 0.93812
g(α)
Time (min)

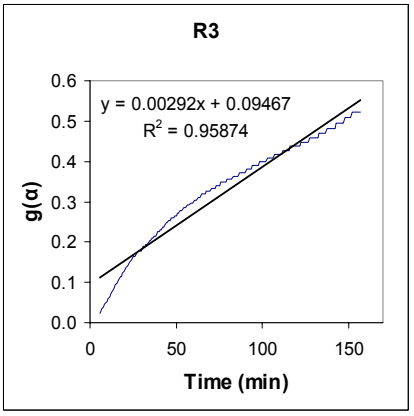
R3
y = 0.00292x + 0.09467
R² = 0.95874
g(α)
Time (min)

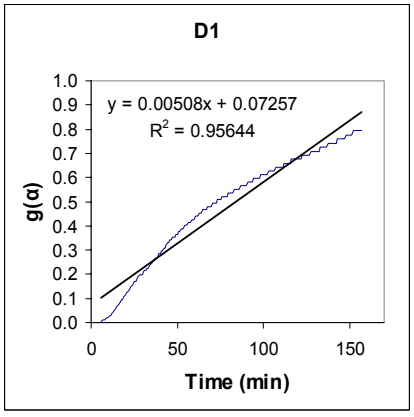
D1
y = 0.00508x + 0.07257
R² = 0.95644
g(α)
Time (min)

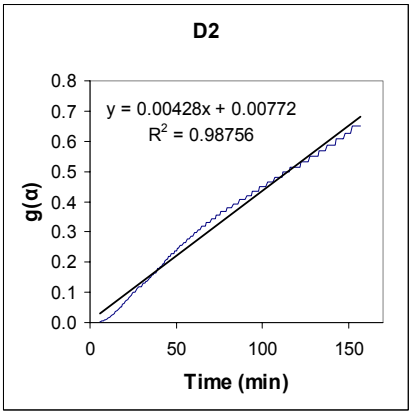
D2
y = 0.00428x + 0.00772
R² = 0.98756
g(α)
Time (min)

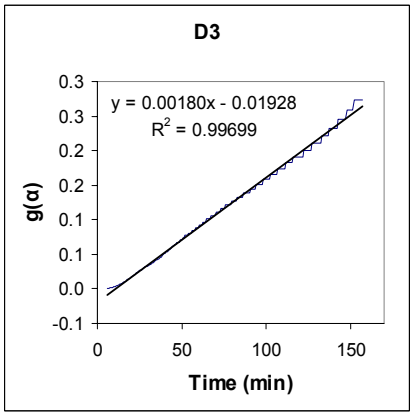
D3
y = 0.00180x - 0.01928
R² = 0.99699
g(α)
Time (min)

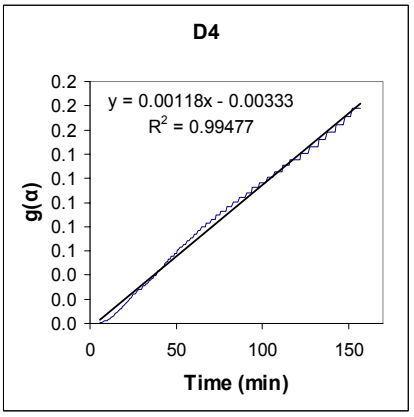
D4
y = 0.00118x - 0.00333
R² = 0.99477
g(α)
Time (min)

APPENDIX B

CALIBRATION CURVES

B.1 CALIBRATION CURVE TO MEASURE CONCENTRATIONS OF SODIUM NAPROXEN IN PURE WATER SOLUTIONS

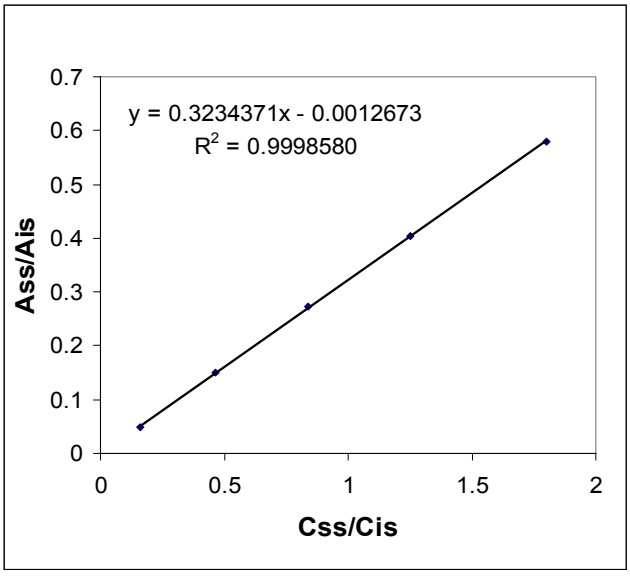

B.2 CALIBRATION CURVE TO MEASURE CONCENTRATIONS OF SODIUM NAPROXEN IN 64 MOL% METHANOL IN AQUEOUS SOLUTIONS

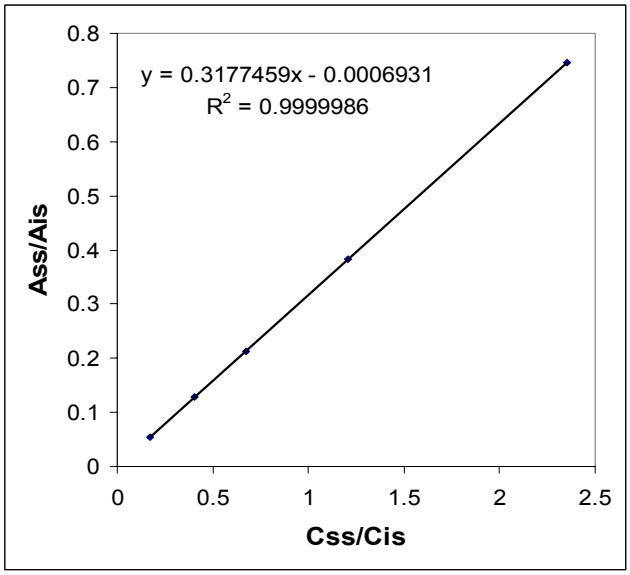

APPENDIX C

DETERMINATION OF DENSITY OF ANHYDROUS SODIUM NAPROXEN BY THE METHOD OF FLOTATION

Density of anhydrous sodium naproxen at an ambient temperature was determined by the method of flotation. Cyclohexane and carbon tetrachloride were prepared whose densities are 0.774 g/cm^3 and 1.59 g/cm^3, respectively. 2-mL vials were used for the experiment. First, a crystal of interest was put into a vial and carbon tetrachloride was added into the vial. The crystal floated because the density for the crystal in the vial is lower than that for carbon tetrachloride. The desired amount of cyclohexane was added into the vial and the density in the vial changes depending on the amount of cyclohexane. If the crystal sank the density of the mixture is higher than the crystal. The density of a mixture of two solvents was estimated with the equation as follows.

$$D_M = \frac{V_1 \times D_1 + V_2 \times D_2}{V_1 + V_2} \tag{C.1}$$

where D is density, V is volume, and subscripts 1, 2 and M are solvent 1 and 2 and a mixture of 1 and 2, respectively. In this equation, it is assumed that two volumes of solvents are additive on mixing. The amount of solvents and calculated densities are listed in Table C.1. In Run 3, upper and lower bounds of densities are very close and the

average of two densities is 1.386 g/cm^3 which is the estimated density of anhydrous sodium naproxen.

Table C-1. Prepared solutions and densities

Run	Carbon Tetrachloride (ml)	Cyclohexane (ml)		Density	
		upper boound	lower bound	upper bound	lower bound
1	0.54025	0.16053	0.19005	1.40308	1.37765
2	0.55588	0.18049	0.18751	1.38999	1.38418
3	0.56641	0.18835	0.18946	1.38637	1.38547

APPENDIX D

CRYSTALOGRAPHY INFORMATION OF THE ANHYDROUS SODIUM NAPROXEN

Table D-1. Fractional hydrogen atomic coordinates and equivalent isotropic thermal parameters for anhydrous sodium naproxen

Atom	*x*	*y*	*z*	U_{eq}
H1	-0.7657	1.3092	-0.3332	0.046
H1'	0.1415	0.2942	0.3836	0.057
H3	-0.5955	1.3931	-0.2296	0.042
H3'	-0.0733	0.3544	0.2971	0.051
H4'	-0.2216	0.2368	0.202	0.046
H4	-0.4186	1.2794	-0.1459	0.039
H6'	0.016	-0.3043	0.1888	0.044
H6	-0.397	0.6805	-0.2354	0.04
H8'	0.2275	-0.3704	0.2752	0.058
H8	-0.5418	0.616	-0.3468	0.055
H9	-0.7254	0.724	-0.4284	0.063
H9'	0.3741	-0.2559	0.3696	0.065
H11'	-0.2946	-0.0267	0.1191	0.036
H11	-0.2446	1.0203	-0.1011	0.035
H13D	-0.286	-0.4	0.1518	0.061
H13E	-0.1612	-0.4421	0.1183	0.061
H13F	-0.306	-0.3871	0.0752	0.061
H13A	-0.1412	0.8179	-0.1752	0.064
H13B	-0.2094	0.599	-0.1545	0.064
H13C	-0.1001	0.7296	-0.1028	0.064
H14A	-0.9056	1.3876	-0.4291	0.106
H14B	-0.9938	1.2371	-0.3919	0.106
H14C	-1.0335	1.2577	-0.4685	0.106
H14D	0.2704	0.2867	0.4876	0.129
H14E	0.3563	0.4062	0.4424	0.129
H14F	0.4305	0.2991	0.5092	0.129

Table D-2. Fractional non-hydrogen atomic coordinates and equivalent isotropic thermal parameters for anhydrous sodium naproxen

Atom	*x*	*y*	*z*	U_{eq}
Na1	-0.10398(10)	0.48664(18)	0.00061(5)	0.0338(3)
Na2	-0.40560(10)	0.25104(19)	-0.00854(5)	0.0346(3)
O1a	-0.33202(19)	0.5662(3)	-0.05815(9)	0.0323(4)
O1b	-0.06803(19)	-0.1564(3)	0.04241(9)	0.0338(5)
O2a	-0.43654(18)	0.8879(4)	-0.04611(9)	0.0337(5)
C1a	-0.7203(3)	1.1676(5)	-0.33536(13)	0.0380(7)
C1b	0.1576(3)	0.1591(6)	0.36098(14)	0.0474(8)
C2a	-0.6072(3)	1.1051(5)	-0.28458(12)	0.0326(6)
C2b	0.0641(3)	0.0937(5)	0.30248(13)	0.0381(7)
C3a	-0.5566(3)	1.2458(5)	-0.23121(13)	0.0347(6)
C3b	-0.0535(3)	0.2190(5)	0.27568(14)	0.0425(7)
C4b	-0.1408(3)	0.1498(6)	0.21891(13)	0.0383(7)
C4a	-0.4528(3)	1.1775(5)	-0.18137(13)	0.0326(6)
C5a	-0.3950(3)	0.9616(5)	-0.18078(12)	0.0282(6)
C5b	-0.1147(3)	-0.0449(5)	0.18498(13)	0.0313(6)
C6b	-0.0021(3)	-0.1694(5)	0.21093(13)	0.0367(7)
C6a	-0.4387(3)	0.8258(5)	-0.23407(13)	0.0334(6)
C7a	-0.5436(3)	0.8935(5)	-0.28734(13)	0.0333(6)
C7b	0.0899(3)	-0.1058(5)	0.27003(13)	0.0360(7)
C8b	0.2085(3)	-0.2346(7)	0.29674(15)	0.0482(8)
C8a	-0.5879(3)	0.7558(6)	-0.34292(14)	0.0457(8)
C9a	-0.6955(3)	0.8202(7)	-0.39107(16)	0.0524(9)
C9b	0.2944(3)	-0.1669(7)	0.35220(16)	0.0538(9)
C10b	0.2705(3)	0.0296(7)	0.38501(15)	0.0507(9)
C10a	-0.7638(3)	1.0262(6)	-0.38696(14)	0.0440(8)
C11b	-0.2102(3)	-0.1069(5)	0.12103(13)	0.0301(6)
C11a	-0.2871(3)	0.8862(5)	-0.12182(12)	0.0294(6)
C12a	-0.3570(2)	0.7688(5)	-0.07157(12)	0.0242(5)
C12b	-0.1486(2)	-0.0253(5)	0.06357(12)	0.0252(5)
C13b	-0.2440(3)	-0.3571(5)	0.11613(15)	0.0405(7)
C13a	-0.1741(3)	0.7452(6)	-0.14027(14)	0.0424(7)
C14a	-0.9586(4)	1.2517(8)	-0.43119(19)	0.0709(12)
C14b	0.3550(5)	0.2839(9)	0.4724(2)	0.0860(15)
O3a	-0.8740(2)	1.0633(5)	-0.43720(11)	0.0599(7)
O3b	0.3664(3)	0.0764(6)	0.44008(12)	0.0704(8)
O2b	-0.17852(19)	0.1665(3)	0.04152(9)	0.0353(5)

Table D-3. Anisotropic thermal parameter with their e.s.d.'s in parentheses for anhydrous sodium naproxen

Atom	U_{11}	U_{22}	U_{33}	U_{23}	U_{13}	U_{12}
Na1	0.0275(6)	0.0249(6)	0.0515(7)	0.0028(5)	0.0142(4)	0.0022(4)
Na2	0.0290(6)	0.0250(6)	0.0531(6)	0.0039(5)	0.0165(5)	0.0029(5)
O1a	0.0330(10)	0.0239(10)	0.0404(10)	0.0017(8)	0.0087(8)	-0.0009(8)
O1b	0.0294(10)	0.0296(11)	0.0463(11)	-0.0017(9)	0.0172(8)	0.0004(9)
O2a	0.0284(10)	0.0346(12)	0.0417(10)	0.0008(9)	0.0152(8)	0.0033(9)
C1a	0.0358(15)	0.0379(17)	0.0382(15)	0.0070(13)	0.0030(12)	0.0049(13)
C1b	0.054(2)	0.049(2)	0.0389(16)	-0.0011(15)	0.0086(14)	-0.0063(16)
C2a	0.0341(15)	0.0320(16)	0.0321(14)	0.0044(12)	0.0076(11)	-0.0009(12)
C2b	0.0432(17)	0.0389(18)	0.0334(14)	0.0021(13)	0.0109(12)	0.0004(14)
C3a	0.0382(15)	0.0258(14)	0.0395(15)	0.0032(13)	0.0064(11)	0.0061(12)
C3b	0.0546(19)	0.0308(17)	0.0435(16)	-0.0077(13)	0.0135(14)	0.0043(14)
C4b	0.0391(16)	0.0339(16)	0.0438(16)	0.0021(14)	0.0132(13)	0.0062(13)
C4a	0.0359(15)	0.0280(15)	0.0326(14)	0.0004(11)	0.0042(11)	0.0020(12)
C5a	0.0255(13)	0.0283(15)	0.0326(14)	0.0061(11)	0.0098(10)	-0.0002(11)
C5b	0.0331(14)	0.0292(15)	0.0347(14)	0.0018(12)	0.0141(11)	0.0001(12)
C6b	0.0393(16)	0.0327(16)	0.0398(15)	-0.0034(13)	0.0121(12)	0.0054(13)
C6a	0.0317(14)	0.0269(15)	0.0412(15)	0.0009(12)	0.0066(11)	0.0039(12)
C7a	0.0334(14)	0.0328(16)	0.0332(14)	0.0019(12)	0.0056(11)	-0.0003(12)
C7b	0.0402(16)	0.0356(17)	0.0344(14)	0.0028(13)	0.0132(12)	0.0010(13)
C8b	0.0431(17)	0.052(2)	0.0505(18)	0.0024(17)	0.0114(14)	0.0125(16)
C8a	0.0502(18)	0.0398(18)	0.0453(17)	-0.0078(15)	0.0053(13)	0.0035(16)
C9a	0.054(2)	0.058(2)	0.0400(17)	-0.0132(17)	-0.0021(14)	0.0004(18)
C9b	0.0415(18)	0.065(2)	0.053(2)	0.0077(18)	0.0040(14)	0.0071(17)
C10b	0.0474(19)	0.065(2)	0.0376(16)	0.0060(17)	0.0044(13)	-0.0085(17)
C10a	0.0389(17)	0.054(2)	0.0362(16)	0.0046(15)	0.0009(12)	-0.0015(15)
C11b	0.0257(13)	0.0276(15)	0.0387(15)	0.0004(12)	0.0107(11)	0.0004(11)
C11a	0.0244(13)	0.0322(16)	0.0327(14)	0.0025(12)	0.0087(10)	-0.0040(11)
C12a	0.0172(11)	0.0252(15)	0.0290(13)	-0.0012(11)	0.0022(9)	-0.0015(10)
C12b	0.0175(12)	0.0256(14)	0.0319(13)	-0.0025(12)	0.0038(9)	-0.0061(11)
C13b	0.0409(17)	0.0352(17)	0.0485(17)	0.0017(14)	0.0163(13)	-0.0031(13)
C13a	0.0296(14)	0.058(2)	0.0424(16)	0.0074(16)	0.0144(12)	0.0084(15)
C14a	0.060(2)	0.079(3)	0.063(2)	0.008(2)	-0.0121(18)	0.021(2)
C14b	0.084(3)	0.101(4)	0.064(3)	-0.013(3)	-0.006(2)	-0.020(3)
O3a	0.0496(14)	0.0727(19)	0.0479(13)	-0.0022(13)	-0.0117(10)	0.0090(13)
O3b	0.0614(16)	0.088(2)	0.0524(15)	0.0003(15)	-0.0092(12)	-0.0126(16)
O2b	0.0311(10)	0.0244(11)	0.0495(11)	0.0093(9)	0.0063(8)	-0.0007(8)

REFERENCES

1. Kuhnertb, M.; Gasser, P., Solvates and Polymorphic Modefications of Steroid Hormones.1. *Microchemical Journal* **1971,** 16, (3), 419-428.

2. Morris, K. R., Structural Aspects of Hydrates and Solvates. In *Polymorphism in Pharmaceutical Solids*, Brittain, H. G., Ed. Marcel Dekker: New York, 1999; pp 125-181.

3. Florey, K., Cephradine. In *Analytical Profiles of Drug Substances*, Florey, K., Ed. Academic Press: New York, 1973; Vol. 2, pp 1-62.

4. Byrn, S. R.; Lin, C. T., Effect of Crystal Packing and Defects on Desolvation of Hydrate Crystals of Caffeine and L-(-)-1,4-Cyclohexadiene-1-Alanine. *Journal of the American Chemical Society* **1976,** 98, (13), 4004-4005.

5. Ressler, C., Solid-State dehydrogenation of S-1,4-Cyclohexadiene-1-anine hydrate to L-phenylananine. *Journal of Organic Chemistry* **1972,** 37, (19), 2933.

6. Poole, J. W.; Owen, G.; Silverio, J.; Freyhof, J. N.; B., R. S., Physiochemical Factors Influencing the Absorption of the Anhydrous and Trihydrate Forms of Ampicillin. *Current Therapeutic Research, Clinical and Experimental* **1968,** 10, (6), 292-303.

7. Lefebvre, C.; Guyot-Hermann, A. M.; Draguet-Brughmans, M.; Bouche, R.; Guyot, J. C., Polymorphic transitions of carbamazepine during grinding and compression. *Drug Development and Industrial Pharmacy* **1986,** 12, (11-13), 1913-1927.

8. Braga, D.; Cojazzi, G.; Abati, A.; Maini, L.; Polito, M.; Scaccianoce, L.; Grepioni, F., Making and converting organometallic pseudo-polymorphs via non-solution methods. *Journal of the Chemical Society-Dalton Transactions* **2000**, (21), 3969-3975.

9. Phan, H. V.; Allen, R. H.; Coats, R. A. Sodium (S)-2-(6-Methoxy-2-Naphthyl)Propionate Monohydrate. US005874614A, FEB 23, 1999.

10. Di Martino, P.; Barthelemy, C.; Palmieri, G. F.; Martelli, S., Physical characterization of naproxen sodium hydrate and anhydrate forms. *European Journal Of Pharmaceutical Sciences* **2001,** 14, (4), 293-300.

11. Kim, Y. B.; Park, Y. I.; Lah, W. R., The Crystal Structure of Naproxen Sodium ($C_{14}H_{13}O_3Na$), a Nonsteroidal Antiinflammatory Agent. *Archives of Pharmacal Research* **1990,** 13, (2), 166-173.

12. Cullity, B. D.; Stock, S. R., *Elements of x-ray diffraction*. 3rd ed.; Prentice Hall: Upper Saddle River, N.J., 2001; p xviii, 664 p.

13. Vippagunta, S. R.; Brittain, H. G.; Grant, D. J. W., Crystalline solids. *Advanced Drug Delivery Reviews* **2001,** 48, (1), 3-26.

14. Kulkarni, G.; Kumaradhas, P.; Rao, C., Charge density study of the polymorphs of p-nitrophenol. *Chemistry of Materials* **1998,** 10, (11), 3498-3505.

15. Blagden, N.; Davey, R.; Lieberman, H.; Williams, L.; Payne, R.; Roberts, R.; Rowe, R.; Docherty, R., Crystal chemistry and solvent effects in polymorphic systems - Sulfathiazole. *Journal of the Chemical Society-Faraday Transactions* **1998,** 94, (8), 1035-1044.

16. Caira, M.; Zanol, M.; Peveri, J.; Gazzaniga, A.; Giordano, F., Structural characterization of two polymorphic forms of piroxicam pivalate. *Journal of Pharmaceutical Sciences* **1998,** 87, (12), 1608-1614.

17. Brittain, H. G.; Bugay, D. E.; Bogdanowich, S. J.; Devincentis, J., Spectral Methods for Determination of Water. *Drug Development and Industrial Pharmacy* **1988,** 14, (14), 2029-2046.

18. Dzidic, I.; Kebarle, P., Hydration of Alkali Ions In Gas Phase - Enthalpies and Entropies of Reactions M+(H2O)N-1+H2O = M+(H2O)N. *Journal of Physical Chemistry* **1970,** 74, (7), 1466.

19. Mullin, J. W., *Crystallization*. 4th ed.; Butterworth-Heinemann: Oxford; Boston, 2001; p xv, 594 p.

20. Ostwald, W., Studdien über die Bildung und Umwandlung fester Körper. *Zeitschrift für Physikalische Chemie* **1897,** 22, 289-330.

21. Burger, A.; Ramberger, R., Polymorphism of Pharmaceutical and Other Molecular-Crystals.1.Theory of Thermodynamic Rules. *Mikrochimica Acta* **1979,** 2, (3-4), 259-271.

22. Grant, D. J. W.; Higuchi, T., *Solubility behavior of organic compounds*. John Wiley & Sons: New York, 1990; p 600.

23. Hildebrand, J. H.; Scott, R. L., *The solubility of nonelectrolytes*. 3d ed.; Reinhold Pub. Corp.: New York, 1950; p x, 488 p.

24. Brittain, H. G.; Byrn, S. R., Structural Aspects of Polymorphism. In *Polymorphism in pharmaceutical solids (Drugs and the pharmaceutical sciences, v. 95)*, Brittain, H. G., Ed. M. Dekker: New York, 1999; Vol. 95, pp 73 -124.

25. Cox, S. R.; Willams, D. E., Representation of the Molecular Electrostatic Potential by a net Atomic Charge Model. *Journal of Computational chemistry* **1981,** 2, (3), 304-323.

26. Gasteiger, J.; Marsili, M., Iterative Partial Equalization of Orbital Electronegativity - A Rapid Access to Atomic Charges. *Tetrahedron* **1980,** 36, (22), 3219-3228.

27. Mulliken, R. S., New electroaffinity scale; together with data on valence states and on valence ionization. *The Journal of Chemical Physics* **1934,** 2, 782-793.

28. Chapra, S. C.; Canale, R. P., *Numerical methods for engineers: with programming and software applications*. 3rd ed.; WCB/McGraw-Hill: Boston, 1998; p xix, 924 p.

29. Reklaitis, G. V.; Ravindran, A.; Ragsdell, K. M., *Engineering optimization: methods and applications*. Wiley: New York, 1983; p xviii, 684 p.

30. Harrison, I. T.; Lewis, B.; Lelson, P.; Rooks, W.; Roszkows, A.; Tomoloni, A.; Fried, J. H., Nonsteroidal Antiinflammatory Agents.1. 6-Substituted 2-naphthylacetic Acids. *Journal of Medicinal Chemistry* **1970,** 13, (2), 203.

31. Harrington, P. J.; Lodewijk, E., Twenty Years and Naproxen Technology. *Organic Process Research & Development* **1997,** 1, 72-76.

32. Crosby, J., Synthesis of Optically-Active Ompounds - A Large-Scale Perspective. *Tetrahedron* **1991,** 47, (27), 4789-4846.

33. Sonawane, H. R.; Bellur, N. S.; Ahuja, J. R.; Kulkarni, D. G., Recent development in the synthesis of optically-active alpha-arypropanoid acids-an important class of nonsteroidal antiinflammatory agents. *tetrahedron-Asymmetry* **1992,** 3, (2), 163-192.

34. Ravikumar, K.; Rajan, S. S.; Pattabhi, V., Structure of naproxen, $C_{14}H_{14}O_3$. *Acta Crystallographica Section C-Crystal Structure Communications* **1985,** 41, (FEB), 280-282.

35. Bednarek, E.; Bocian, W.; Dobrowolski, J.; Kozerski, L.; Sadlej-Sosnowska, N.; Sitkowski, J., The conformation of the naproxen anion studied by H-1 NMR and theoretical methods. *Journal of Molecular Structure* **2001,** 559, (1-3), 369-377.

36. Bansal, P.; Haribhakti, K.; Subramanian, V.; Plakogiannis, F., Effect of Formulation and Process Variables on the Dissolution Profile of Naproxen Sodium from Tablets. *Drug Development and Industrial Pharmacy* **1994,** 20, (13), 2151-2156.

37. Dong, Z. D.; Salsbury, J. S.; Zhou, D. L.; Munson, E. J.; Schroeder, S. A.; Prakash, I.; Vyazovkin, S.; Wight, C. A.; Grant, D. J. W., Dehydration kinetics of neotame monohydrate. *Journal of Pharmaceutical Sciences* **2002,** 91, (6), 1423-1431.

38. Sestak, J., Study of the Kinetics of the Mechanism of Solid-State Reactions at Increasing Temperatures. *Thermochimica Acta* **1971,** 3, 1-12.

39. Pikal, M. J.; Lang, J. E.; Shah, S., Desolvation Kinetics of Cefamandole Sodium Methanolate: the Effect of Water Vapor. *International Journal of Pharmaceutics* **1983,** 17, 237-262.

40. Shefter, E.; Fung, H. L.; Mok, O., Dehydration of crystalline theophylline monohydrate and ampicillin trihydrate. *Journal of Pharmaceutical Sciences* **1973,** 62, (5), 791-794.

41. Sekiguchi, K.; Shirotani, K.; Sakata, O.; Suzuki, E., Kinetic study of the dehydration of sulfaguanidine under isothermal conditions. *Chemical & pharmaceutical Bulletin* **1984,** 32, (4), 1558-1567.

42. Niazi, S., Thermodynamics of mercaptopurine dehydration. *Journal of Pharmaceutical Sciences* **1978,** 67, (4), 488-491.

43. Allen, P. V.; Rahn, P. D.; Sarapu, A. C.; Vanderwielen, A. J., Physicla Characterization of Erythromycin - Anhydrate, Monohydrate, and Dihydrate Crystalline Solids. *Journal of Pharmaceutical Sciences* **1978,** 67, (8), 1087-1093.

44. Moore, D. E.; Chappuis, P. P., A comparative-study of the photochemistry of the non-steridal anti-inflammatory drugs, naproxen, benoxaprofen and indomethacin. *Photochemistry and Photobiology* **1988,** 47, (2), 173-180.

45. Méndez del Río, J. R. Solubility and phase transitions in batch and laminar-flow tubular crystallizers. Available online, Georgia Institute of Technology, 2004: http://etd.gatech.edu/theses/available/etd-11182004-120908/unrestricted/mendezdelrio%5Fjose%5Fr%5F200412%5Fmast.pdf

46. Prausnitz, J. M.; Lichtenthaler, R. N.; Azevedo, E. G. d., *Molecular thermodynamics of fluid-phase equilibria*. 3rd ed.; Prentice-Hall PTR: Upper Saddle River, N.J., 1999; p xvii, 860 p.

47. Beiny, D. H. M.; Mullin, J. W., Solubilities of Higher Normal Alkanes in M-Xylene. *Journal of Chemical and Engineering Data* **1987,** 32, (1), 9-10.

48. Urakami, K.; Shono, Y.; Higashi, A.; Umemoto, K.; Godo, M., A novel method for estimation of transition temperature for polymorphic pairs in pharmaceuticals using heat of solution and solubility data. *Chemical & Pharmaceutical Bulletin* **2002,** 50, (2), 263-267.

49. Terada, K.; Kitano, H.; Yoshihashi, Y.; Yonemochi, E., Quantitative correlation between initial dissolution rate and heat of solution of drug. *Pharmaceutical Research* **2000,** 17, (8), 920-924.

50. Suryanarayanan, R.; Mitchell, A. G., Phase transitions of calcium gluceptate. *International Journal of Pharmaceutics* **1986,** 32, (2-3), 213-221.

51. Shefter, E.; Higuchi, T., Dissolution behavior of crystalline solvated and nonsolvated forms of some pharmaceuticals. *Journal of Pharmaceutical Sciences* **1963,** 52, (8), 781.

52. Suryanarayanan, R.; Mitchell, A. G., Evaluation of 2 concepts of crystallinity using calcium gluceptate as a model-compound. *International Journal of Pharmaceutics* **1985,** 24, (1), 1-17.

53. Khankari, R. K.; Law, D.; Grant, D. J. W., Determination of water-content in pharmaceutical hydrates by differential scanning calorimetry. *International Journal of Pharmaceutics* **1992,** 82, (1-2), 117-127.

54. Kim, Y.; Rousseau, R. W., Characterization and solid-state transformations of the pseudopolymorphic forms of sodium naproxen. *crystal Growth & Design* **2004,** 4, (6), 1211-1216.

55. Stark, J. G.; Wallace, H. G., *Chemistry Data Book*. 2nd ed.; John Murray: London, 1976.

56. Kim, Y.; R. Mendez Del Rio, J.; Rousseau, R. W., Solubility and Prediction of the Heat of Solution of Sodium Naproxen in Aqueous Solutions. *Journal of Pharmaceutical Sciences* **2005,** 94, Accepted.

57. Khankari, R. K.; Grant, D. J. W., Pharmaceutical Hydrates. *Thermochimica Acta* **1995,** 248, 61-79.

58. Domiano, P.; NarDelli, M.; Balsamo, A.; Macchia, B.; Macchia, F., Crystal and Molecular-Structure of Para-Methoxybenzyl 2-Alpha-Methyl-2-Beta-[(R)]Acetoxy(Methoxy)Methyl]-6-Beta-Phenoxyacetamidopenam-3-Alpha-Carboxylate. *Acta Crystallographica Section B-Structural Science* **1979,** 35, (JUN), 1363-1372.

59. Cox, J. S. G.; Woodard, G. D.; Mccrone, W. C., Solid-State Chemistry of Cromolyn Sodium (Disodium-Cromoglycate). *Journal of Pharmaceutical Sciences* **1971,** 60, (10), 1458-1465.

60. Te, R. L.; Griesser, U. J.; Morris, K. R.; Byrn, S. R.; Stowell, J. G., X-ray diffraction and solid-state NMR investigation of the single-crystal to single-crystal dehydration of thiamine hydrochloride monohydrate. *Crystal Growth & Design* **2003,** 3, (6), 997-1004.

61. Bettinetti, G.; Mura, P.; Sorrenti, M.; Faucci, M.; Negri, A., Physical characterization of picotamide monohydrate and anhydrous picotamide. *Journal of Pharmaceutical Sciences* **1999,** 88, (11), 1133-1139.

62. Reutzel-Edens, S. M.; Bush, J. K.; Magee, P. A.; Stephenson, G. A.; Byrn, S. R., Anhydrates and hydrates of olanzapine: Crystallization, solid-state characterization, and structural relationships. *Crystal Growth & Design* **2003,** 3, (6), 897-907.

63. Kim, Y.; VanDerveer, D.; Rousseau, R. W.; Wilkinson, A. P., Anhydrous sodium naproxen. *Acta Crystallographica Section E-Structure Reports Online* **2004,** 60, M419-M420.

64. Cameron, T. S.; Mannan, K. M.; Rahman, M. O., Crystal-Structure of Sodium Acetate Trihydrate. *Acta Crystallographica Section B-Structural Science* **1976,** 32, (JAN15), 89-90.

65. Ceccarelli, C.; Jeffrey, G. A.; Taylor, R., A Survey of O-H. O Hydrogen-bond Geometries Determined by Neutron-Diffraction. *Journal of Molecular Structure* **1981,** 70, (JAN), 255-271.

66. Harris, K. D. M.; Tremayne, M., Crystal structure determination from powder diffraction data. *Chemistry of materials* **1996,** 8, (11), 2554-2570.

67. Harris, K.; Tremayne, M.; Kariuki, B., Contemporary advances in the use of powder X-ray diffraction for structure determination. *Angewandte Chemie-International Edition* **2001,** 40, (9), 1626-1651.

68. David, W. I. F., *Structure determination from powder diffraction data*. Oxford University Press: Oxford; New York, 2002; p xvii, 337 p.

69. Visser, J. W., A fully automatic program for finding unit cell from powder data. *Journal of Applied Crystallography* **1969,** 2, 89.

70. Werner, P.; Eriksson, L.; Westdahl, M., Treor, A Semi-Exhaustive Trial-And-Error Powder Indexing Program For All Symmetries. *Journal of Applied Crystallography* **1985,** 18, (OCT), 367-370.

71. Boultif, A.; Louer, D., Indexing of Powder Diffraction Patterns For Low-Symmetry Lattices By the Successive Dichotomy Method. *Journal of Applied Crystallography* **1991,** 24, 987-993.

72. Rietveld, H. M., a Profile refinement method for nulcear and magnetic structures. *Journal of Applied Crystallography* **1969,** 2, 65-71.

73. Harris, K. D. M.; Tremayne, M.; Lightfoot, P.; Bruce, P. G., Crystal structure determination from powder diffraction data by monte-carlo methods. *Journal of the American Chemical Society* **1994,** 116, (8), 3543-3547.

74. Lanning, O. J.; Habershon, S.; Harris, K. D. M.; Johnston, R. L.; Kariuki, B. M.; Tedesco, E.; Turner, G. W., Definition of a 'guiding function' in global optimization: a hybrid approach combining energy and R-factor in structure solution from powder diffraction data. *chemical Physics Letters* **2000,** 317, (3-5), 296-303.

75. Turner, G. W.; Tedesco, E.; Harris, K. D. M.; Johnston, R. L.; Kariuki, B. M., Implementation of Lamarckian concepts in a Genetic Algorithm for structure solution from powder diffraction data. *chemical & Physics letters* **2000,** 321, (3-4), 183-190.

76. Dong, C., PowderX: Windows-95-based program for powder X-ray diffraction data processing. *Journal of Applied Crystallography* **1999,** 32, (4), 838.

77. Werner, P. E.; Eriksson, L.; Westdahl, M., Teror, A semi-exhaustive trial and error powder indexing porgram for all symmetries. *Journal of Applied Crystallography* **1985,** 18, (OCT), 367-370.

78. Shirley, R. Progress in Automatic Powder Indexing. http://www.ccp14.ac.uk/poster-talks/shirley_powdind_epdic2000/index.htm (May 19, 2005)

79. Larson, A. C.; Von Dreele, R. B. *General Structure Analysis System*; Los Alamos National Laboratory: Los Alamos, NM, 2000; pp Report LAUR 86-748.

80. Toby, B. H., EXPGUI, a graphical user interface for GSAS. *Journal of Applied Crystallography* **2001,** 34, 210-213.

81. berendsen, H. J. C.; Grigera, J. R.; Straatsma, T. P., The Missing Term in Effective Pair Potentials. *Journal of Physical Chemistry* **1987,** 91, (24), 6269-6271.

82. Mohan, V.; Smith, P. E.; Pettitt, B. M., Molecular-Dynamics Simulation of Ions and Water Around Triplex DNA. *Journal of Physical Chemistry* **1993,** 97, (49), 12984-12990.

83. Uchida, H.; Matsuoka, M., Molecular dynamics simulation of solution structure and dynamics of aqueous sodium chloride solutions from dilute to supersaturated concentration. *Fluid Phase Equilibria* **2004,** 219, (1), 49-54.

84. Bhatt, D.; Chee, R.; Newman, J.; Radke, C., Molecular simulation of the surface tension of simple aqueous electrolytes and the Gibbs adsorption equation. *Current Opinion in Colloid & Interface Science* **2004,** 9, (1-2), 145-148.

85. Chandrasekhar, J.; Spellmeyer, D. C.; Jorgensen, W. L., Energy Component Analysis For Dilute Aqueous-Solutions of Li+, Na+, F-, and Cl- Ions. *Journal of Applied Crystallography* **1984,** 106, (4), 903-910.

86. Moloy, E. C.; Cygan, R. T.; Bonhomme, F.; Teter, D. M.; Navrotsky, A., Molecular simulations of anhydrous Na-6[Al6Si6O24] sodalite. *chemistry of Materials* **2004,** 16, (11), 2121-2133.

87. Smith, D. E.; Dang, L. X., computer simulation of NaCl Association in Polarizable water. *Journal of Chemical Physics* **1994,** 100, (5), 3757-3766.

88. Rietveld Method Short Course. In Georgia Institute of Technology, Continuing Education: Atlanta, Georgia, USA, 2003.